CARBON DIOXIDE CAPTURE FROM NATURAL GAS USING REGENERABLE KAOLIN BASED SORBENTS

BY

QUSAY YOUSEF IBRAHIM BKOUR

A Thesis Presented to the

DEANSHIP OF GRADUATE STUDIES

KING FAHD UNIVERSITY OF PETROLEUM & MINERALS

DHAHRAN, SAUDI ARABIA

In Partial Fulfillment of the

Requirements for the Degree of

MASTER OF SCIENCE

In

CHEMICAL ENGINEERING

December 2014

KING FAHD UNIVERSITY OF PETROLEUM & MINERALS

DHAHRAN- 31261, SAUDI ARABIA

DEANSHIP OF GRADUATE STUDIES

This thesis written by **Qusay Y. Bkour** under the direction of his thesis advisor and approved by his thesis committee, has been presented and accepted by the Dean of Graduate Studies, in partial fulfillment of the requirements for the degree of **MASTER OF SCIENCE IN CHEMICAL ENGINEERING.**

Dr. Reyad Al-Shawabkeh
(Advisor)

Dr. Naim M. Faqir
(Co-Advisor)

Dr. Usamah Al-Mubaiyedh
(Member)

Dr. Adnan Al-Amer
(Member)

Dr. Mustafa Naser
(Member)

Dr. Mohammad Ba-shammakh
Department Chairman

Dr. Salam A. Zummo
Dean of Graduate Studies

1/1/15
Date

`

2014

`

DEDICATION

This work is dedicated to my beloved parents and wife.

`

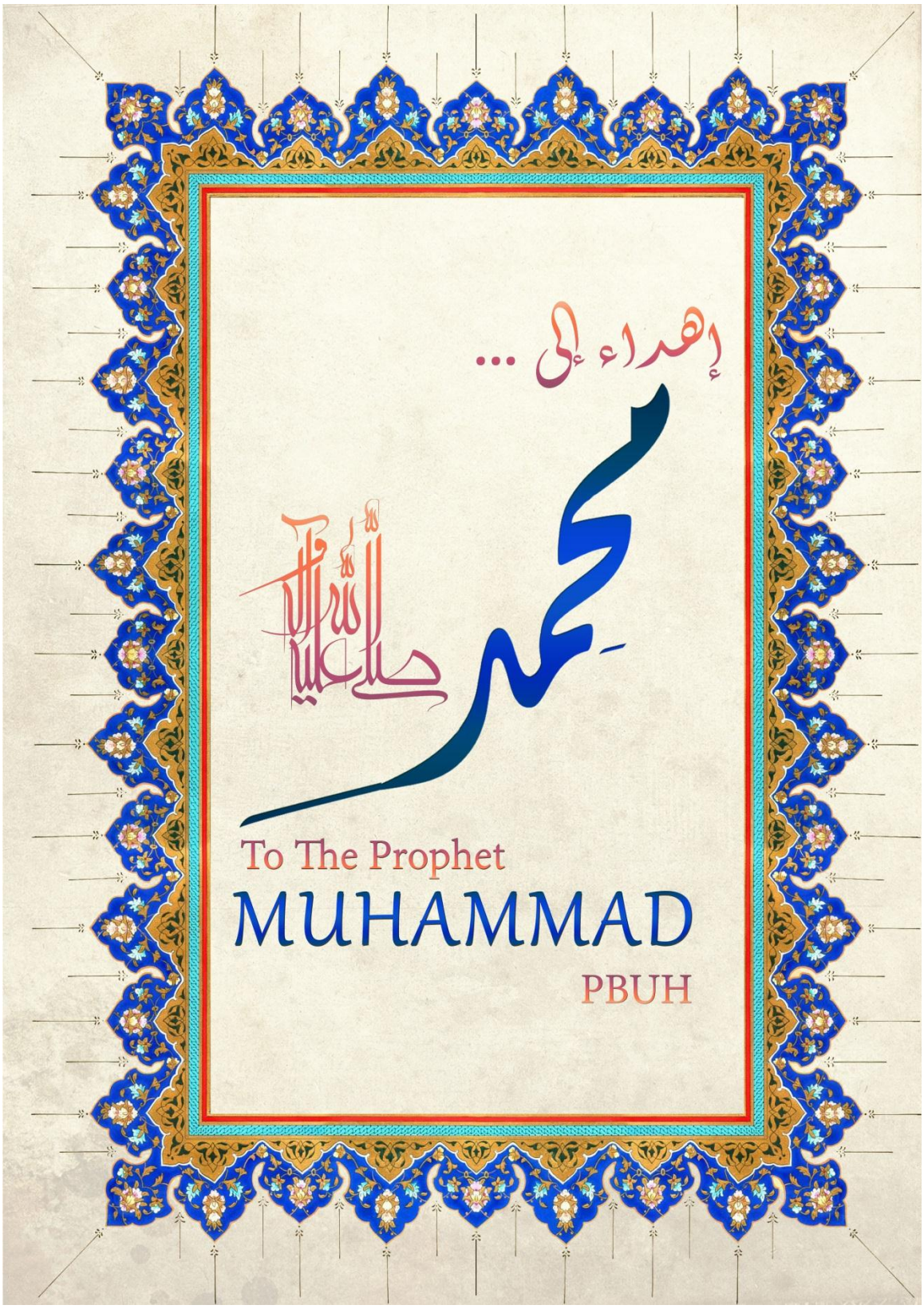
إهداء إلى ...
محمد صلى الله عليه وآله
To The Prophet
MUHAMMAD
PBUH

`

ACKNOWLEDGMENTS

All praise due to Almighty Allah, Most Gracious and Most Merciful, for his immense beneficence and blessings. He bestowed upon me health, knowledge and patience to complete this work. May peace and blessings be upon prophet Muhammad (PBUH), His Family, His Companions, and those who follow Him.

Thereafter, acknowledgement is due to KFUPM for the support extended towards my research through its remarkable facilities and for granting me the opportunity to pursue graduate studies.

I acknowledge, with deep gratitude and appreciation, the inspiration, encouragement, valuable time, patience, and continuous guidance given to me, pushing me to the front, and teaching me life skills by my thesis advisor, Dr. Reyad Awwad Alshawabkeh, His strong support and co-operation towards my this research during experiments was a boon to me. I am highly grateful and thankful to my thesis co-advisor Dr. Naim Faqir for his valuable guidance, suggestions and motivation. I extend my deep gratitude to my committee members: Dr. Mustafa Nasser, Dr. Usamah Al-Mubaiyedh and Dr. Adnan Al-Amer for their constructive guidance and support. My sincere appreciation goes to the Chemical Engineering Department staff for their support.

My heartfelt thanks are due to my beloved parents, wife, brothers, and friends for their prayers, guidance, and moral support throughout my academic life. My parents' advice, to strive for excellence has made all this work possible.

`

TABLE OF CONTENTS

DEDICATION……..iv

ACKNOWLEDGMENTS……...….vi

TABLE OF CONTENTS……...….vii

LIST OF TABLES…….……x

LIST OF FIGURES…….……xi

LIST OF ABBREVIATIONS…….……...xiii

ABSTRACT…….……xiv

ملخص الرسالة……..xvi

CHAPTER 1 INTRODUCTION..... 1

1.1 Greenhouse Gases (GHG) and Global Warming 1

1.2 CO_2 as greenhouse gas 3

1.3 Objectives of this work..... 5

CHAPTER 2 LITERATURE REVIEW 6

2.1 Absorption 7

2.2 Membrane Separation 9

2.3 Cryogenic Separation 10

2.4 Adsorption 10

2.4.1 Fundamentals of adsorption..... 14

2.4.2 Adsorption isotherms..... 15

2.4.3 Breakthrough curve..... 18

2.4.4 Hydrothermal Synthesis 20

`

CHAPTER 3 EXPERIMENTAL DESCRIPTION 24

3.1 Materials 24

3.2 Methods 24

3.3 Characterization 26

3.3.1 Fourier transform infrared spectroscopy (FTIR) 26

3.3.2 X-ray diffraction spectroscopy (XRD) 27

3.3.3 Scanning electron microscope (SEM) 27

3.3.4 Energy dispersive X-ray analysis (EDX) 27

3.3.5 Brunauer-Emmett-Teller (BET) technique 28

3.4 Adsorption and desorption studies 28

CHAPTER 4 RESUTLS AND DISCUSSION 31

4.1 Synthesis of product adsorbent 31

4.2 Characterization 32

4 .2.1 X-ray diffraction analysis (XRD) 32

4.2.2 Energy dispersive X-ray (EDX) analysis 35

4.2.3 Brunauer-Emmett-Teller (BET) technique 36

4.2.4 Pore Size Distribution 41

4.2.5 N_2 adsorption/ desorption isotherm analysis 43

4.2.6 Barrett–Joyner–Halenda (BJH) adsorption 46

4.2.7 Scanning Electron Microscopy (SEM) 47

4.2.8 Fourier transform infrared spectroscopy (FTIR) 49

4.3 Breakthrough profiles 50

4.4 Adsorption capacity 54

4.5 Regeneration and desorption results 56

4.6 Effect of temperature 60

`

4.7 Effect of initial concentration 62

4.8 Results of characterization of regenerated material 63

4.9 Effect of humidity 67

CHAPTER 5 MATHEMATICAL IINTERPRETATION 70

5.1 Breakthrough curve analysis 70

5.2 CO_2 adsorption isotherm analysis 71

5.3 Thermodynamic parameters 74

5.4 Fixed Bed Adsorption Column Modeling 77

CHAPTER 6 CONCLUSIONS AND RECOMMENDATIONS 81

6.1 Conclusions 81

6.2 Recommendations 85

APPENDIX 86

REFERENCES 101

VITAE 111

`

LIST OF TABLES

Table 1 Calculation of unit cell mass of Kaolinite [68]. 13
Table 2 Statistical analysis design of the experiment. 25
Table 3 Elemental analysis (Weight% (atomic %)) of synthesized adsorbent and raw kaolin by EDX. 35
Table 4 Textural properties of kaolin adsorbent materials. 38
Table 5 IUPAC classification of pore sizes [60]. 42
Table 6 BET and t-plot modelsurface area. 46
Table 7 Adsorption capacities of CO2 for different adsorbents. 55
Table 8 Statistical analysis of elemental data. 65
Table 9 Elemental analysis from SEM results for sample after five cycles. 66
Table 10 Residence time calculations. 98
Table 11 Adsorption capacity calculations sample. 99

`

LIST OF FIGURES

Figure 1 Global surface temperature. [46] 2
Figure 2 Total U.S greenhouse gas emissions by economic sector in 2011.[47] 3
Figure 3 Carbon dioxide concentration. [46] 4
Figure 4 Process technologies for CO_2 capture. [49] 6
Figure 5 Flow diagram of simplified MEA absorption process [8]. 9
Figure 6 Morphology of Kaolinite crystal [68] 13
Figure 7 A typical breakthrough curve [69]. 19
Figure 8 Reaction mechanism for zeolite synthesis from coal fly ash [88]. 23
Figure 9 The autoclave 26
Figure 10 experiment setup. 30
Figure 11 XRD spectrum for Kaolin. 33
Figure 12 XRD spectrum for limestone. 34
Figure 13 XRD spectrum for synthesized adsorbent. 34
Figure 14 N_2 adsorption/desorption isotherm for raw kaolin. 39
Figure 15 N_2 adsorption/desorption isotherm for treated kaolin. 39
Figure 16 N2 adsorption/desorption isotherm for limestone. 40
Figure 17 IUPAC classification for adsorption isotherm [59]. 40
Figure 18 pore size distribution for kaolin material. 42
Figure 19 BET surface area linear plot fro trated kaolin. 44
Figure 20 Hakins and Jura t-plot of treated kaolin. 45
Figure 21 BJH adsorption comulative pore volume for kaolin adsorbent and limestone. 47
Figure 22 SEM micrograph (a) 2kx magnification (b) 30kx magnification (c) 50kx magnification (d) 100kx magnification. 48
Figure 23 FTIR spectra for treated and untreated Kaolin. 50
Figure 24 Breakthrough curve of treated kaolin at flow rate of 4 L/min, concentration of 1630 ppm, and temperature of 25 C. 52
Figure 25 Breakthrough curve of raw kaolin at flow rate of 4 L/min, concentration of 1630 ppm and temperature of 25 C. 53
Figure 26 Breakthrough curves of raw Kaolin and limestone at flow rate of 4 L/min and temperature of 25 ^{o}C. 53
Figure 27 Complete breakthrough curve of treated Kaolinite at flow rate of 4 L/min, temperature of 25 ^{o}C. 54
Figure 28 Adsorption curves of treated Kaolin after several regeneration cycles. 57
Figure 29 Effect of regeneration cycles on amount of CO_2 adsorbed 58
Figure 30 Effect of regeneration cycles on amount of CO_2 desorbed. 59
Figure 31 Effect of regeneration cycles on amount of CO_2 adsorbed, desorbed, and reacted. 60

`

Figure 32 Effect of temperature on the adsorption of treated kaolin. 62
Figure 33 Effect of initial concentration on the adsorption of treated kaolin. 63
Figure 34 SEM micrographs of the treated sample after five cycles. 64
Figure 35 Spectrum of x-rays for treated sample after five cycles. 65
Figure 36 Breakthrough curve for treated kaolin at relative humidity of 63% and 20%. 68
Figure 37 Adsorption capacity at different sets of humidity conditions. 69
Figure 38 Definition of mean reciedence time on the breakthrough curve. 71
Figure 39 CO_2 adsorption isotherm at 22 C. 72
Figure 40 Linear form of BET isotherm for CO_2 adsorption on treated kaolin at 22C. .. 73
Figure 41 Fitting between experimental isotherm data and n-BET equation. 73
Figure 42 Relationship between equilibrium constant and temperature for treated kaolin. 75
Figure 43 Experimental and dispersion model for CO_2 adsorption 80
Figure 44 CO_2 uptake of treated kaolin (4 L/min, 19140 ppm, 20% RH,15 C). 86
Figure 45 CO_2 uptake of treated kaolin (4 l/min, 18710 ppm, 20% RH,25 C)..... 86
Figure 46 CO_2 uptake of treated kaolin (4 l/min, 18350 ppm, 20% RH,35 C)..... 87
Figure 47 CO_2 uptake of treated kaolin (4 l/min, 18140 ppm, 20% RH,50 C)..... 87
Figure 48 CO_2 uptake of treated kaolin (4 l/min, 18420 ppm, 20% RH,60 C)..... 88
Figure 49 CO_2 uptake of treated kaolin (4 l/min, 18710 ppm, 20% RH,70 C)..... 88
Figure 50 Adsorption-desorption curve for raw kaolin at %RH = Low, Conc= 1200ppm, flowrate= 4 L/min and Temp=25 C. 89
Figure 51 Adsorption-desorption curve for raw limestone at %RH = Low, Conc= 1200ppm, flowrate= 4 L/min and Temp=25 C. 89
Figure 52 Adsorption-desorption curve for treated kaolin at fresh regeneration cycle. .. 90
Figure 53 Adsorption-desorption curve for treated kaolin at first regeneration cycle. 90
Figure 54 Adsorption-desorption curve for treated kaolin at second regeneration cycle. 91
Figure 55 Adsorption-desorption curve for treated kaolin at third regeneration cycle.... 91
Figure 56 Adsorption-desorption curve for treated kaolin at fourth regeneration cycle. 92
Figure 57 Adsorption-desorption curve for treated kaolin at fifth regeneration cycle. ... 92
Figure 58 Adsorption-desorption curve for treated kaolin at low humidity. 93
Figure 59 Adsorption-desorption curve for treated kaolin at high humidity. 93
Figure 60 Adsorption-desorption curve for treated kaolin at 5 C. 94
Figure 61 Adsorption-desorption curve for treated kaolin at 15 C. 94
Figure 62 Adsorption-desorption curve for treated kaolin at 25 C. 95
Figure 63 Adsorption-desorption curve for treated kaolin at 35 C. 95
Figure 64 Adsorption-desorption curve for treated kaolin at 50 C. 96
Figure 65 Adsorption-desorption curve for treated kaolin at 60 C. 96
Figure 66 Adsorption-desorption curve for treated kaolin at 70 C. 97
Figure 67 Experimental and dispersion model isotherm for CO_2 adsorption (70 C)..... 100

`

LIST OF ABBREVIATIONS

GHG	:	Green House Gases
MOF	:	Metal Organic Framework
MEA	:	Monoethaneolamine
TNT	:	Titanium Nanotube
ZIF	:	Zeolitic Imidazolate Framework
SAPO	:	Silica Alumino Phosphates
AIPO	:	Alumino Phosphates
MTZ	:	Mass Transfer Zone
MRT	:	Mean Residence time
PFR	:	Plug Flow Reactor

`

ABSTRACT

Full Name : [Qusay Yousef Ibrahim Bkour]

Thesis Title : **[Carbon Dioxide Capture from Natural Gas using Regenerable Kaolin-Based Sorbents]**

Major Field : [Chemical Engineering]

Date of Degree : [December 2014]

The increasing demand worldwide to capture CO_2 from natural gas is forcing the industry to establish efficient and cost-effective approaches. In this work, a new aluminosilicates material was synthesized from kaolin clay and used for carbon dioxide capture from gases. This material was prepared by the hydrothermal reaction of kaolin and limestone with sodium hydroxide solution. Then it was characterized according to its crystalline phase. Several reaction conditions such as reaction temperature, pressure, kaolinite to limestone mass ratio and reaction time were investigated. It was found that by increasing the reaction temperature and pressure, the sodium hydroxide concentration has a noticeable effect on the formation of new aluminosilicate phases containing calcium and sodium in its structure. The produced sample was tested for its adsorption capacity against carbon dioxide from a gas stream. The adsorption/desorption breakthrough curves showed maximum saturation capacity of 4.7 mmol/g at a relative humidity of 55 %, and initial flow rate and concentration of CO_2 of 4 L/min and 1630 ppm, respectively. Thermodynamic studies of adsorption of carbon dioxide on the new adsorbent surface were investigated. It was found that increasing the bed temperature increases the rate of adsorption, where an endothermic nature of interaction took place in the adsorption column. The heat of adsorption ΔH, Gibbs free energy ΔG, and change in entropy ΔS

were calculated to be 144 kJ/mol, -7.4 kJ/mol and 444 kJ/mol.K, respectively. The experimental data was fitted using the axial dispersion model to predict the rate of adsorption of CO_2 by the obtained adsorbent. The effective diffusivity was calculated to be $2.8*10^{-3}$ cm^2/s. The produced adsorbent was regenerated several times using NaOH solution. The adsorption capacity increased by increasing the NaOH concentration as a result of opening more mesopores on the adsorbent surface and more sodium oxides linked in the structure.

This adsorbent is a low cost raw material and has a high adsorption capacity, which can be considered a cost effective sorbent for carbon dioxide removal from gas streams.

Keywords: Adsorption, CO_2 capture, Desorption, Regeneration, Kaolinite, adsorption capacity.

`

ملخص الرسالة

الاسم الكامل: **قصي يوسف ابراهيم بكور**

عنوان الرسالة: امتصاص ثاني اكسيد الكربون من الغاز الطبيعي باستخدام الكاولين

التخصص: الهندسة الكيميائية

تاريخ الدرجة العلمية: تشرين الثاني ٢٠١٤

الغاز الطبيعي يحتوي على نسبه من غاز ثاني اكسيد الكربون الامر الذي يؤدي الى حدوث مشاكل صناعيه

مختلفه .في هذا البحث تم استخدام مواد ماصه sorbent لل CO_2 تم تحضيرها كيميائيا ,هاذه الماده عباره عن سليكات الالمنيوم(كالونايت)المعالجه كيميائيا ,وهي مواد اقتصاديه وفعاله لفصل ال CO_2 عن الغاز الطبيعي حيث انها تتفاعل مع ال CO_2 ليتم فصله .في هذا البحث تم دراسه صفات الماده فيزيائيا من ناحيه مساحة السطح، توزيع حجم المسمامات ,وخصائص السطح .بعد ذلك تم فحص الماده على امتصاص ال CO_2 باستخدام تراكيز مختلفه من ال CO_2. وايضا تم دراسع عملية فض الCO_2 عن الماده باستخدام ال غاز النتيروجين .هذه الدراسه اظهرت انه على درجة حراره الجو وسرعة جريان للغاز 4 لتر/دقيقه القدره الامتصاصيه لل CO_2 على هذه الماده هي 2.79 (مل مول/غرام) ومقارنة بلمواد الاخرى تعتبر منافسه على الرغم من قلة مساحة سطحها وايضا اظهرت الدراسه ان هذه الماده يمكن استخدامها اكثر من مره حيث انها عملية اعادة تجديد الماده سهله واقتصاديه

`

واحيانا تزيد من القدره الامتصاصيه حيث انها تغير التركيبه الكيميايه للماده حيث بعد استخدامها ب 5 مرات زادت القدره الامتصاصيه الى الضعف.

`

CHAPTER 1

INTRODUCTION

1.1 Greenhouse Gases (GHG) and Global Warming

Even since the industrial revolution recorded the highest rate in the 19th century, increasing amounts of fossil fuels like oil, coal, and natural gas have been burned in different industrial sectors as manufacturing and electricity power generation plants. When fossil fuels are burned, greenhouse gases are released which cause global warming. When the sun's energy falls on the atmosphere, the ozone layer screens out the ultraviolent high frequency light and the visible light is transmitted to the earth. Part of this light is reflected back and the other part is absorbed as thermal energy by the earth. It is transferred as infrared long wavelength radiation using the gases present in the atmosphere, mainly carbon dioxide, water vapor, sulfur oxides, nitrogen oxides, hydrogen sulfide and methane. These gases are called greenhouse gases because they absorb the infrared radiation and hold it within the atmosphere, this leads to an increase in the global surface temperature.

`

Several studies have showed that the average global surface temperature has increased by 0.6-0.9 ^{o}C in the last 150 years and the rate of increase has doubled in last 50 years (Figure 1) [42]. The global warming has caused increases in melting of iceberg, raising the sea level, and inducing flooding in low lying areas [43] [44] [45].

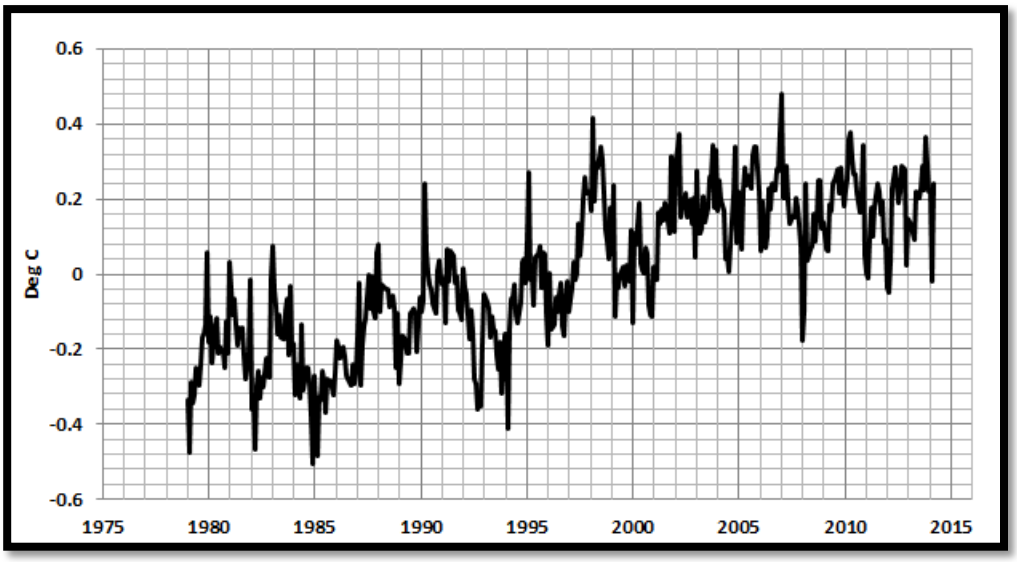

Figure 1 Global surface temperature. [46]

Human activities are the major sources of most of the greenhouse gases in the atmosphere, these activities are mainly burning of fossil fuels [45]. As shown in figure 2, the transportation, electricity generation and industry are the major greenhouse emission contributors with 28% and 33% and 20% respectively of the total emissions in US in 2011 [47, 48].

There are many of studies that aim to reduce greenhouse gases by improving energy efficiency, utilizing the non-carbon sources of energy, and CO_2 capture and sequestration.

`

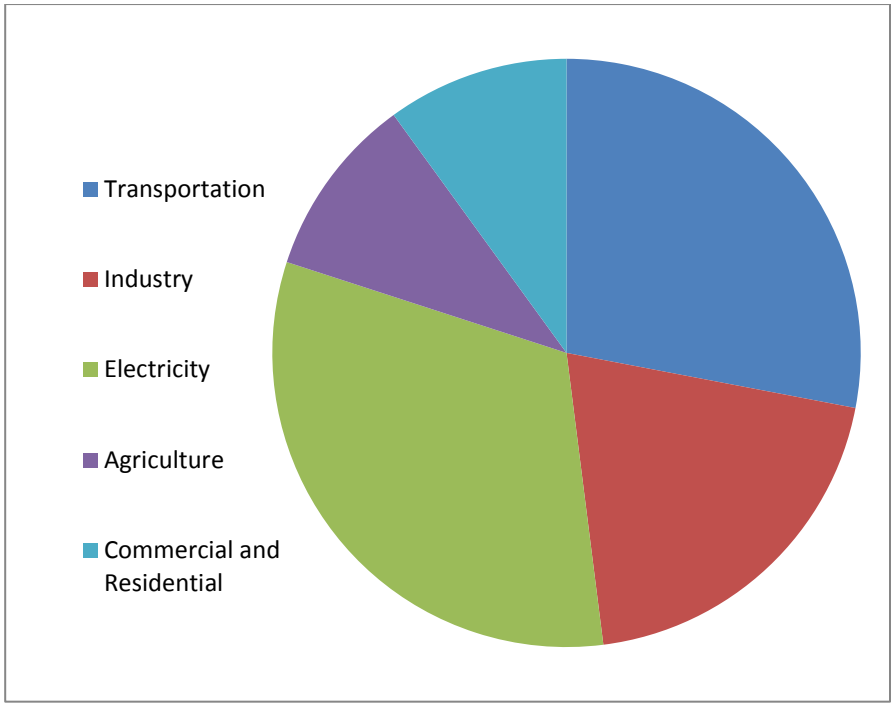

Figure 2 Total U.S greenhouse gas emissions by economic sector in 2011.[47]

1.2 CO_2 as greenhouse gas

Carbon dioxide (CO_2) is the major causative of the global warming phenomena among the greenhouses gases as it contributes about 60% to global warming [1]. As shown in figure 3, the CO_2 growth rate increased from less than 1 ppm/yr in 1960s to more than 2 ppm/yr in recent years [2]. Consequently, the atmospheric level of CO_2 rose from 315 ppm in 1985 to 399 in 2014 [3]. The Intergovernmental Panel on Climate Change (IPCC) expected that the CO_2 concentration will rise from 500 up to 1000 ppm by the year 2100 [4].

The rising level of CO_2 is already affecting the sea level, atmosphere, and ecological systems. The global sea level has risen by 130 m over the last 22,000 years, and 10 to 20

`

cm over the past century with rate of 1.7 mm yr^{-1}, which would results from melting of the ice caps [44].

Therefore, it is important to establish efficient approaches to capture the CO_2 from post combustion effluents before direct sequestration since about 30% of CO_2 is generated by combustion of fossil fuels [5]. Natural gas accounts for the emission of large quantities of CO_2. The global emission of CO_2 from natural gas was 53.1 kg CO_2 per million Btu, while coal and oil produced 95.3 and 71.3 kg CO_2 per million Btu [84].

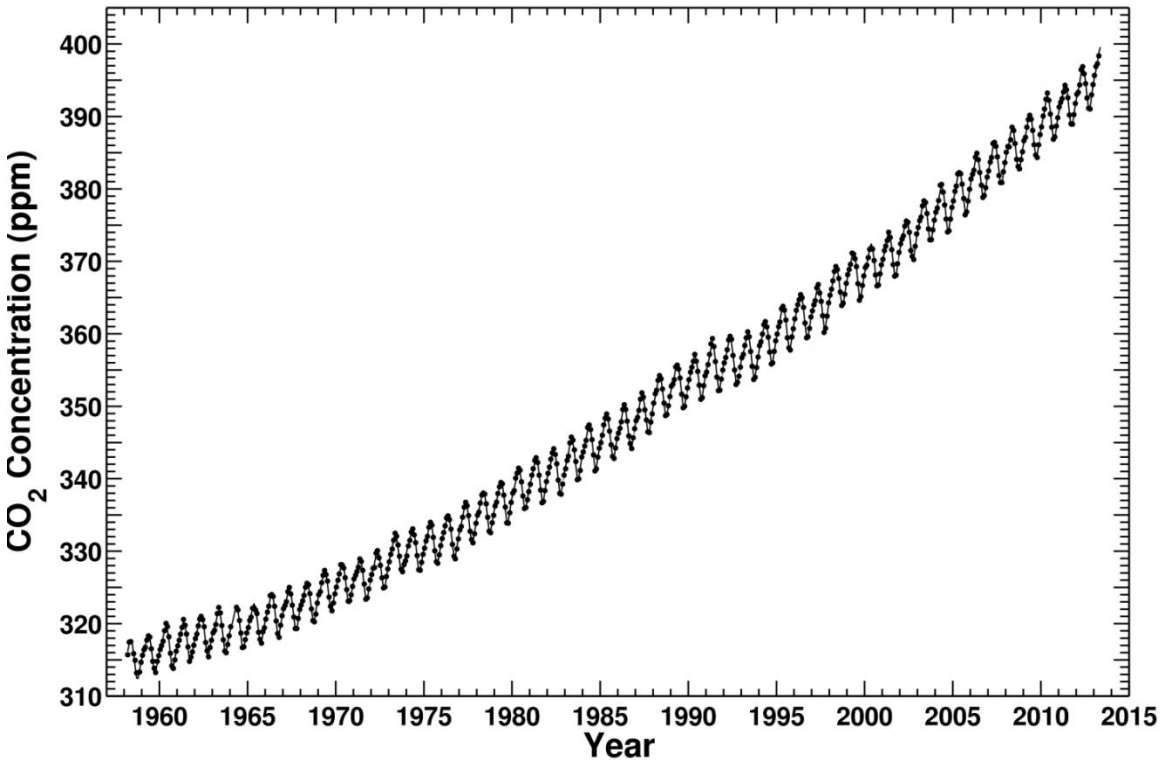

Figure 3 Carbon dioxide concentration. [46]

`

1.3 Objectives of this work

1. The main objective of this work is to synthesize a novel, cost effective and high adsorption capacity sorbent from natural Kaolin and limestone to be used for CO_2 removal from gas stream.

2. The obtained adsorbent is characterized according to its surface area and morphology using BET, XRD, SEM, EDX and FTIR.

3. Study the adsorption capacity and kinetics of CO_2 by the synthesized material at different operation conditions such as temperature, flow rate, initial concentration, and humidity.

4. Study the desorption and regeneration capacity, and hence the adsorbent activity.

5. Develop a kinetic model that simulates the rate of adsorption at different operation temperatures.

This literature survey pertaining to this work is presented in chapter 2. Experimental methods and procedures are shown in chapter 3. The results and discussion section is covered in chapter 4. The mathematical interpretation is shown in chapter 5. Finally, chapter 6 lists the conclusions and recommendations points.

`

CHAPTER 2

LITERATURE REVIEW

There are numerous techniques that can be used for post combustion and natural gas separation and capture; absorption, cryogenic separation, membrane separation, micro algal, bio fixation and adsorption [6]. Figure 4 summarizes these techniques.

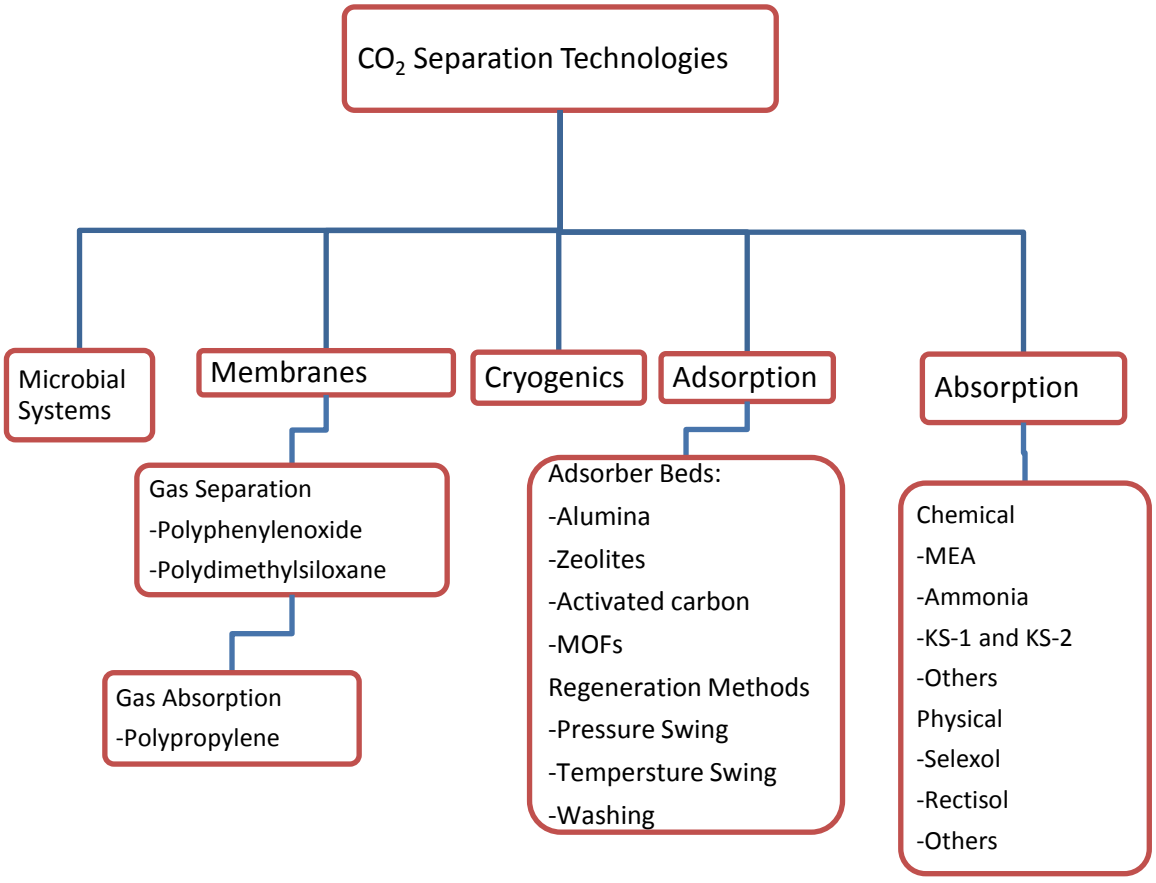

Figure 4 Process technologies for CO_2 capture. [49]

`

2.1 Absorption

Gas absorption using amine solutions has been used for CO_2 scrubbing on industrial scale for decades. Chemical absorption is an amine based process involving the reaction of CO_2 with amine compounds such as monoethanolamine (MEA), diethanolamine (DEA), diethyleneglycol (DEG) or triethyleneglycol (TEG) [14, 12]. Monoethaneolamine (MEA) has been widely used for CO_2 separation in natural gas industries for decades, and produced relatively pure CO_2. There were several works reported for capturing CO_2 using chemical absorption. Kvamsdal et al. [8] in figure 5 showed the conventional MEA absorption process, where two columns were used; the absorber and stripper column, the flue gas enters counter currently with MEA that absorbs the CO_2 and the effluent solution is treated in the stripper using steam generated from the power plant. CO_2 is collected from the top of the columns to be used as a chemical or fuel feedstock. Some researchers have developed a dynamic model of the CO_2 absorber of chemical absorption plant [9, 10]. Wanga et al. [7] studied CO_2 capture with alkanolamine solutions such as, MEA solvent. They tried to predict future challenges and potential developments. Tong et al. [85] studied the solubility of CO_2 in blends of 2-amino-2-methyl-1-propanol (AMP) and piperazine (PZ). They found that the PZ+AMP blends have CO_2 absorption capacities about 12.5% smaller than the aqueous AMP solution without PZ. Kim et al. [86] investigated the effect of polyamines containing multiple amino groups in their structure on the CO_2 absorption capacity and heat of absorption, they found that these aqueous solutions such as tetraethylenepentamine (TEPA), diethylenetriamine (DETA), triethylenetetramine (TETA), and EDA showed better absorption capacity than that of MEA due to the increased number of amino groups that can react with CO_2. Yamini et al.

`

[87] synthesized amino acid anion based ionic liquids; they found that amino acid anion - ionic liquids showed 70% more CO_2 absorption capacity than primary amine-cation ionic liquids.

There are many disadvantages associated with the absorption process including operational problems such as solvent degradation and corrosion of the equipment. Also the regeneration process of the solvent requires a high amount of energy, thus the operational cost of the process using MEA is high [11].

The chemical absorption is limited to low pressure gas streams (between 3%-25%), so physical absorption can be used for the high pressure feed or high CO_2 content. It depends on Henry's law which requires the CO_2 loading capacity of the solvent is higher at high CO_2 partial pressures [12]. The typical solvents are Selexol, Rectisol (cold methanol), and n-alkane [14, 12]. The regeneration in physical absorption is appropriated by heating or pressure reduction using flash units, so it requires relatively little energy [13]. The physical absorption process is limited for CO_2 rich gas streams or high CO_2 pressure.

`

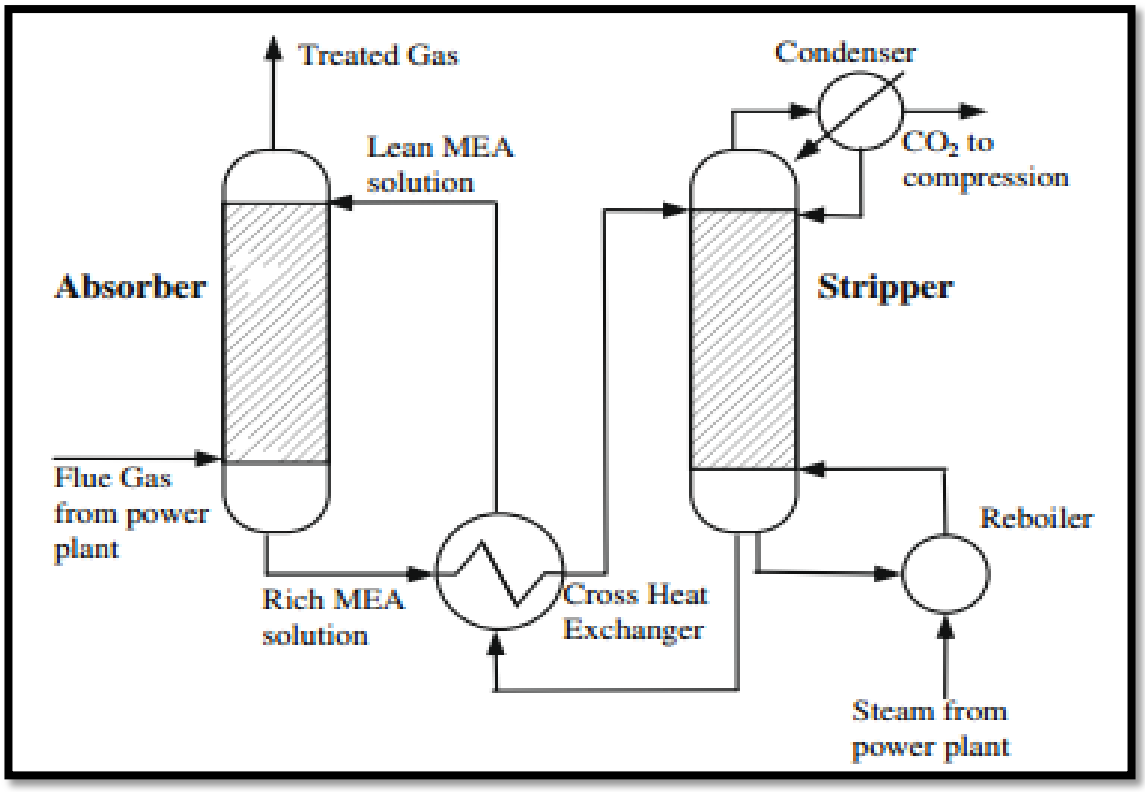

Figure 5 Flow diagram of simplified MEA absorption process [8].

2.2 Membrane Separation

Membrane separation is a newly developed process which depends on the utilization of thin polymeric films that provide selectivity to permeate specific gases based on their molecular sizes. The difference in partial pressure of the compound in both sides of membrane is the driving force for the penetration of the compounds through the membrane. There are a number of advantages of this method. For example, there is no corrosion associated with the presence of aqueous solution, thus low level of maintenance is required. Also there is no phase change or need for a regeneration step like the absorption method because of the absence of chemicals, so it requires low thermal energy

`

[13]. However, there might be a decline in the membrane performance due to natural gas contaminants [12].

When the partial pressure of CO_2 is low, the driving force for separation of the gas is low, so a solvent can be used with the membrane, where the membrane maintains the surface area between the liquid solvent and gas phase. The CO_2 diffuses first through the pores of membrane, and then it is adsorbed. This method solves flow problems in traditional absorption like channeling and foaming.

2.3 Cryogenic Separation

CO_2 can be captured without any absorption solvents and at atmospheric pressure using the cryogenic separation approach. This technology is based on the fact that CO_2 liquefies at low temperatures, since CO_2 condenses at -56.6 ^{o}C at 1 atm [14]. When the mixture gases is cooled, the CO_2 and water freeze forming hydrates which are ice crystals with trapped CO_2 while other gases are released. The problem of this process is the relatively high cost of cooling.

2.4 Adsorption

Adsorption is a promising technology for CO_2 separation. Over other methods that are used for CO_2 capture and separation, adsorption is a more economical, naturally occurring and easier one. Several types of adsorbents can be used for removal of CO_2 from gas stream. These include physical adsorbents such as activated carbonaceous materials, aluminasilicates (zeolites, alumino-silico-phosphates SAPOs, and alumino-phosphates AlPOs), and Metal organic frameworks MOFs, and may include chemical adsorbents such

`

as amine groups into mesoporous silica. Suitable adsorbents for CO_2 separation should combine several aspects, including high CO_2 adsorption capacity, high CO_2 selectivity, fast kinetics, mild conditions for regeneration, low cost, tolerance to the presence of moisture and impurities in the feed, and the stability during extensive adsorption/desorption cycling. Several research efforts were focused on developing the existing materials or synthesis new ones. Konduru et al. [23] used Zeolite 13X with 1.77 mmol/g adsorption capacity. Other Zeoilites types used such as Zeolite T [24], NaZSM-5 [25], MWW zeotype [26], silica-alumino-phosphates (SAPO) and Alumino-phosphates (AlPO) [27]. Zhang et al. [28] found that the adsorption capacity for CO_2 on modified activated carbon was 2.92 mmol/g at 1 atm and 298 K. Xin et al. [15] studied the photo-catalytic reduction of CO_2 to methanol CH_3OH using titanium nanotube (TNT) modified with CdS and Bi_2S_3 metals to improve the rate of visible light adsorbed. This TNT demonstrated low price, high surface area, 3-D regular structure, and hydrophilic behavior. It was found that the modified TNT decreased the surface area and capacity of CO_2 adsorption (0.269 mmol/g TNT at 1 atm and 298K) where the adsorption is a favorable physical process, however, photo-catalytic activity increased. The metal organic frameworks (MOF) are a class of new adsorbents that have extra high surface area, natural porous [16], high thermal stability and ordered structure [17]. Andrew et al. [18] studied the adsorption of CO_2 on MOF-177; he found that the adsorption capacity of CO_2 was 34mmol/g (1496 mg/g) at 43bar. Llewellyn et al. [19] studied the adsorption of CO_2 over novel mesoporous MIL-100 and MIL-101. They were formed from rigid carboxylate ligands and trimmers of chromium octahedral. It was found that MIL-100 and MIL-101 recorded an adsorption capacity of 18 and 40 mmol/g respectively at 304 K and 50 bar.

`

Hideki et al. [20] identified new organic frameworks called zeolitic imidazolate frameworks (ZIFs) that have high thermal and chemical stabilities. Banerjee et al. [21] found that the adsorption capacity of CO_2 on ZIF-69 was 209.8 mg/g at 1 bar and 273 K. Zhijuan et al. [22] studied the performance of ZIF-8, modified by using ammonia impregnation towards CO_2, and found that its capacity was 330 mg/g at 298K and 25 bar, the increase of the capacity was because of basic sites.

However, there are many of drawbacks of using of MOFs for CO_2 separation; these materials are expensive and most of the MOFs show unfavorable adsorption isotherms in the low pressure range. It adsorbs considerable amounts of CO_2, affecting the CO_2 selectivity and it shows hydrothermal instability.

Kaolinite can be used as an adsorbent after modification. The layer of the Kaolinite consists of an alumina octahedral sheet and a silica tetrahedral sheet that share a common plane of oxygen atoms and repeated layers of the mineral are hydrogen bonded together [67]. The unit formula of Kaolinite is: $Si_4\ O_{10}\ A_{l4}\ (OH)_8$ [68]. Table 1 shows the calculation of unit cell mass of Kaolinite. The crystal shape of the Kaolinite is shown in figure 6. Table 8 shows the adsorption capacities for different adsorbents that have been used in the literature.

`

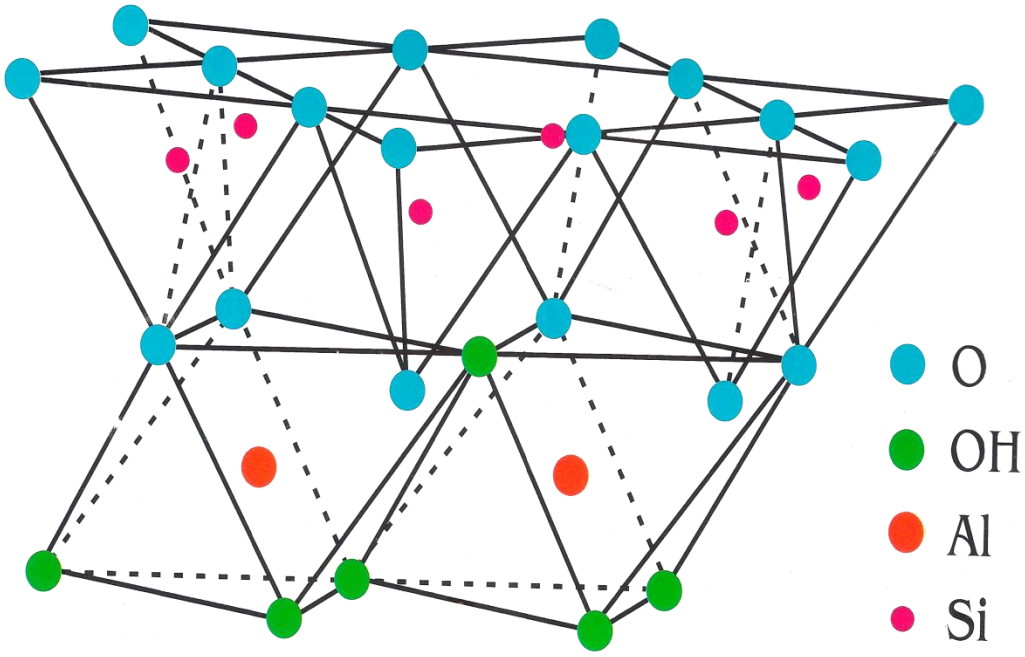

Figure 6 Morphology of Kaolinite crystal [68].

Table 1 Calculation of unit cell mass of Kaolinite [68].

Element	Mass	Stoich. coef
Si	28.09	4
Al	26.98	4
Mg	24.3	10.57
O	16	18

`

2.4.1 Fundamentals of adsorption

Adsorption can be classified into two types; chemical adsorption (chemisorption) or physical adsorption (physisorption) based on the type of attraction forces between adsorbate and adsorbent. The concept of physisorption refers to the adsorption of molecules on the solid surface without presence of chemical reactions or catalysis. This type of the adsorption is preferred because of its simplicity and its industrial applications, and moreover, it can be studied based on proven macroscopic experiments without needing more conjecture. Adsorption equilibrium is the dynamic equilibrium between the number of the molecules adsorbed and the others desorbed within a certain time interval (i.e. there is a match between molecules flow to and from the surface). The fluid phases that its molecules are intermingling with the surface atoms of a solid phase are called adsorptive, while the solid phase with external and internal surfaces are called adsorbents.

The strength or interaction energy can be used to distinguish between physisorption, physico-chemical adsorption and chemisorption phenomena. The forces in physisorption phenomena are van der Waals and/or dispersion forces in which adsorbed molecules are weakly bound. The interaction energy between admolecules and the sorbent atoms or molecules are strong in chemisorption because they are subject to chemical reaction where the character of their electrons shells change. The adsorbed molecules in physisorption system can be desorbed by either increasing temperature or lowering the sorptive gas pressure, while they cannot reversibly be desorbed in chemisorption where the kinetics are slow. In physico-chemical adsorption the interactions are weak but there

`

are catalytic properties of the sorbent that make strong associations between adsorbed molecules and sorbents.

2.4.2 Adsorption isotherms

The adsorption isotherms are used to present the equilibrium between molecules in the gas phase and those adsorbed on the active sites of the solid adsorbent. The Langmuir or Freundlich relationships are the most isotherms used in the literature. Langmuir assumes that the adsorbed species form the monolayer on the surface of the adsorbent (each site hold only one adsorbed species), and the uniform energy of adsorption (so same probability adsorption on all sites) [64].

The Langmuir isotherm can be derived based on the equilibrium conditions between the adsorbed molecules and the desorbed on the surface according:

The adsorption process can be represented by the following equation:

$$S + A \leftrightarrow SA$$

Where S: the vacant surface sites, A: fluid phase molecules, and SA: occupied surface sites.

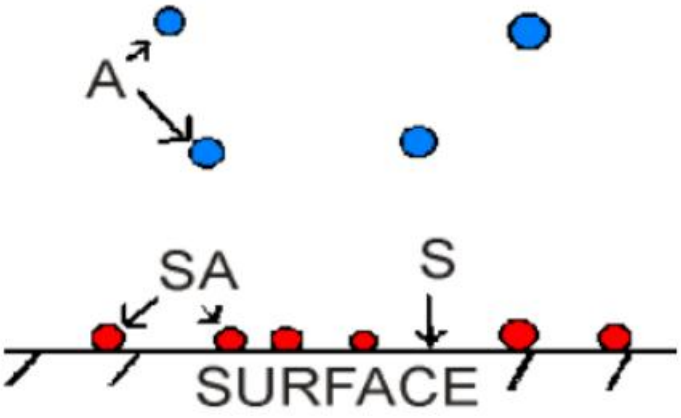

`

Rate of forward reaction R_f, and the rate of backward reaction R_b can be illustrated by:

$$R_f = k_a[\mathrm{A}][\mathrm{S}]$$

$$R_b = k_b[\mathrm{SA}]$$

An equilibrium constant K can be written as:

$$\mathrm{K} = \frac{k_a}{k_b} = \frac{[SA]}{[S][A]}$$

$$\mathrm{K} = \frac{k_a}{k_b} = \frac{\Theta}{(1-\Theta)P}$$

Where Θ is the fraction of the surface sites occupied, and it value ranged from 0 to 1.

Writing the equation in term of Θ:

$$\Theta = \frac{k_a\,\mathrm{P}}{k_b + k_a\,P}$$

Dividing the numerator and denominator by k_b:

$$\Theta = \frac{\mathrm{K\,P}}{1 + K\,P}$$

The Θ can be replaced with q_e/q_m, where q_e is the amount of the gas adsorbed at equilibrium, q_m is amount of gas adsorbed at high pressure to cover the surface with monolayer molecules.

$$q_e = \frac{q_m.K.P}{1 + K.P}$$

`

Where C_e is the concentration of species at equilibrium (mg/ dm^3), q_m is the quantity of metal ions needed for forming a monolayer on the surface of the adsorbent (mg /g), K the Langmuir constant of equilibrium.

If the experimental data is available, the constants can be obtained by linearization of the Langmuir isotherm:

$$\frac{P}{q_e} = \frac{P}{q_m} + \frac{1}{K\, q_m}$$

The Langmuir isotherm has a number of limitations, for example, it is applicable for monolayer adsorption at low pressure and high temperature, when the temperature is lowered and the pressure is increased additional layers are formed.

Freundlish isotherm equation is used to describe the adsorption on heterogeneous surfaces. It can be derived based on first order kinetics equation:

$$\frac{d\, C}{d\, t} = \mathrm{K\, C}$$

Where K is the first order rate constant and C is the concentration as function of time.

In general the rate law can be written as:

$$\frac{d\, C}{d\, t} = K_f C^n$$

Where K_f is the forward rate coefficient.

Writing the forward and backward reaction:

$$\frac{d\, C}{d\, t} = \mathrm{K1}\; C^{n1} + \mathrm{K2}\; S^{n2}$$

`

At equilibrium the equation can be solved for S as:

$$S = (\frac{K1}{K2})^{1/n2}\, C^{n1/n2}$$

This leads to Freundlish equation with K= $\frac{K1}{K2}$ and b= $n1/n2$:

$$S = K\, C^{b}$$

Where S is the amount adsorbed.

When there is a chemical interaction between the adsorbed molecules and the surface, Langmuir and Freundlish models may not fit the experimental data adequately. Hence, Shawabkek-Tutunji [66] isotherm correlation was developed to account for chemical interaction of adsorbed molecules with adsorbent surface as:

$$q_e = q_s\,(1 - \alpha\, {C_e}^{\beta})$$

Where:

$$\alpha = \frac{k\,\Delta t}{m_s\, q_s}$$

The linear form of the equation:

$$\ln\,(1 - \frac{q_e}{q_s}) = \ln\alpha + \beta \ln C_e$$

2.4.3 Breakthrough curve

A breakthrough curve is used to characterize the rate of adsorption with time. It represents the concentration of the adsorbate at the exit of the adsorption bed as a function of time (Figure 7).

`

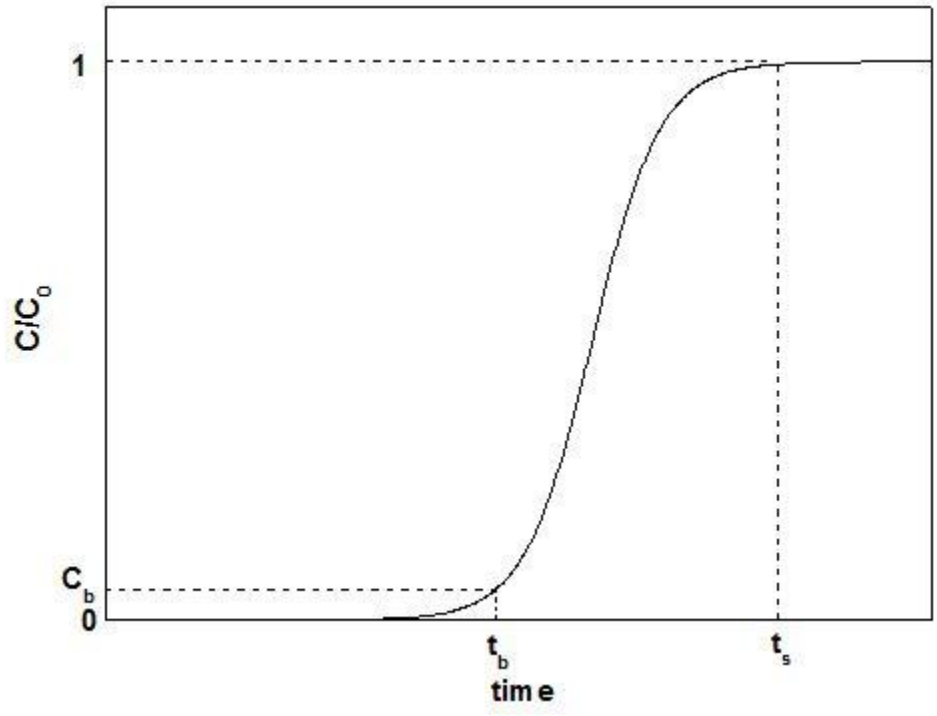

Figure 7 A typical breakthrough curve [69].

Initially, the relative concentration is zero because all molecules are adsorbed on the column until it reaches t_b at $C_{out}/C_F = 0.05$ where the adsorbent starts to get saturated with the adsorbate. At time t_s ($C_{out}/C_F = 0.95$) the adsorbent is almost completely saturated, so the outlet concentration equals the initial concentration and any adsorbate which enters the column will pass without being adsorbed.

The area between t_b and t_s is the mass transfer zone. A Sharp breakthrough curve and long adsorption time t_b are desirable to have good separation [69].

Different parameters affect the shape of breakeven curve for adsorption of gas in packed column such as flow rate, bed height, and void fraction of bed. About the effect of the bed height on the shape of breakthrough curve, when the bed height is increased, the mass

`

transfer zone becomes broader and the breakthrough time is increased because of increasing the adsorbent loading and the length of the diffusion path. Moreover, by increasing the gas flow rate through the adsorption column at a constant height bed, the breakthrough time decreases [70].

The bed void fraction, which is the ratio between the free volumes in the column to the total volume of column, depends on the geometry of adsorbent materials. By increasing the void fraction at the same mass of adsorbent, the mass transfer zone becomes broader because of the longer diffusion path length. Small pellet diameter generates a steep slope breakthrough curve due to negligible diffusion and mass transfer in the bed [70].

2.4.4 Hydrothermal Synthesis

Hydrothermal synthesis is related to the synthesis of materials that have characteristic 3D framework with sequences of tetrahedron XO_4, where X is silicon, aluminum, etc. Sodium hydroxide as a high alkaline solvent is incorporated into source material rich in Al_2O_3 and SiO_2 as source of the sodium. The detailed mechanism of the hydrothermal reaction is still not clear. However some researchers have been trying to investigate the general mechanism. Murayama et al. [88] clarified the mechanism of the hydrothermal reaction for zeolite synthesis from coal fly ash in various alkali solutions. He investigated three steps for hydrothermal reaction of zeolite synthesis; first step is the dissolution of the Al and Si in the ash by OH- and keep them in the alkali solution, Second step is the formation of the aluminosilicate gel by condensation or gelation of aluminate and silicate ions that react with each other in alkali solution, third step is the crystallization of aluminosilicate gel to form zeolite structure, after deposition of the gel on the particle

`

surface as big flake. Na^{+} in alkali solution has a role of crystallization of zeolite. The change of Al^{+3} and Si^{+4} concentration in liquid phase during the hydrothermal reaction is also studied by Murayama, at the beginning of the heating stage the Al rapidly increases and then decreases in the temperature rising stage because of the consumption of aluminate ion during condensation reaction of an aluminosilicate gel, while Si is dissolved with time with linear relation in the temperature rising stage. Si and Al ingredients are not consumed when aluminate ions are completely consumed in an alkali solution (Figure 8). Franus [89] studied the transformation of coal fly ash to X- type zeolite using two types of synthesis; low temperature and hydrothermal synthesis. Zeolitic material with rich Na-X phase was yielded by alkaline reaction of fly ash with NaOH. He frond that the BET surface area of Na-X formed by hydrothermal reaction is five times higher (332.5 m_2/g) than that formed by low temperature reaction (73 m_2/g). Also the ratios of Si/Al were 1.2 and 1.04 for Na-X obtained by hydrothermal and low temperature reaction respectively. The amount of zeolitic phase rich in Na-X was from 55 to 60% from total reaction products in hydrothermal reaction, whereas from 42 to 55% in low temperature reaction.

The synthesis of the kaolinite with elements substituted for Al has been studied by several researchers. Bentabol et al. [90] studied the transformation of kaolinite within range of PH values, variable run times, and temperature range of 200 to 400 in solution containing variables amount of Na, K, Li and Mg. They found that Mg^{+2} cation in $Mg(OH)_2$ substitute for Al^{+3} in the kaolinite. Co–kaolinite and Al–Co–serpentine were hydrothermally synthesized at 200 °C by mixing the kaolinite with $Co(OH)_2$ forming $CoO–Al_2O_3–SiO_2–H_2O$ [91]. In this work, Ca-kaolinite was synthesized by reaction of NaOH with mixing of kaolin and limestone under hydrothermal conditions, where the

`

solution was placed in the autoclave at a range of 200 ^{o}C and pressure of 15 bar to avoid evaporation from the solution. The sample is further calcinated or thermal activated at 550 ^{0}C to form spinal of Si and Al oxides.

Some reports discussed the substitution of Mg, Fe, Mn and Co. Bentabol et al. [90] synthesized Mg and Mg-Ni kaolinite under hydrothermal conditions. They also studied Co-kaolinite at 200^{0}C. Peter et al [94] studied the formation of Gehlenite ($Ca_2SiAl_2O_7$) from the mixture of kaolinite and calcite according to the following equation:

$$2CaCO_3 + Al_2Si_2O_7 \cdot 2H_2O \rightarrow Ca_2Al_2SiO_7 + SiO_2 + 2H_2O + 2CO_2$$

Kerfa et al [95] studied the Gehlenite crystallization from calcium and metakaolinite, under the reaction:

$$Al_2Si_2O_7 + (2+n)\ CaCO_3 \rightarrow Ca_2Al_2SiO_7 + nCaOSiO_2$$

Stilbite is a natural zeolite has a chemical composition of (Na Ca_4 ($Si_{27}Al_9$) $O_{72}\cdot 30H_2O$). Hua et al. [96] studied the characterization of geopolymers formed from Stillbite/kaolinite mixtures, they found that Stilbite contains 7.56 mass % of CaO.

Seliem et al. [103] showed the SEM image for Mn-kaolinite that synthesized hydrothermally, the sample showed needle like morphology at 150 ^{0}C, and the particles were well defined.

Kallai et al. [104] showed the SEM for samples were formed from the reaction of kaolinite and metakaolinite with NaOH, the untreated kaolinite sample showed undefined aggregates with lower Na content, and treated kaolinite sample showed well developed cubes related to zeolite A.

`

Rios et al. [106] studied the synthesis of zeolites by hydrothermal transformation of kaolinite, kaolinite sample showed platy morphology and hexagonal outlines, while zeolitic materal that obtained after hydrothermal reaction showed a mainly lephispheric morphology.

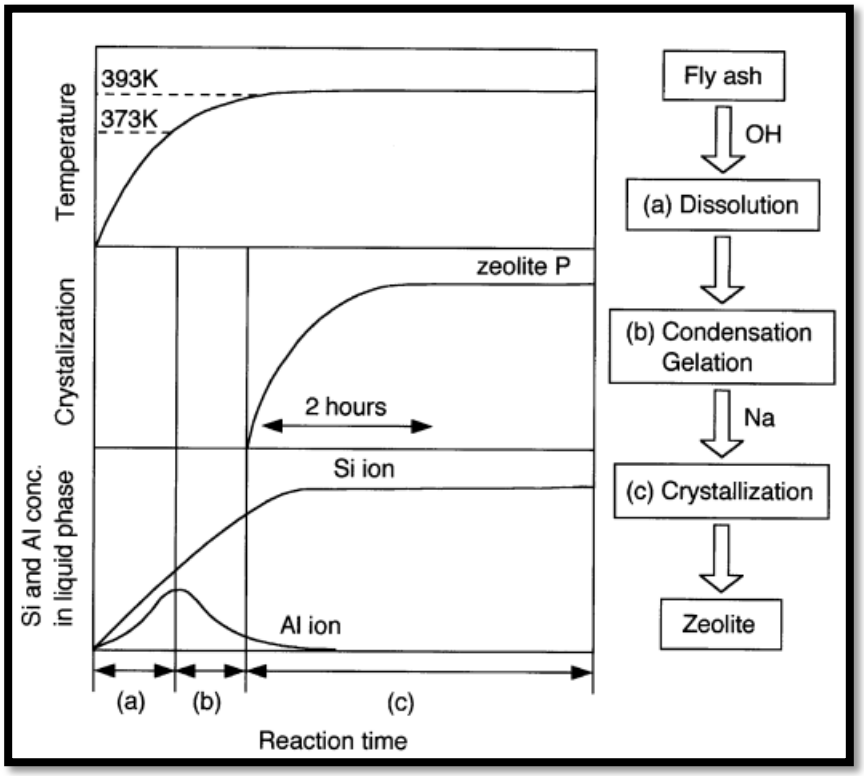

Figure 8 Reaction mechanism for zeolite synthesis from coal fly ash [88].

`

CHAPTER 3

EXPERIMENTAL DESCRIPTION

The Fixed bed absorber is the main tool that is used to assess the CO_2 from natural gas capturing using regenerable Kaolin – based sorbents. This chapter describes the fixed bed absorber, experimental procedures and techniques that are used in this research study, and the properties and synthesis of the Kaolin – based sorbent materials. More than one technique was used to characterize the sorbent materials; Fourier transform infrared (FTIR) spectroscopy, Scanning electron microscopy (SEM), X-Ray diffraction (XRD), Energy dispersive X-ray analysis (EDX), and Brunauer, Emmett, and Teller Surface area test (BET). This chapter also discusses some calculations that were used to support the conclusions.

3.1 Materials

The raw materials used for synthesis of CO_2 adsorbent are Kaolinite and limestone. They were supplied from Riyadh area- Saudi Arabia. Carbon dioxide and nitrogen gas cylinders were supplied by Saudi gas industries. The purity of CO_2 was 99.99% of CO_2 with 20 ppm of moisture.

3.2 Methods

The adsorbent material was synthesized using chemical and thermal treatment of kaolin clay, and limestone. Firstly, the raw limestone and natural kaolin were pulverized and screened to get powdered materials.

`

After that, a solid mixture of powder limestone and kaolin was dissolved in NaOH solution, and agitated isothermally (22 ^{o}C) for 90 min. The mixture was placed in 500 ml closed vessel and kept under isothermal and isobaric conditions at different temperature and pressure values for 6 h, and then cooled to room temperature. The mixture was then calcinated in a muffle furnace at 550 ^{o}C for 5 hours. The calcinated material was screened to get different size distribution of the produced adsorbent and stored in caped flasks for further uses. The synthesis parameters such as kaolin/limestone (K/L) mass ratio, NaOH concentration, solution temperature, and reaction pressure were varied according to full statistical analysis design of experiment as shown in table 2.

Table 2 Statistical analysis design of the experiment.

Variations	Lower limit	Upper limit
Kaolinite/Limestone (g/g)	0	3
[NaOH] (g/100 ml)	0	36
T (^{o}C)	25	225
P (bar)	0	15

`

Figure 9 The autoclave.

3.3 Characterization

3.3.1 Fourier transform infrared spectroscopy (FTIR)

The Fourier transform infrared spectroscopy (FTIR) is used to identify functional groups on the surface of particles. The infrared spectra of the sample were recorded using FPC FTIR Perkin-Elmer spectrophotometer. A mass of 1.5 mg of the sample was mixed with 1 g of KBr powder and pressed hydraulically to obtain the transparent disk. The disk was then dried in an oven for 2h at 110 ^{o}C to remove any water vapor. Transmission mode was applied to take the FTIR spectra.

The IR spectrum signifies an identity verification of sample with peaks that represent the vibrations frequencies between the bonds of the atoms in the material.

`

It provides information about the qualitative analysis and quantitative analysis of materials present based on the size of the spectrum peaks.

3.3.2 X-ray diffraction spectroscopy (XRD)

The phase identification and crystallinity of the adsorbent was determined using X-ray diffractometer. The diffraction patterns (XRD) were collected using D/tex Ultra powder diffractometer using Ni-filtered Cu K α radiation source at 40 mA and 40 mV for 1 hour to record the 2 theta diffraction from 0^o to 80^o , the identification of the phase present was done using high score plus software. XRD experiment was done by mounting the sample on the sample holder and it was flushed with the surface of the holder, then the desired slit width (1mm) was loaded with the beveled edge down.

3.3.3 Scanning electron microscope (SEM)

The scanning electron microscope was used to determine the morphology and qualities characteristic of the adsorbent sample using JEOL, model JSM 6400. Adsorbent sample was coated with carbon to make it a conductive surface and fixed with double side masking type. The sample was viewed on FE-SEM to get information about the surface topography of the sample.

3.3.4 Energy dispersive X-ray analysis (EDX)

The energy dispersive X-ray (EDX) was used to determine the chemical composition of the synthesized adsorbent material using OXFORD instrument. The sample was placed in the holder in the way where the flat edge of the mount was against the flat area of the stage. The data was obtained using INGA software. EDX is a fast, non-destructive analysis and it can be used for a range of elements.

`

3.3.5 Brunauer-Emmett-Teller (BET) technique

The Brunauer-Emmett-Teller (BET) technique is used to calculate the specific surface area, micropores area and micropores volume distribution. Liquid nitrogen adsorption was conducted at 77 K using micrometric 2020 to obtain the adsorption isotherm of the sample. A sample of 0.3 g was pulverized and dried very well at 150 ^{o}C and then degassed for 6h under vacuum.

3.4 Adsorption and desorption studies

The setup for adsorption/desorption experiment is shown in Figure (10). It is composed of adsorption column made from a jacketed glass (20 cm, 1 cm ID, and 1.2 cm OD). The column was filled with 10 g of sorbents and glycerol/water solution was circulated to maintain the isothermal conditions. Pure N_2 was mixed with pure CO_2 at different volume ratios and introduced into the column. The flow rates of gas mixture were controlled using two mass flow controllers (Matheson, model 8200). The effluent gas stream was monitored continuously using a gas detector. In a typical run, N_2 was initially introduced to the column to free the surface of the adsorbent material, and then CO_2/N_2 gas mixture was allowed to pass over saturated water at 60 ^{0}C to gain the desired humidity. Then the gas mixture was introduced to the column. The experiments were repeated for different flow rates, CO_2 concentration, temperatures, and humidity values. The desorption experiments were repeated in similar manner but only N_2 gas was introduced instead of CO_2/N_2 mixture.

`

The breakthrough curve is a vital factor that represents the working capacity. The CO_2 adsorption capacity (mmol CO_2/g sorbent) was determined by integrating the area above the CO_2 breakthrough curve. The adsorption capacity values were calculated using this relation:

$$q = \frac{FC_0t_q}{m}$$

Where C_0 is the feed concentration of CO_2 (mg/l), m is the mass of treated kaolin adsorbent loaded in the column (g), and t_q is the stoichiometric time that is calculated from the breakthrough data (min) according to this equation [73]:

$$t_q = \int_0^{\infty} \left(1 - \frac{C(t)}{C_o}\right) dt$$

Where C(t) and C_0 are the concentration of CO_2 at the outlet and inlet of the column respectively.

Also the adsorption capacity for the produced samples was measured using Rubotherm's high pressure TGA. Pure CO_2 gas is allowed to be introduced at room temperature and the weight of the adsorbent was recorded at different dosing pressure.

`

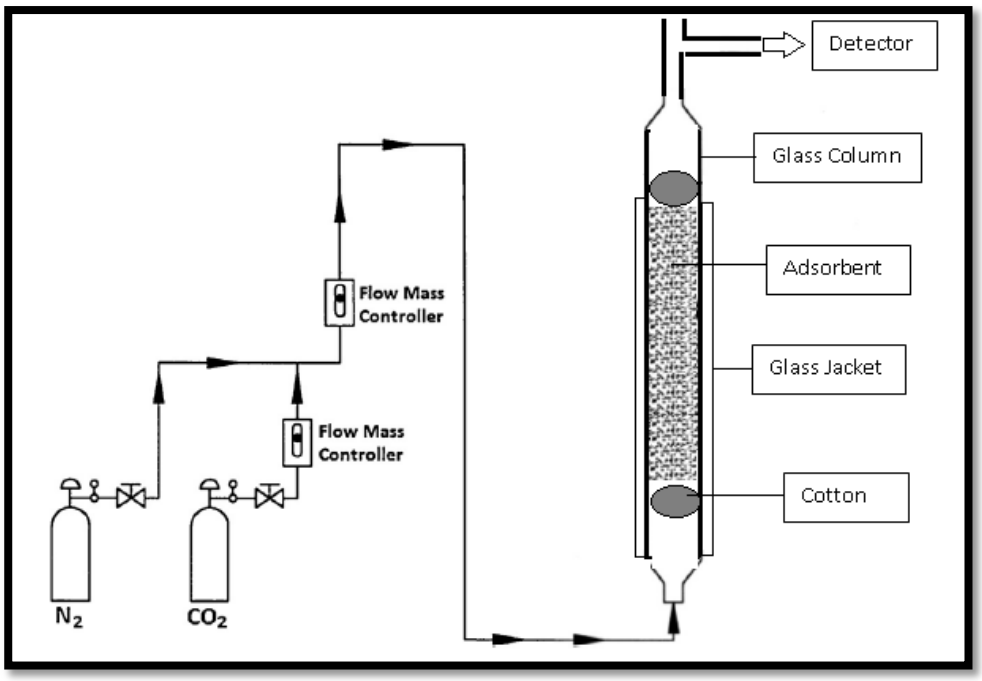

Figure 10 experiment setup.

`

CHAPTER 4

RESUTLS AND DISCUSSION

4.1 Synthesis of product adsorbent

The product adsorbent that has general structure of Ca-Na-SiO_2-Al_2O_2 was obtained by treating mixtures of minerals by heating and calcination. Synthesis methodology is focused on so called "hydrothermal synthesis" or "activation" in closed system for solutions of NaOH. This process is related to the synthesis of materials that have characteristic 3D framework with sequences of tetrahedron XO_4, where X is silicon, aluminum, etc. Sodium hydroxide as a high alkaline solvent is incorporated into source material rich in Al_2O_3 and SiO_2 as source of the sodium. Kaolin is a convenient clay mineral that was used as a precursor to the product adsorbent composition as it is the source of aluminum and silicon for alkali reaction. Although variations in chemical composition of kaolin are exists, it has an idealized chemical composition of $Al_2Si_2O_5$. Parameters, such as reaction temperature, NaOH concentration, reaction pressure, and reaction time which are important parameters affecting the behavior of the adsorption process. Samples of kaolin and limestone were mixed at different mass fractions with NaOH (2-36 M). Limestone ($CaCO_3$) is the source of the calcium in the product adsorbent. The Al and Ca in the kaolin were dissolved by OH^- in the alkali solution. Then aluminosilicate gel was formed with calcium oxide, after that, the gel was crystallized to form Calcium-Sodium-Aluminum-silicon oxides as big flake.

`

4.2 Characterization

4 .2.1 X-ray diffraction analysis (XRD)

XRD analysis is used to determine the phases and crystallinity of both raw kaolin and limestone and the synthesized material. Figure 11 shows XRD spectrum for raw Kaolin sample; there are two phases, one is Kaolinite $Al_2(Si_2O_5)(OH)_4$ (83.5 w.t %) and the other is Anatase TiO_2 (16.5 w.t %). Gougazeh et al [92] showed that the XRD pattern of the natural Jordanian kaolin contains 72 w.t% kaolinite (appeared at 12.34° and 24.64° 2θ), 27 w.t% quartz, and 1 w.t% other component. Figure 12 shows the main phases in raw limestone sample which are Calcite $CaCO_3$ (34.4 w.t %) and Quartz SiO_2 (66 w.t %). Ghorab et al. [93] also showed that the XRD pattern of limestone contains mainly two phase; Calcite and quartz.

Figure 13 Shows XRD patterns of the synthesized adsorbent, it is obvious that the main two phases are Gehlenite (Ca_2 Al ($Al_{1.22}$ $Si_{0.78}$ $O_{6.78}$) (O H)$_{0.22}$) appeared at 4, 10,7,8,14, and 17 2Ɵ peaks , with 43% weight ratio. And the other main phase is Stilbite ($Na_{5.76}$ $Ca_{4.96}$ ($Al_{5.68}$ $Si_{56.32}$ O_{144}) (H_2O)$_{48.88}$) with 57% weight ratio. There are very small amounts of calcite ($CaCO_3$) and quartz (SiO2) (11, 12, 15, 16 peaks). Hence after the chemical and thermal treatment of Kaolin using limestone and NaOH new phases are introduced in the structure of the raw adsorbent which contains Ca-Al-Si-Na oxide. X-ray diffraction was confirmed the new phases that were formed after treating.

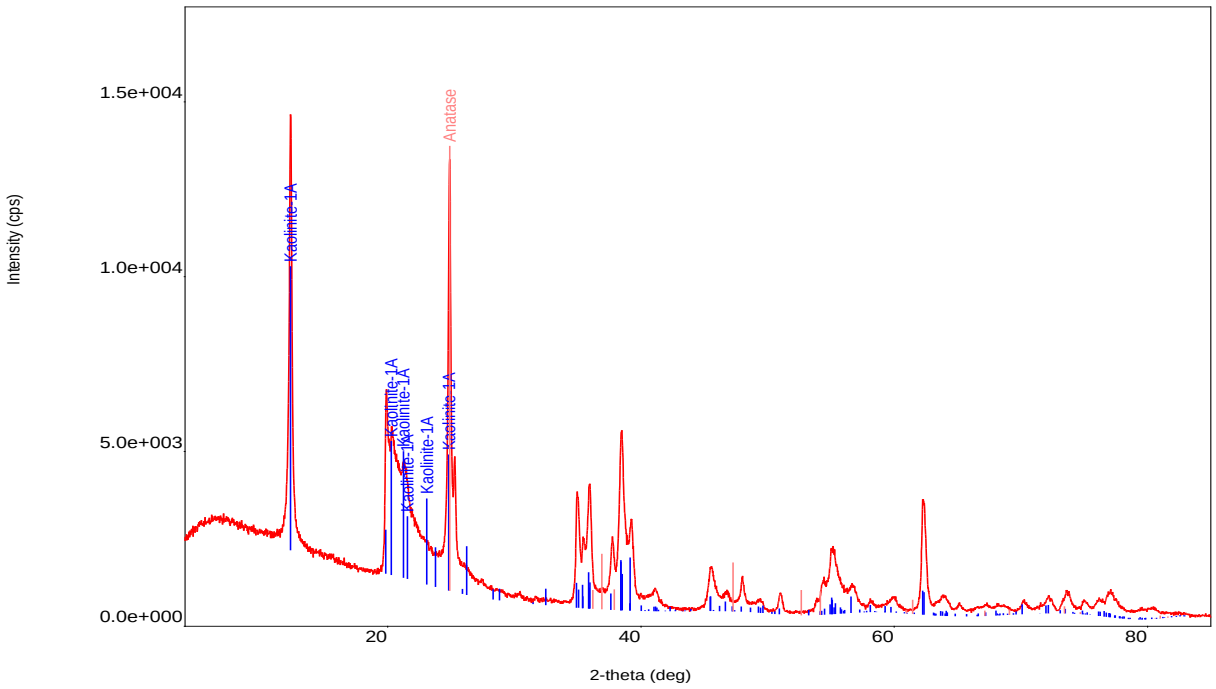

Figure 11 XRD spectrum for Kaolin.

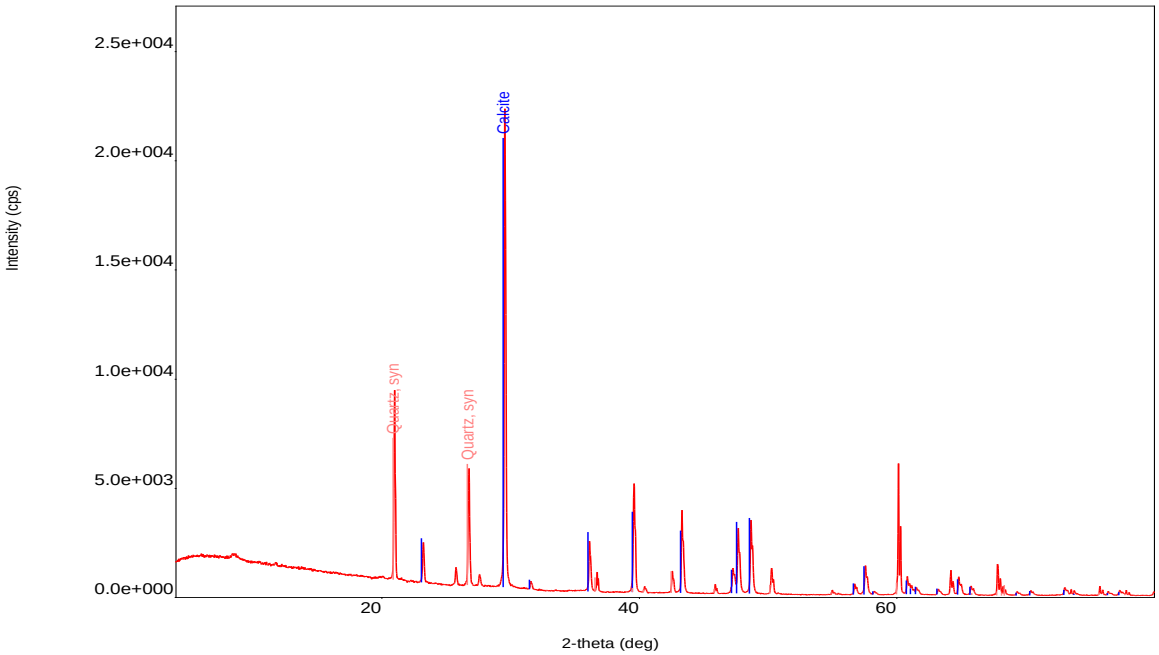

Figure 12 XRD spectrum for limestone.

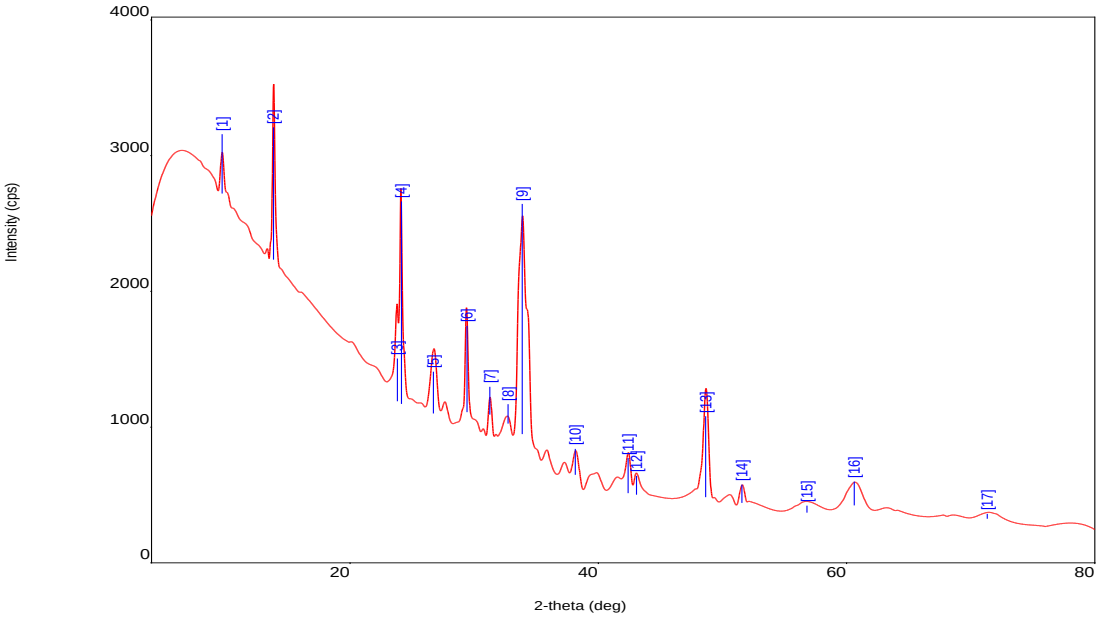

Figure 13 XRD spectrum for synthesized adsorbent.

`

4.2.2 Energy dispersive X-ray (EDX) analysis

Table 3 shows the elemental analysis of the Ca-Al-Si oxides adsorbent material and raw kaolin material. The produced material is composed of Ca, Al, Si, Na, C and O. While kaolin material is composed mainly of Al, Si, Ti, there are small traces of Ca and Fe. Based on the chemical composition analysis; the raw kaolin did not show the characteristic signal of Ca and Na, whereas for treated kaolin, clear signals of the presence of Ca and Na were observed. Accordingly, we can conclude that Ca and Na are inserted in the structure of Kaolin forming new crystalline phase material. Several researchers proved that Na is inserted in the structure after reaction [88-91]. The weight percent of Al in the structure decreased during hydrothermal reaction because of the dissolving of aluminate ions [88].

Table 3 Elemental analysis (Weight% (atomic %)) of synthesized adsorbent and raw kaolin by EDX.

Element	Produced adsorbent	kaolin
C	23.57 (33.94)	-
Al	3.26 (2.09)	15.86 (11.36)
Si	19.91(12.26)	15.36 (10.57)
Ca	2.91(1.25)	0.45 (0.34)
Na	12.07 (9.08)	-
O	38.28 (41.38)	38.28 (75.44)
Ti	-	5.33 (2.15)
Fe	-	0.84 (0.29)

`

4.2.3 Brunauer-Emmett-Teller (BET) technique

Table 4 shows the textural properties of the kaolin adsorbent before and after treatment; also it presents comparison between the surface properties of the raw materials and produced adsorbent after different duration of usage. The nitrogen adsorption/desorption of kaolin materials at 77 K was used to evaluate surface areas and pore diameters. The average pore widths were determined using BET method, and the surface areas were determined using BET and t-plot. The specific surface area was evaluated in the range of 0.05 -0.2 of the relative pressure. The nitrogen molecule cross-sectional area was 0.162 nm^2 [57]. The BET analysis showed that the produced adsorbent has better surface area (1.96 m^2/g) than the raw materials and adsorption cumulative micropores surface area (5.831 m^2/g) compared with raw Kaolin (0.8043, 4.518 m^2/g respectively) and raw limestone (0.8161, 3.468 m^2/g respectively). There was no significant decrease in the BET surface area between the fresh produced adsorbent and the used one, as after regeneration new phases were formed.

Figure 14, 15, 16 shows the nitrogen adsorption – desorption isotherm for raw kaolin, produced adsorbent and limestone. The International Union of Pure and Applied Chemistry (IUPAC) published classification of adsorption isotherm in 1985 [58], which reflects the adsorption potential and pore size as planar nonporous surface, mesopores, or micropores. However, the macropores are wide so they can be considered as flat surfaces, and micropores adsorption behavior is dominated by the interaction between fluid molecules and the pore walls., while the adsorption behavior in mesopores depend on the attractive interaction between fluid and the pore wall and between fluid molecules.

`

Pore condensation happens when the pressure is less than the saturation pressure of the bulk liquid where the gas condenses in pores to a liquid like phase. The IUPAC classification is shown in figure 17. Type 1 isotherms are found when the adsorption to only few layers, this condition is encountered in physical adsorption on microporous materials. Type II isotherms are found in case of macroporous or nonporous where multilayer adsorption can occur and the inflection point of isotherm indicates the completion of monolayer and beginning of multilayer adsorption. Type III isotherms indicate that the adsorbate – adsorbent interaction is relatively weak. Type IV isotherms are typical for mesoporous materials, and the hysteresis loop is an important characteristic feature which is related to pore condensation. The initial part of the isotherm as type III related to weak adsorbate interaction. The plateau of isotherm at the high range of P/P0 indicates complete pore filling, and the initial part of isotherm related to monolayer – multilayer adsorption. Type V also shows hysteresis and pore condensation. Type VI isotherms are obtained for non-porous surfaces and stepwise multilayer adsorption. The produced adsorbent isotherm belongs to type V isotherm according to IUPAC classification. It indicates that the treated adsorbent sample is almost mesoporous ($2 < d < 50$ nm). The narrow and uniform pore size distribution is proved by the overlapping of the adsorption/desorption curves.

The specific surface of kaolinite depends on the source of kaolin. Several researchers have investigated the specific surface area of kaolin and modified kaolin. Chen et al. [97] showed that the specific surface area, pore diameter, and pore volume for unmodified kaolinite are 74.3 m^2/g, 15.3 nm, and 0.305 cm^3/g. And in the case of amine-modified kaolinite are 8.9 m^2/g, 22.3 nm, and 0.05 cm^3/g. They observed that the reduction in the

`

textural properties is because of the blocking of the surface pore of kaolinite by amine molecules. Castellano et al. [98] investigated that the specific surface area of kaolinite is 10 to m^2/g. All limestones have low surface area. Alton [99] showed that the specific surface area of limestone is 1.66–1.95 m^2/g. The specific surface area of crystalline Gehlenite was 5 m^2/g [100].

Table 4 Textural properties of kaolin adsorbent materials.

Compounds	t-plot External surface area (m^2/g)	BET surface area (m^2/g)	t-plot micropore volume (cm^3/g)	Adsorption average pore width (4v/A by BET) A^0
limestone	2.04	0.816	0.000295	765.9
Raw kaolin	4.00	0.804	0.000187	861.6
Treated kaolin (fresh)	4.05	1.96	0.000415	879.4
Treated used one	6.23	1.95	0.000302	689.3
Treated used once (after regeneration)	3.01	0.902	0.000428	759.4
Treated used 5 times (after regeneration)	0.873	0.742	0.000435	1446.0

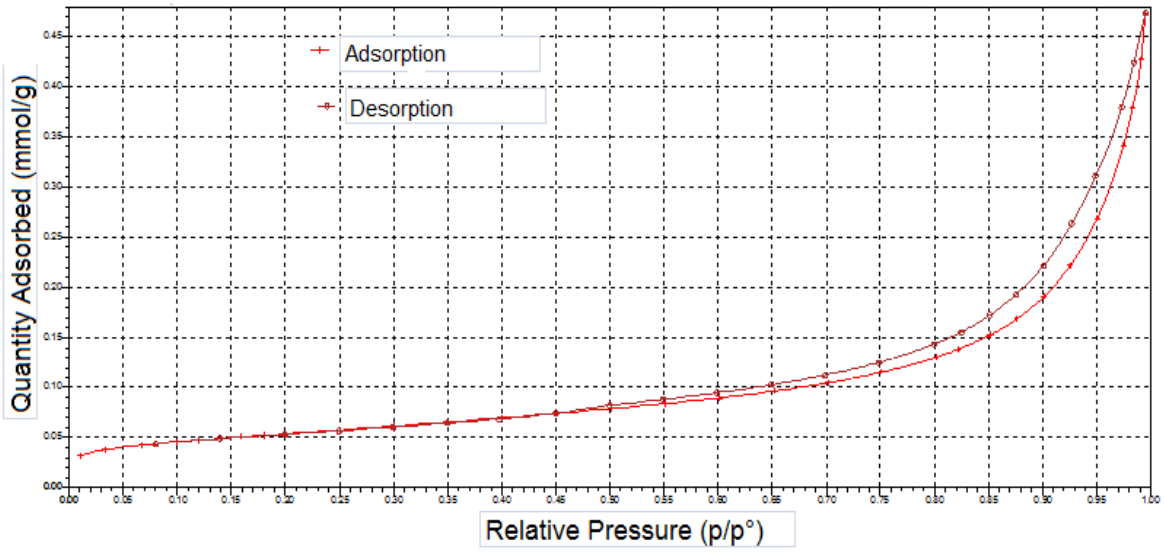

Figure 14 N_2 adsorption/desorption isotherm for raw kaolin.

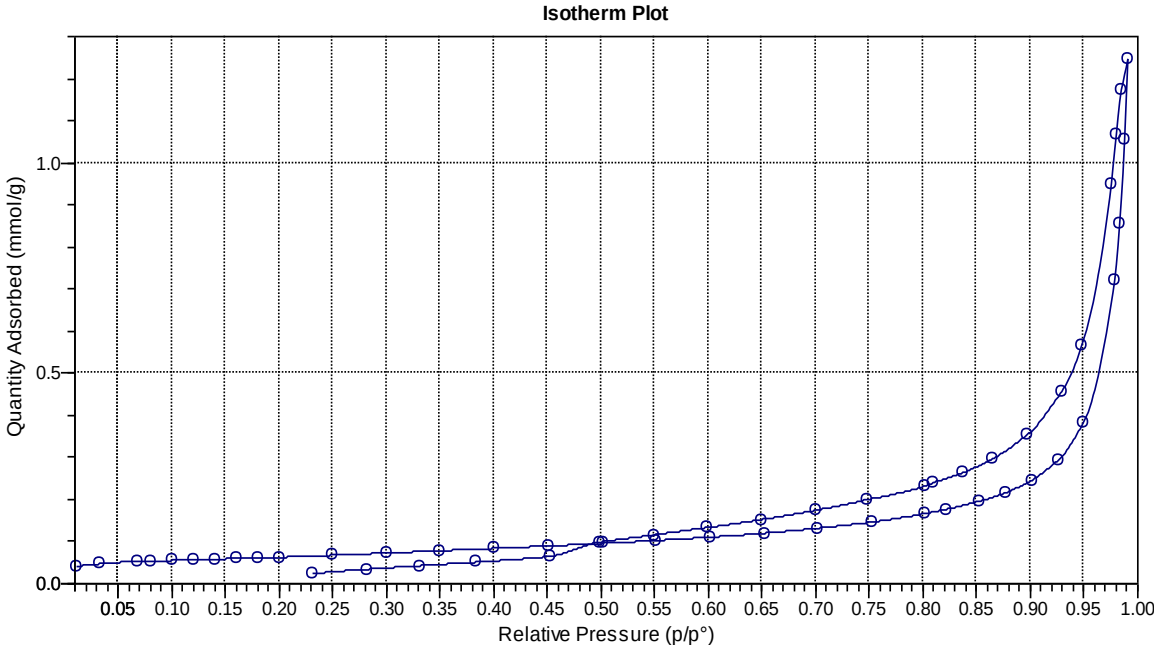

Figure 15 N_2 adsorption/desorption isotherm for treated kaolin.

`

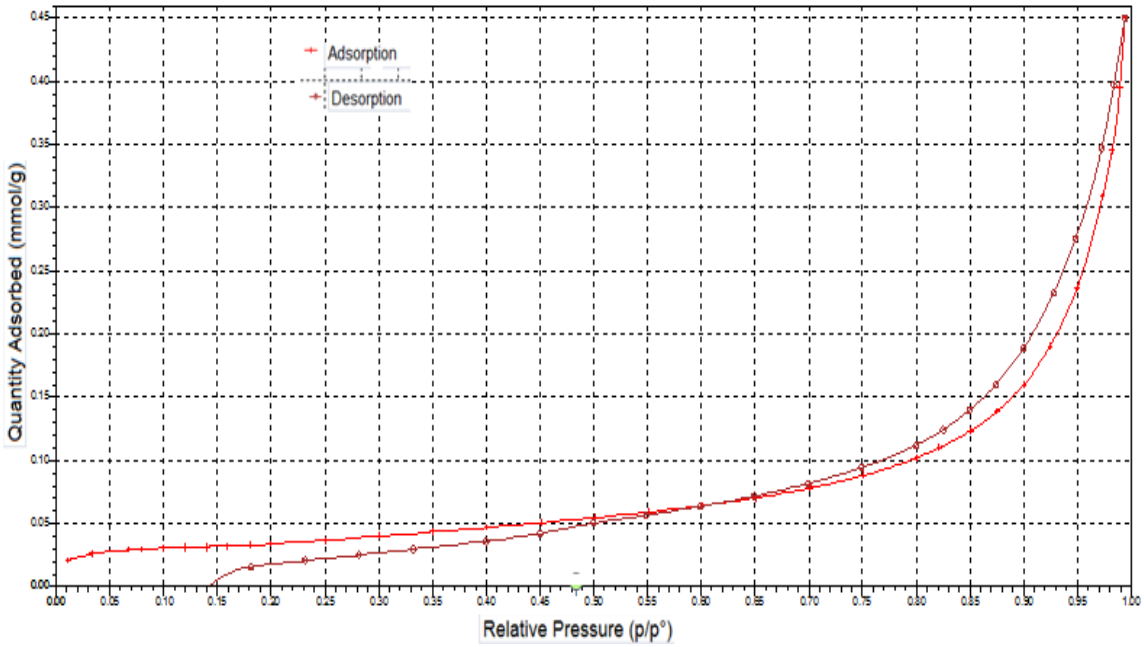

Figure 16 N2 adsorption/desorption isotherm for limestone.

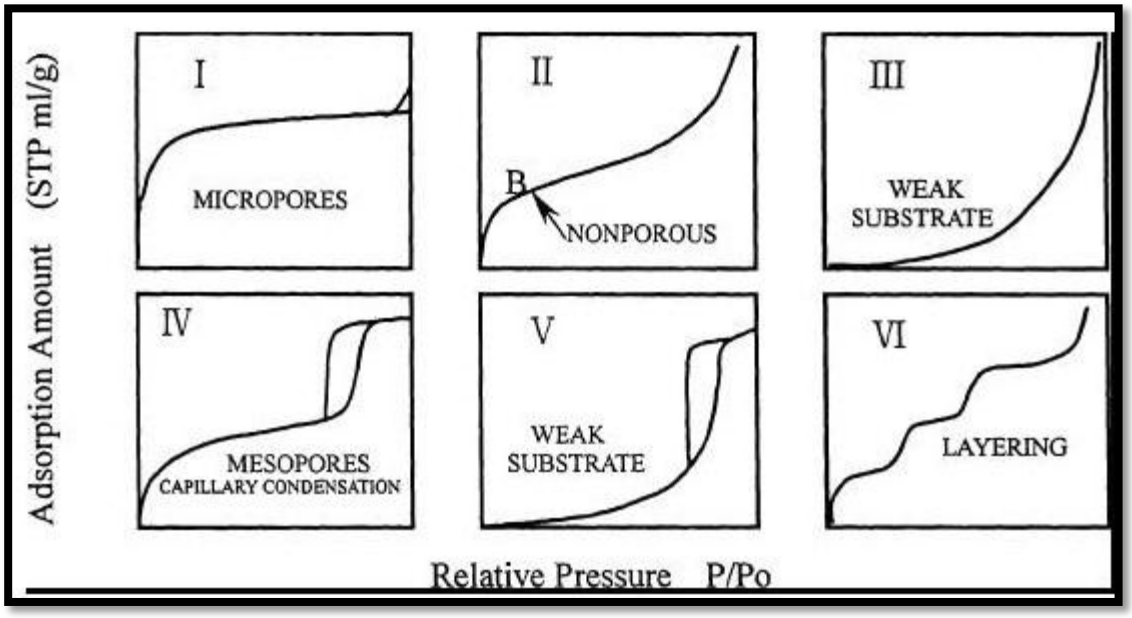

Figure 17 IUPAC classification for adsorption isotherm [59].

`

4.2.4 Pore Size Distribution

Pore size distribution and macroporosity are usually determined by mercury porosimetry. The results are commonly displayed either as dV_p/dr against pore radius r, or as a cumulative distribution V_p against r. Nitrogen adsorption method can also be used to determine pore size distribution; however, in some cases the use of this method is not possible for small pores that have molecular sieving abilities. When the adsorption of nitrogen is carried out at 77.34 K, both capillary condensation in the pores and adsorption of nitrogen in the surface take place. The size of the pore r_k, where the condensation occurs and the thickness of adsorbed layer t, depend on the nitrogen partial pressure. By assuming appropriate relation between r_k, t and partial pressure P, the adsorption isotherm can be converted to pore size distribution. When change of pore size distribution is involved, cumulative pore size distribution is preferred.

The distribution of pore sizes can be classified into micropores, mesopores, and macropores according to the classification of Dubinin [60]. Table 5 shows these classifications. Figure 18 shows the mean pore diameter varies from 473.8 A^0 for treated kaolin to 481.7 A^0 for raw kaolin, thus the treated kaolin is mesoporous. The shape of pore size distribution was bimodal. It can also be observed that the permeability of the produced adsorbent was better than that of raw kaolin, larger permeability value, and better filtration properties of material. The narrow particle size distribution maintains the void spaces between the particles. The maximum pore volume of produced adsorbent is much larger than that of raw kaolin.

`

Table 5 IUPAC classification of pore sizes [60].

Type	Pore Size (A^0)
Macropore	≥ 500
Mesopore	20 to 500
Supermicropore	7 to 20
Ultramicropore	≤ 7

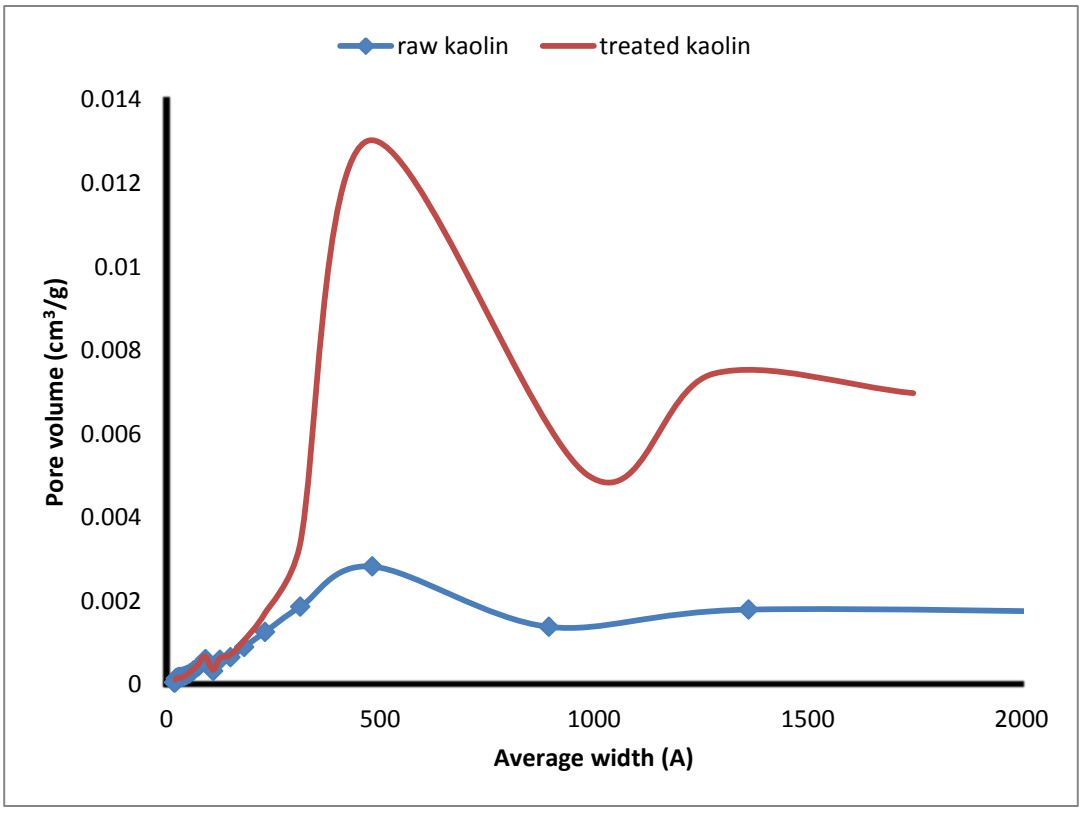

Figure 18 pore size distribution for kaolin material.

`

4.2.5 N_2 adsorption/ desorption isotherm analysis

The N_2 adsorption – desorption isotherm is used to calculate the surface area and pore diameter. There are several methods that can be used such as BET model, which is an extension from monolayer molecules adsorption to multilayer [62]. The linear form of BET isotherm is:

$$\frac{1}{\mathrm{Q}\left(\frac{P_o}{\mathrm{P}}-1\right)}=\frac{1}{V_m\,\mathrm{C}}+\frac{\left(\frac{\mathrm{P}}{P_o}\right)(\mathrm{C}-1)}{V_m\,\mathrm{C}}$$

Where Q is the adsorbed volume at equilibrium (cm^3/g), P is equilibrium pressure (MPa), P_o is saturated vapor pressure (MPa), V_m is adsorbed volume in a monolayer, at STP, and C is the BET constant. After obtaining the V_m, the specific surface area S_{BET} (m^2/g) was obtained using this formula:

$$\mathrm{S}=\frac{N_A\ \mathrm{a}\ V_m 10^{-20}}{\mathrm{m}\ V_M}=\ 4.35\ \mathrm{Vm}*10^6\ (\frac{m^2}{\mathrm{g}})$$

Where N_A is Avogadro's number, m is mass of adsorbate sample (g), and V_M is molar volume (22.414 cm3/ mol at STP), a is cross section of adsorbate (0.16 nm^2). Figure 19 shows the BET surface area plot for fresh treated Kaolin.

`

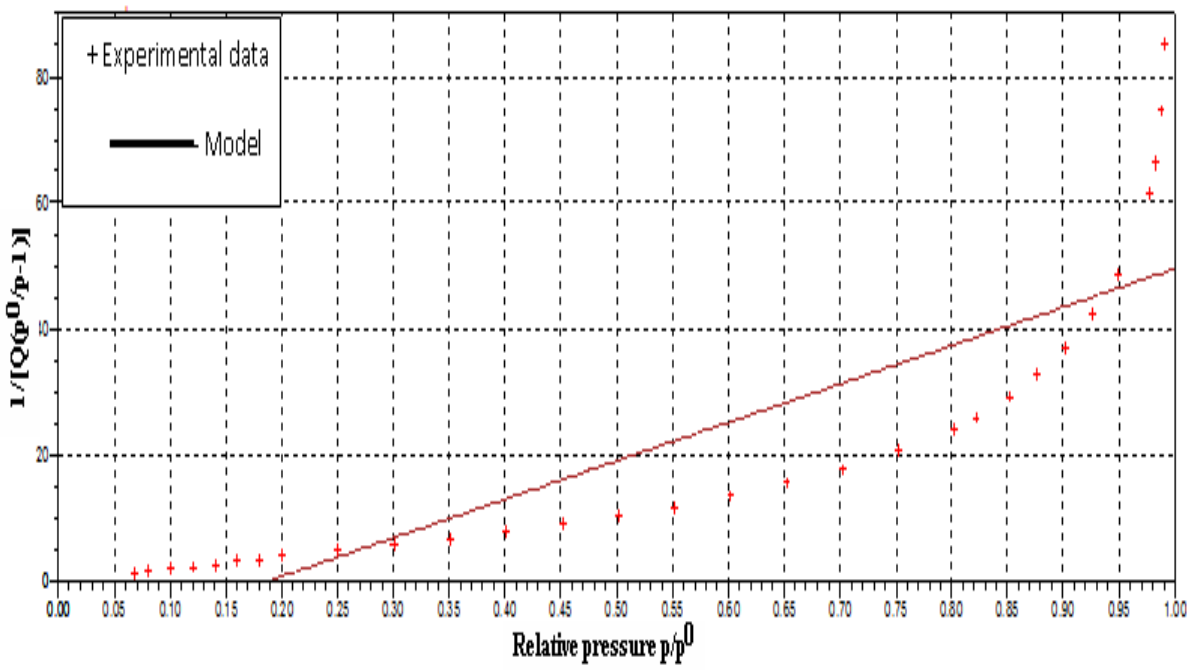

Figure 19 BET surface area linear plot fro trated kaolin.

It is obvious from the above figure 19 that the BET model is applicable for a range of $0.05< P/P^0 <0.35$. The surface area can be also obtained from the t-plot model by plotting the quantity adsorbed (Q) as a function of layer thickness (t) at different values of P/P^0 as shown in figure 20. The thickness of the adsorbed layer as a function of reduced pressure is called t-plot of flat surface. The plot of the amount adsorbed against thickness is a straight line. The amount adsorbed can be either decreased of increased for the porous solid, if it decreases, then it indicates the presence of slit shape pores ($t_{slit}<t_{flat}$). On the other hand, if it increases, this indicates cylindrical pores ($t_{cyl}>t_{flat}$). This method can be analyzed by obtaining data of amount adsorbed versus (P/P_0), and for each value of (P/P_0), the thickness t can be obtained from the t-plot. Finally, the amount adsorbed versus thickness can be plotted.

`

The t-plot equation is:

$$Q\left(\frac{\mathrm{P}}{P_o}\right) = Q(micro) + k\,S_{\mathrm{ex}}\,t\left(\frac{\mathrm{P}}{P_o}\right)$$

Where k is the equilibrium constant of adsorption. The model separates the micropores from external surface (mesopores, macropores, and outside surface) by the above equation. From the slope and intercept, the external and micropore surface areas were obtained. The layer thickness in the above equation can be replaced by Harkins and Jura [63] equation:

$$t = \left(\frac{13.99}{0.034 - log(\frac{\mathrm{p}}{\mathrm{p}}°)}\right)^{0.5}$$

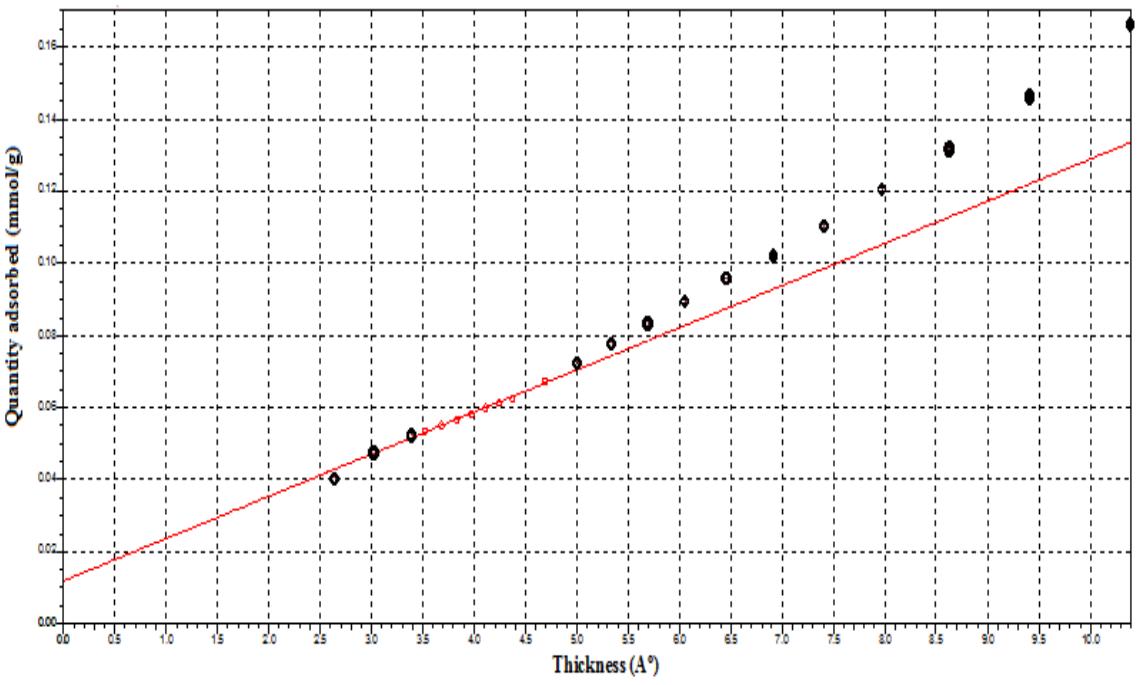

Figure 20 Hakins and Jura t-plot of treated kaolin.

`

Table 6 summarized the parameters for two models, which leads to the conclusion that the surface area from t-plot model is more accurate for treated kaolin sample.

Table 6 BET and t-plot modelsurface area.

Model	Slope	Y-intercept	Surface area (m^2/g)	Correlation coefficient
Hakins and Jura t-plot	0.0116	0.0119	4.05	0.999
BET	60.9	-11.28	1.96	0.858

4.2.6 Barrett–Joyner–Halenda (BJH) adsorption

The Berrett Joyner Halenda (BJH) method was initially proposed for coarse porous adsorbent with wide range of pore sizes [101]. Later on, the applicability of the method was proved for all types of porous materials. BJH method is useful to obtain the pore volume and total surface area by analyzing the adsorption and desorption divisions of the nitrogen isotherm. BJH method calculations cylindrical pores [102].

Figure 21 shows the difference between the pore volume and the pore width for raw kaolin and limestone and treated kaolin (fresh and after using five time and regeneration). It can be noticed that fresh treated kaolin has a higher value of total pore volume and wider pores. Also it has a monomodel of pore size distribution.

`

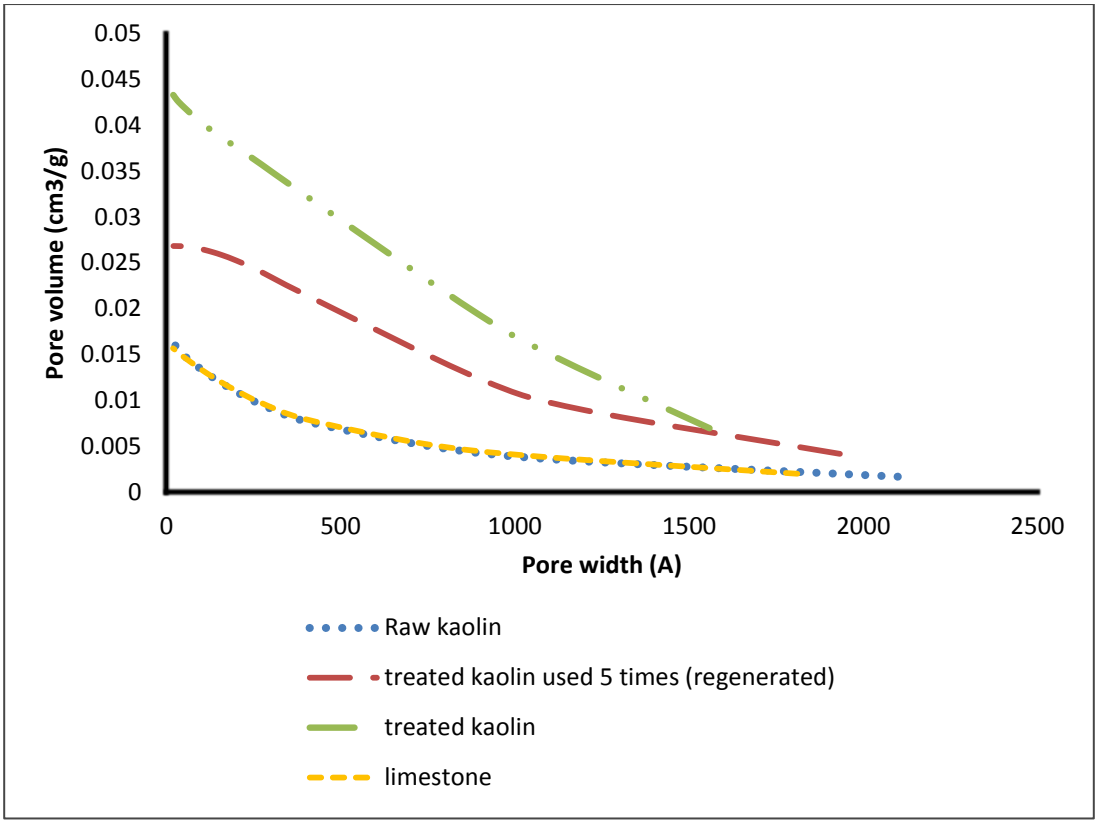

Figure 21 BJH adsorption comulative pore volume for kaolin adsorbent and limestone.

4.2.7 Scanning Electron Microscopy (SEM)

The qualitative and morphological characteristics of produced adsorbent were examined using SEM technique. Fig 22 (a) – (d) shows the SEM micrographs of treated Kaolinite. White particles can be seen in the structure surface, which are Ca particles that were inserted during chemical treatment with limestone. The produced sample is composed of agglomerates. Murat et al. [105] studied the synthesis of zeolite from thermally activated kaolinite. They showed that zeolite crystals appear in the form of large agglomerates, and the agglomeration may start before crystallization of zeolite. The surface morphologically of samples was not uniform, showing noticeable pores.

`

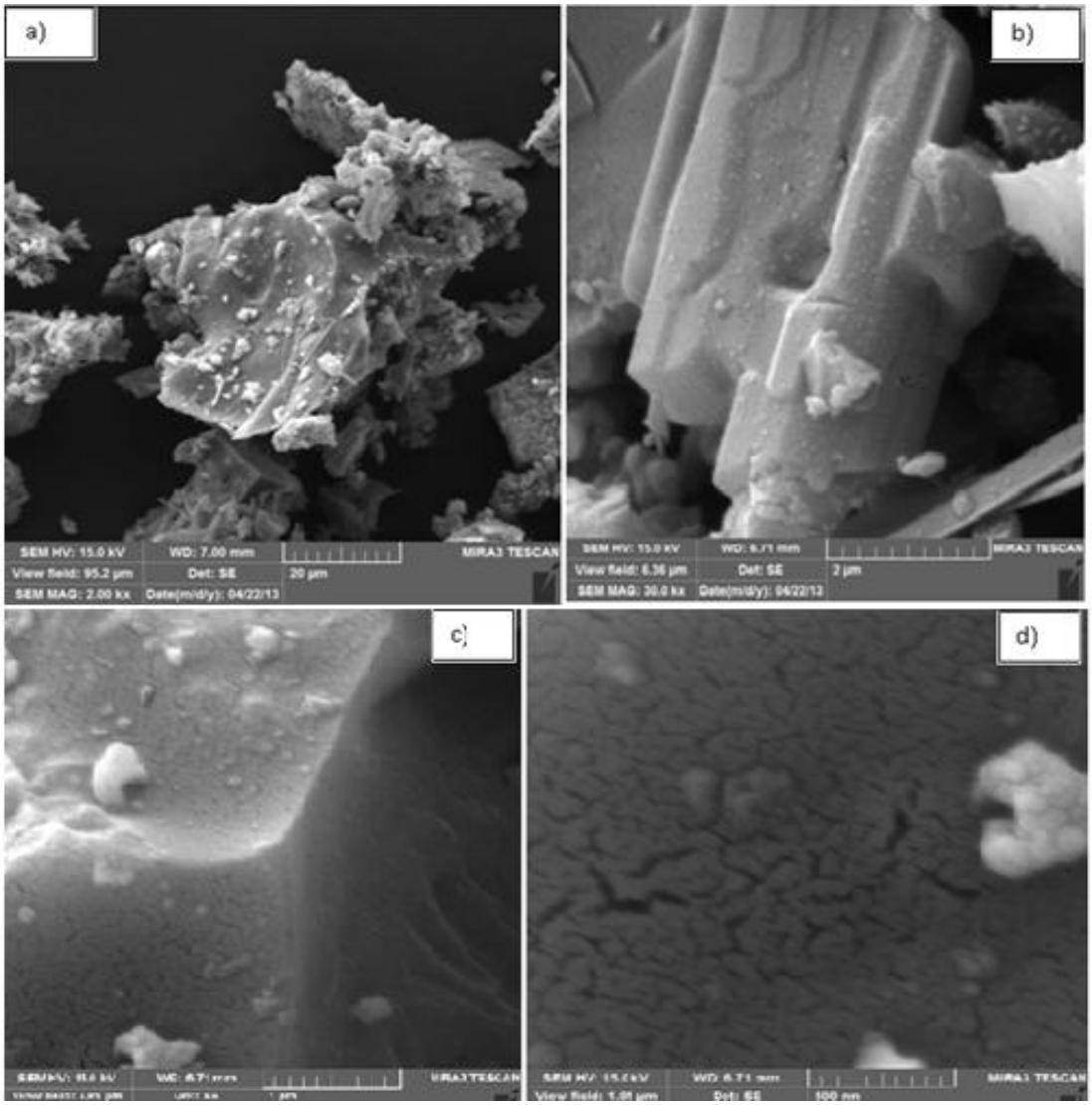

Figure 22 SEM micrograph (a) 2kx magnification (b) 30kx magnification (c) 50kx magnification (d) 100kx magnification.

`

4.2.8 Fourier transform infrared spectroscopy (FTIR)

The change in the surface chemistry of adsorbent samples after treatment was studied using FTIR spectroscopy. Figure 23 shows the FTIR spectra for both treated and raw kaolin. In the kaolin sample, a peak of 3696 cm-1 which is related to OH stretching of inner surface hydroxyl groups disappeared during treatment. The characteristic absorbance peak at 3622 cm-1 which is assigned to OH stretching of inner hydroxyl groups, also vanished during treatment. However, peaks at 3420 and 2967 cm-1 appeared in the treated sample. These peaks are related to hydroxyl acid functional groups. Another minor peak appeared for treated sample at 831 cm-1 which is related to OH or OCH3 group. The peak at 2364 cm-1 was clearly observed for treated kaolin due to NH+=N+H or CO_2. In addition, four major peaks were observed at 1640, 1562, 1467, 1207 cm-1, which are related to –NH2, =NH, N-N=O, and N+-O- respectively. In raw kaolin sample, a peak of 1118 cm-1 is assigned to Si-O stretching (longitudinal mode) and peak of 1039 cm-1 related to in-plane Si-O stretching, shifted to 1041 cm-1 for treated sample. However, a new peak of 935 cm-1 appeared in the treated sample, which corresponds to the OH deformation of inner surface hydroxyl groups. The absorption bands observed at 758, 699, 547 cm-1 for raw kaolin could be assigned to Si-O (perpendicular), Si-O, and Al-O-Si; these bands disappeared in the treated sample. Gougazeh et al. [93] showed that the band ranged from 690 cm^{-1} to 925 cm^{-1} assigned to Al-O, and did not appear in the zeolite product. Peaks at 662, 693, 718 cm^{-1} assigned to T-O-T vibrations (T=Al or Si).

`

Alkan et al. [110] showed that the band at 3696 cm^{-1} assigned to the inner surface O-H group, the peak at 3622 cm^{-1} is related to inner hydroxyl group, and the peak at 1115 cm^{-1} corresponds to Si-O stretching, peak at 755 assigned to Si-O-Si

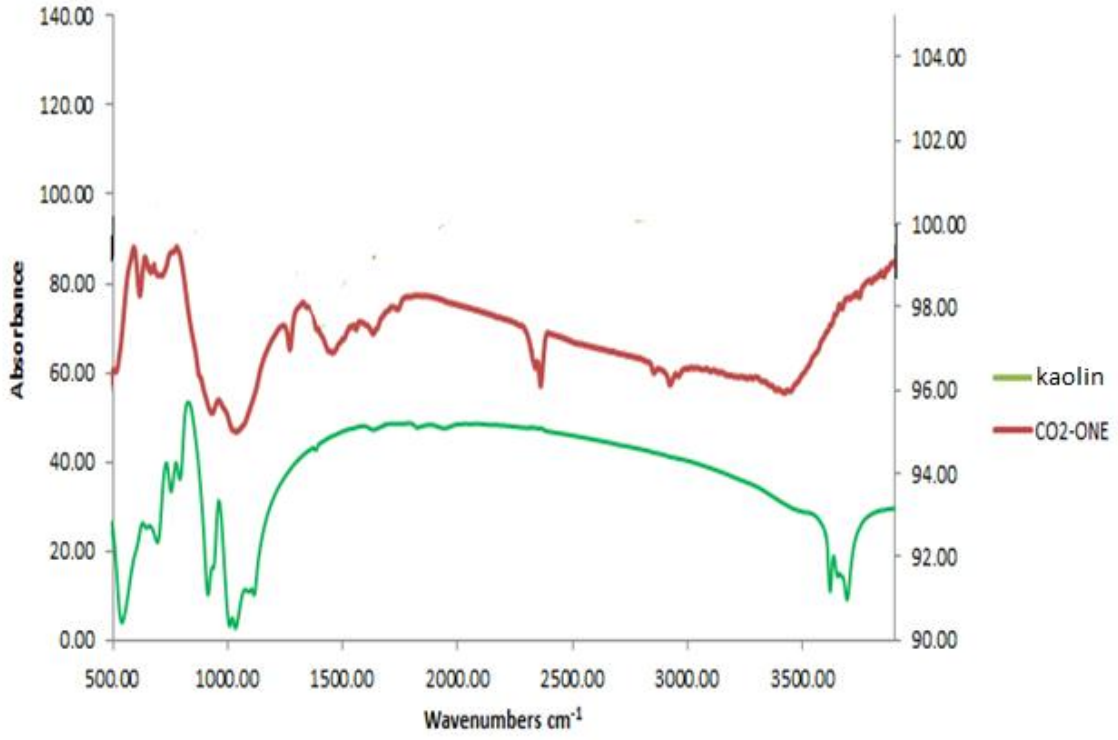

Figure 23 FTIR spectra for treated and untreated Kaolin.

4.3 Breakthrough profiles

The treated kaolin adsorbent which is a mixture of aluminosilicates and calcium and sodium oxides was tested for adsorption of CO_2 acidic gas from the gas stream. A method of sorption of a sample of CO_2 is carried out by placing certain amounts of sample in an isothermal column. CO_2 is introduced into the bed from the bottom of the column using a fixed flow rate. Ranges of initial concentration of CO_2 were used and the flow rate is in the range of 2 L/min, 4 L/min, and 6 L/min. Preferably, the initial concentration of CO_2 is

`

1.87% and the flow rate is 4 L/min. The desorption procedure was similar to the above procedure except that nitrogen gas was introduced instead of CO_2.

The concentration of CO_2 at the exit stream was then measured at different periods of time and the difference in concentration between the inlet and outlet streams were calculated. Figure 24, 25 and 26 shows the breakthrough curves for CO_2 adsorption, which were obtained for produced adsorbent, limestone and raw Kaolin at room temperature and a flow rate of 4 L/min. Figure 24 shows that at an initial concentration and flow rate of CO_2 of 1630 ppm and 4 L/min respectively and a given mass of sample of 10 g, the breakthrough curves of adsorption of treated kaolin sample took about 55 min to get saturated with CO_2 and at this time all CO_2 was adsorbed on the surface, while the raw limestone and Kaolinite (Figure 25 and 26) took about 10 s to reach the same saturated value of treated sample. The adsorption of CO_2 by the treated samples was followed by the chemisorption process where a chemical reaction between CO_2 and the surface took place. While for raw kaolin and limestone the physical adsorption is dominant. Hence, the adsorption capacity of the treated sample is very high compared to the raw materials. Fig. 27 shows the complete breakthrough curve for treated Kaolin.

`

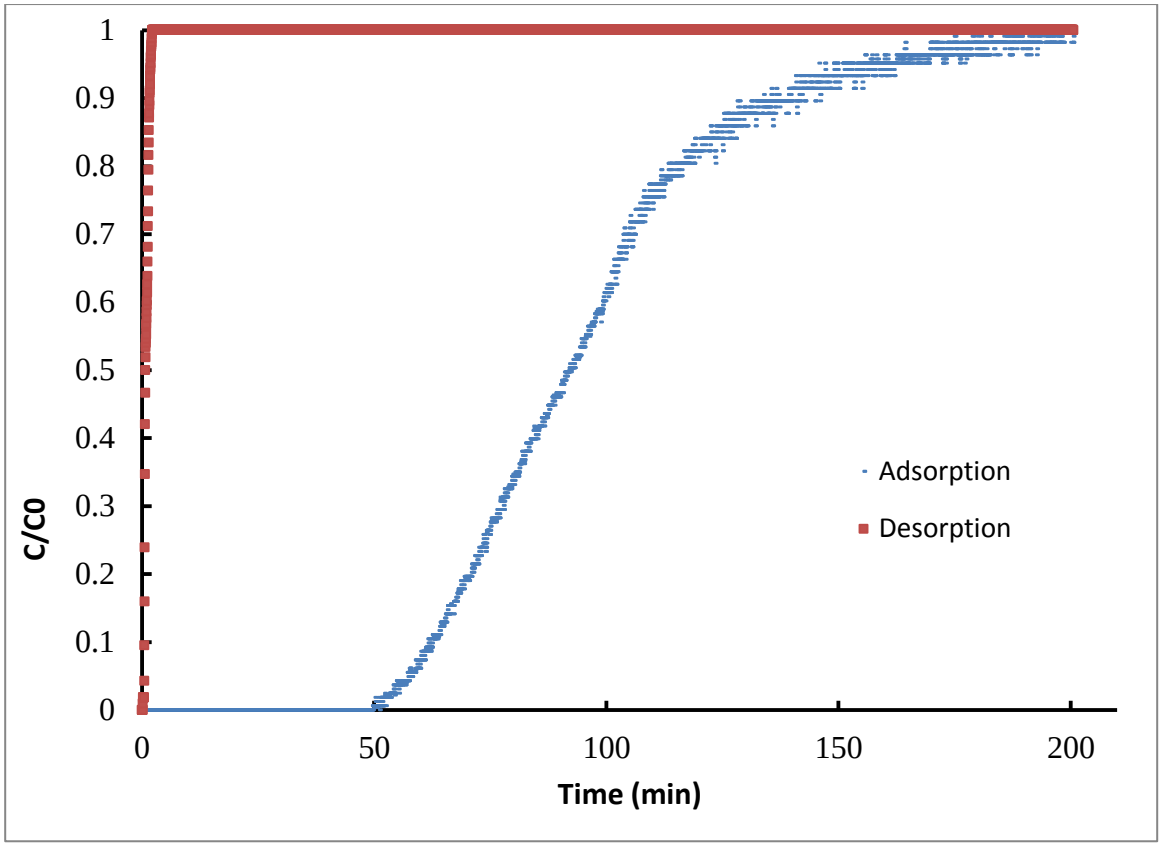

Figure 24 Breakthrough curve of treated kaolin at flow rate of 4 L/min, concentration of 1630 ppm, and temperature of 25 C.

`

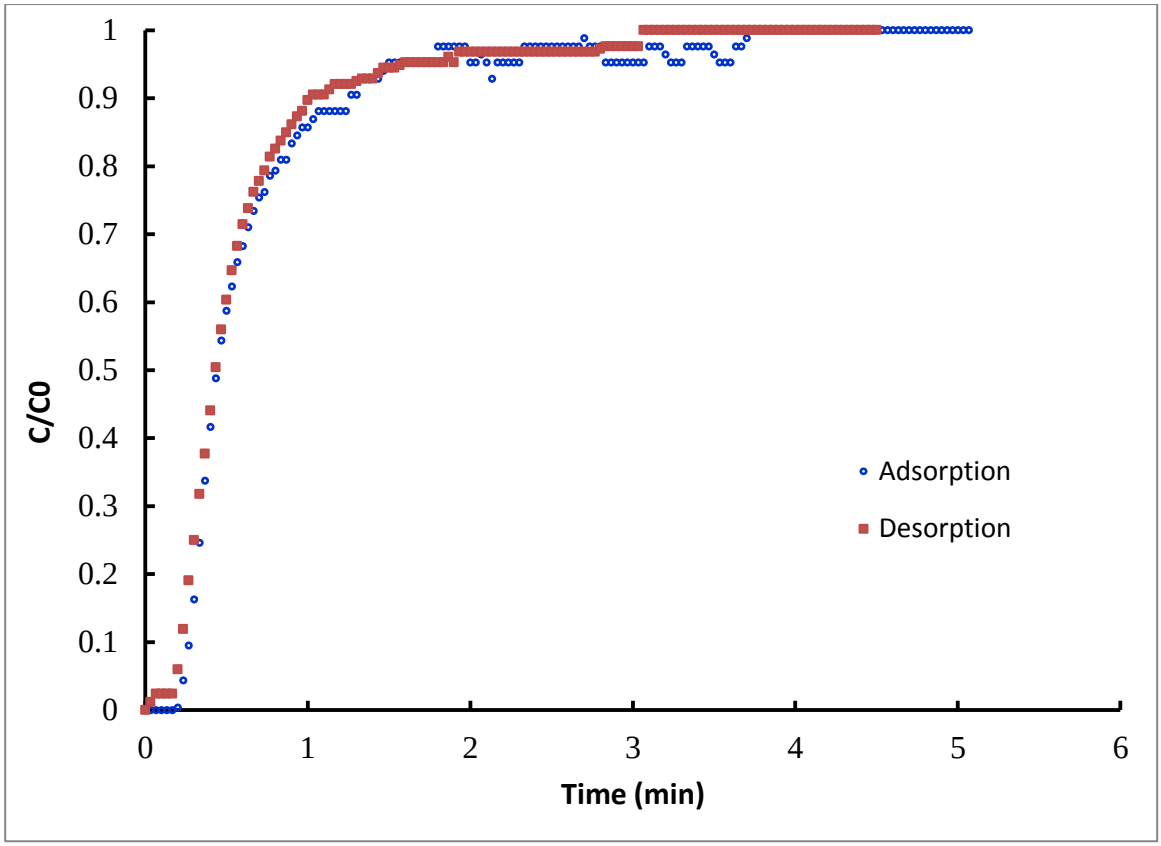

Figure 25 Breakthrough curve of raw kaolin at flow rate of 4 L/min, concentration of 1630 ppm and temperature of 25 C.

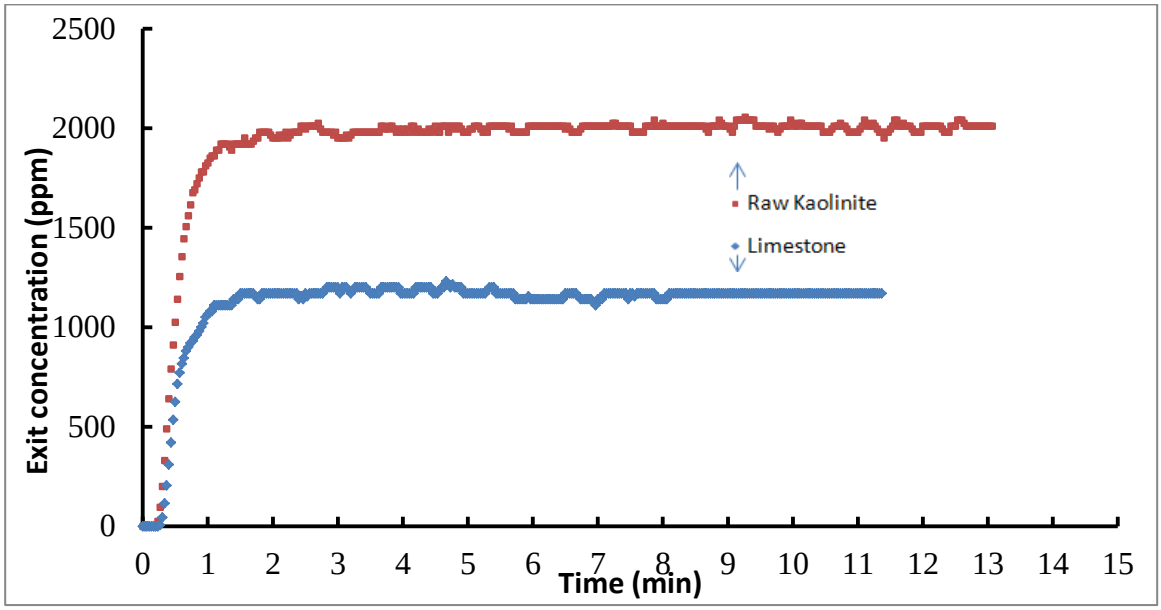

Figure 26 Breakthrough curves of raw Kaolin and limestone at flow rate of 4 L/min and temperature of 25 ^{o}C.

`

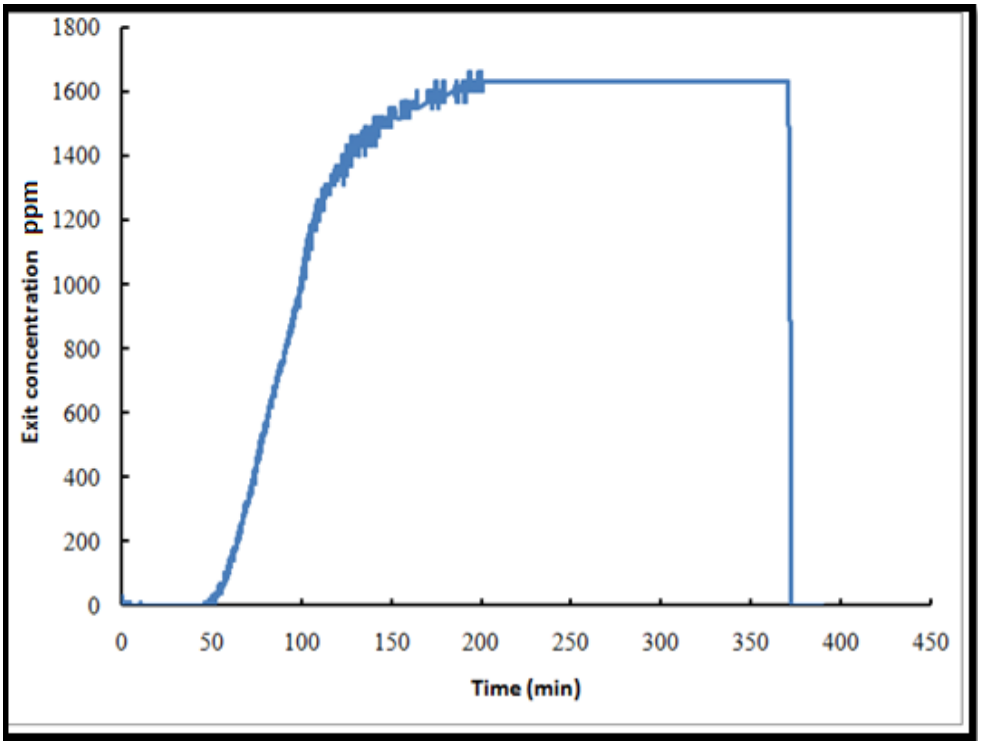

Figure 27 Complete breakthrough curve of treated Kaolinite at flow rate of 4 L/min, temperature of 25 ^{o}C.

4.4 Adsorption capacity

The chemical treatment of Kaolin using limestone and NaOH formed a mixture of Ca-Na-SiO_2-Al_2O_3 that increased the affinity for CO_2 adsorption because there are more CO_2 consuming sites in the structure. The new phases make the adsorption capacity much higher (2.79 mmol/g) at 4 L/min, 298 K and 1 bar, comparing to the raw kaolin (0.013 mmol/g) at the same conditions. The adsorption capacity of different adsorbents materials in the literature at different conditions are listed in the table 7. Even though the product material has a low surface area; the adsorption capacity is competitive with other adsorbents at the same conditions.

`

Table 7 Adsorption capacities of CO2 for different adsorbents.

Adsorbent	T (K)	P (bar)	q (mmol/g)	Reference
Treated Kaolin	298	1	2.79	This work
(TNT) modified with CdS and Bi_2S_3	298	1	0.269	15
Zeolite 13X	298	1	1.77	23
Mg-MOF-74	298	1	8.61	37
Modified activated carbon	298	1	2.92	28
MOF-177	298	35	34	18
MIL-100	304	50	18	19
MIL-101	604	50	40	19
Activated fly ash	313	-	5.48	32
Lithium-based fly ash	773	-	2.43	33
Zr-MOF	273	9.8	8.1	34
Amine-modified mesocellular slilca foams	348	-	7.73	35
UiO-67 MOF	308	1	6.86	36
MCM-41PEI	348	1	6	38
Zeolite 13X	298	32	7.4	18
MAXSORP	298	35	25	18
ZIF-8	298	25	7.5	21

`

4.5 Regeneration and desorption results

After having adsorbed CO_2, the Ca-Na-SiO_2-Al_2O_3 composition may be regenerated and/or recycled by desorbing the previously-adsorbed CO_2. Desorption may be carried out by heating the CO_2 containing composition and passing one or more inert gases over the CO_2 composition. At a sufficient temperature, CO_2 will be desorbed from the structure.

A method of desorption of a sample of N_2 is carried out by placing a fixed amount of different ranges of sample sizes in an isothermal column. N_2 is introduced from the bottom in different ranges of flow rates.

The new adsorbent was tested after several regeneration cycles with NaOH (14 M) and was found that its capacity increases by increasing the regeneration cycles as a result of more Na oxide linked aluminosilicate structure with the treatment of NaOH.

The regeneration of the chemisorbed material was carried out using the washing of the consumed material with NaOH, so it will react with calcium carbonate, after which calcinations was done. Figure 28 shows that the adsorption capacity for the material after regeneration after five times of using it is much higher than the fresh one, which is because the washing with NaOH generates new phases, which contain higher amounts of Na with Ca-Si-Al oxides.

`

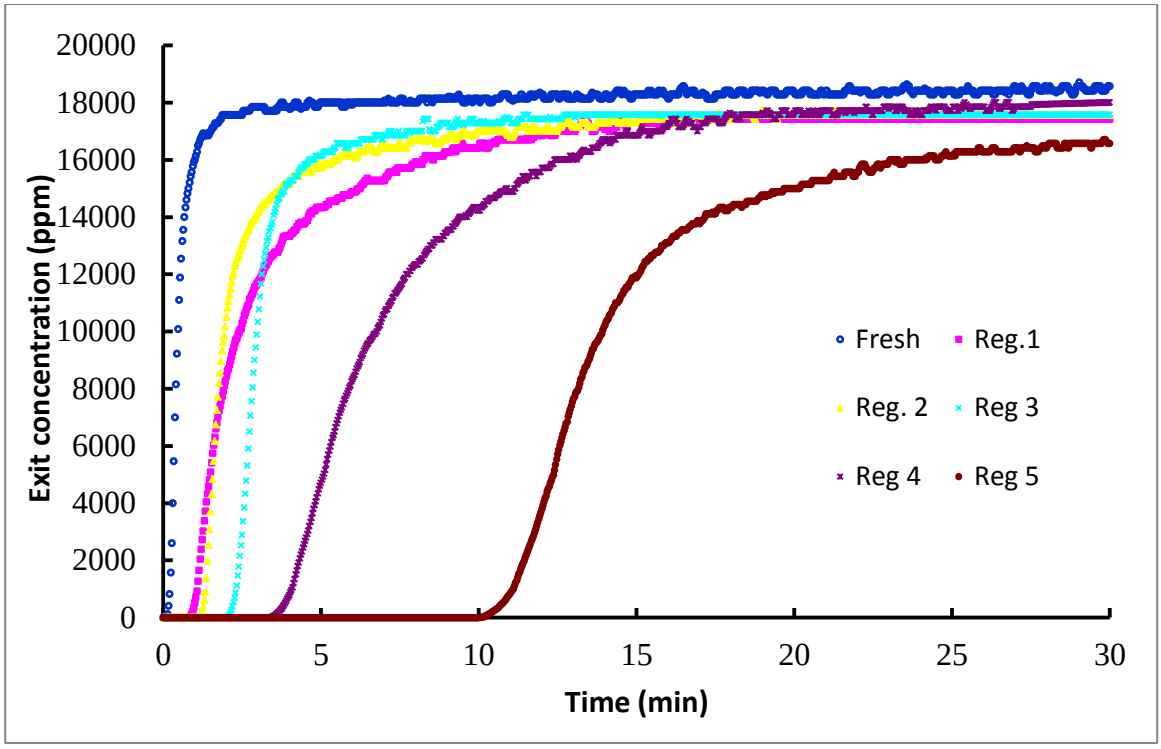

Figure 28 Adsorption curves of treated Kaolin after several regeneration cycles.

When the initial concentration is 1.87% and the flow rate is 4 L/min, the maximum adsorption capacity initially is 0.467 mmol/g, followed by 1.018 mmol/g after the first regeneration, by 0.861 mmol/g after the second regeneration, by 1.043 mmol/g after the third regeneration, by 2.97 mmol/ g after the four times of regeneration and by 4.7 mmol/g after the fifth regeneration. Figure 29 is a graph depicting the effect of regeneration cycles on the amount of CO_2 adsorbed. The initial CO_2 concentration was 18700 ppm (1.87%).

`

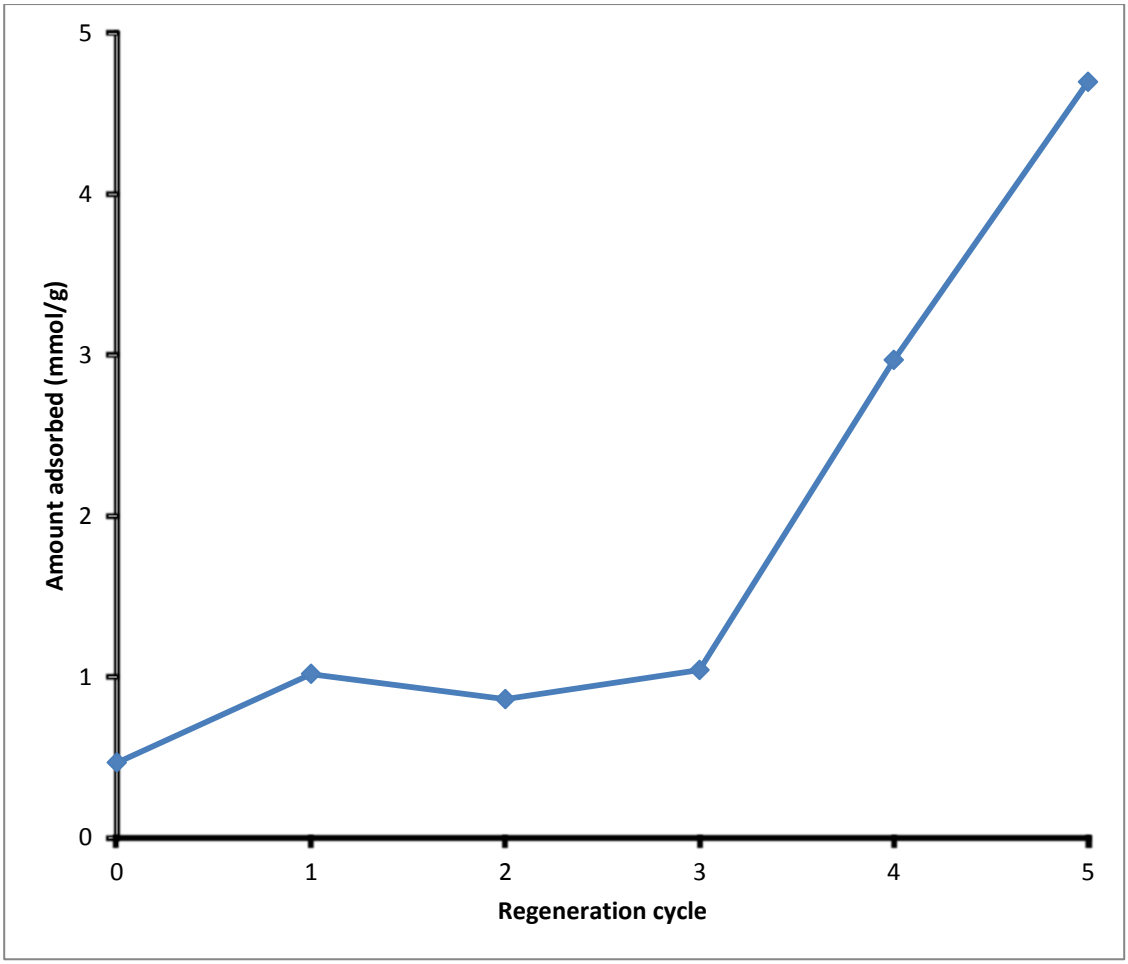

Figure 29 Effect of regeneration cycles on amount of CO_2 adsorbed .

Also the quantity of CO_2 desorbed from the treated kaolin was almost the same at room temperature for the different times of regeneration. The amount of CO_2 desorbed at an initial gas concentration of 1.87% and flow rate of 4 L/min is 0.2 mmol/g after first regeneration, followed by 0.21 mmol/g after the second regeneration, by 0.201 mmol/g after the third regeneration, by 0.186 mmol/g after the fourth regeneration, and by 0.201 mmol/g after the fifth regeneration (Figure 30).

`

Figure 31 shows the effect of regeneration cycles on the amount of CO_2 adsorbed, desorbed and reacted on the treated kaolin material. The amount of reacted CO_2 is the difference between the adsorbed and desorbed amounts.

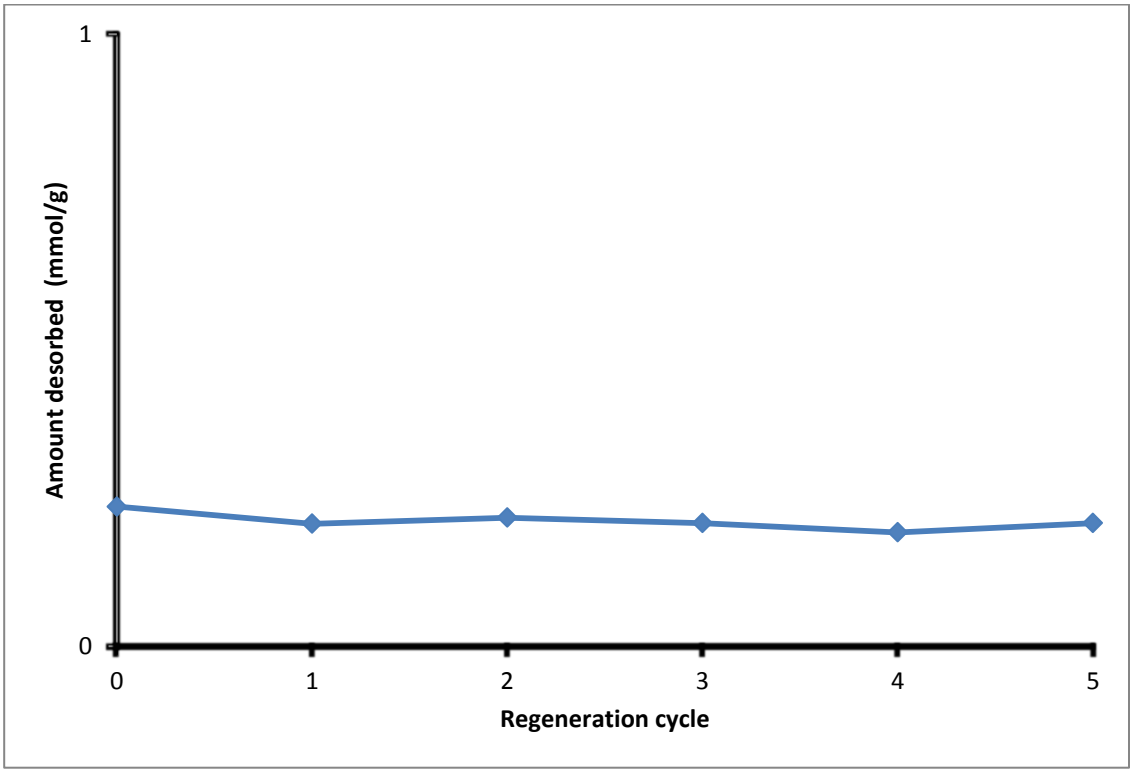

Figure 30 Effect of regeneration cycles on amount of CO_2 desorbed.

`

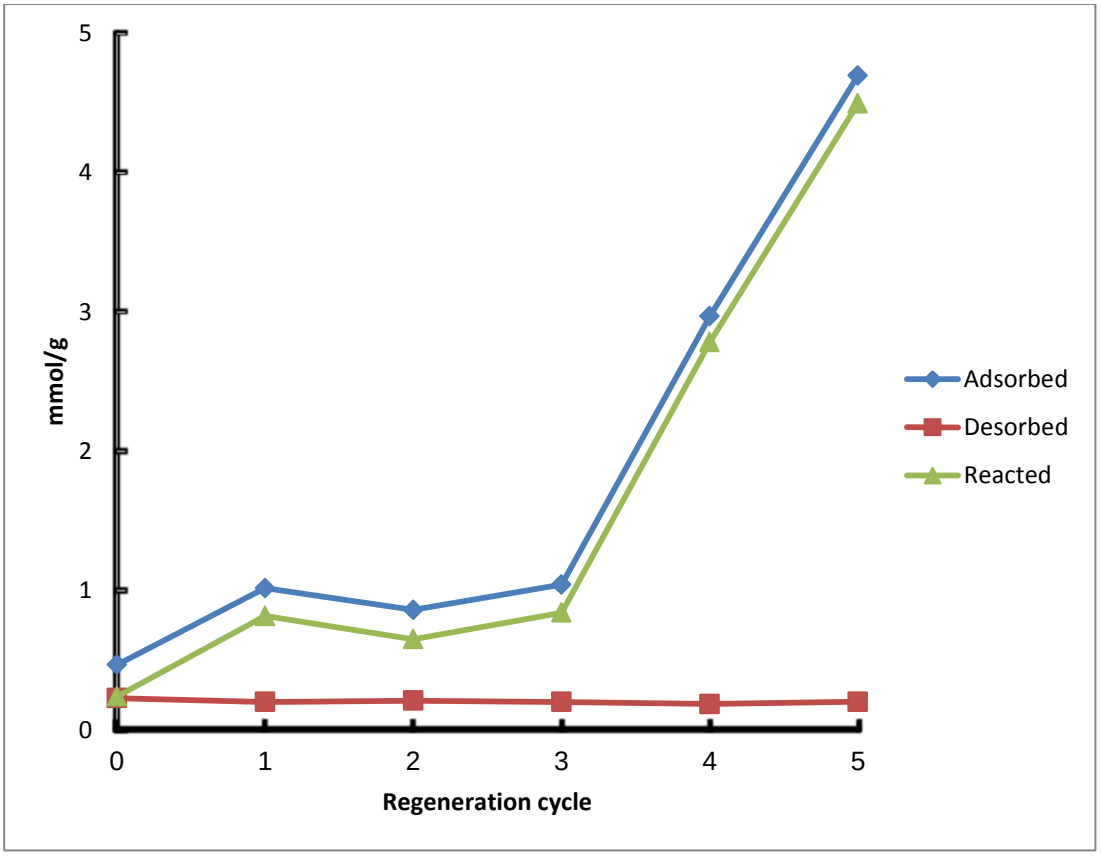

Figure 31 Effect of regeneration cycles on amount of CO_2 adsorbed, desorbed, and reacted.

4.6 Effect of temperature

Figure 32 describes the effect of temperature on the adsorption of CO_2 on the treated kaolin adsorbent. Different temperatures were tested (5, 15, 25, 35, 50, 60, and 70 ^{o}C) at initial CO_2 concentration of 18700 ppm (1.87%) and a flow rate of 4 L/min. It is obvious that for high temperatures, it took more time to get saturated so it has a higher adsorption capacity. The adsorption of CO_2 by the treated samples was followed by the chemisorption process where a chemical reaction between the CO_2 and the surface took place. This sorption was enhanced with increasing bed temperature from which it can be concluded that there was an endothermic process at the surface of the produced samples.

`

Although, an increase in the temperature makes the gas molecules active energized and harder to be adsorbed, an increase in the flow rate and negligible effect of pressure will make the effect disappear and increasing the temperature will increase the rate of the reaction on the surface and therefore increase the adsorption capacity. Bear [74] showed that the CO_2 adsorption capacity for AC-MDEA sample was increased with temperature therefore increasing the indication of the chemisorption process. Al-Degs et al .[82] studied the effect of temperature on the adsorption behavior of dyes on activated carbon, they found that the adsorption of dyes was an endothermic process because the adsorption capacity of dyes increased at higher temperatures, and the surface coverage also increased. They suggested that the enhancement of adsorption capacity with high temperatures may be because of an increase in the penetration of dyes inside micropores or the creation of new active sites. Akso [107] investigated that the adsorption of cadmium (II) by C. vulgaris was exothermic, so adsorption increased with decreasing temperature, and the optimum adsorption temperature was 20 ^{0}C. Martins et al. [108] found that the adsorption of zinc on F. antipyretica is an endothermic process, and the capacity enhanced with temperature from 11.5 mg g^{-1} at 5°C to 14.7 mg g^{-1} moss at 30°C. The increase can be caused by a change in adsorbent pore size and enhanced ion exchange. On the other hand, cadmium adsorption capacity was independent of the temperature. Namasivayam et al. [109] found that the adsorption capacity of Congo Red on activated carbon increased slightly with temperature. The endothermic nature of the adsorption process was confirmed from the positive values of ΔH^0. The spontaneous nature of adsorption was confirmed by the negative value of ΔG^0 at 60 ^{0}C, while at low temperature, the ΔG^0 values were positive and the spontaneity was not favored.

`

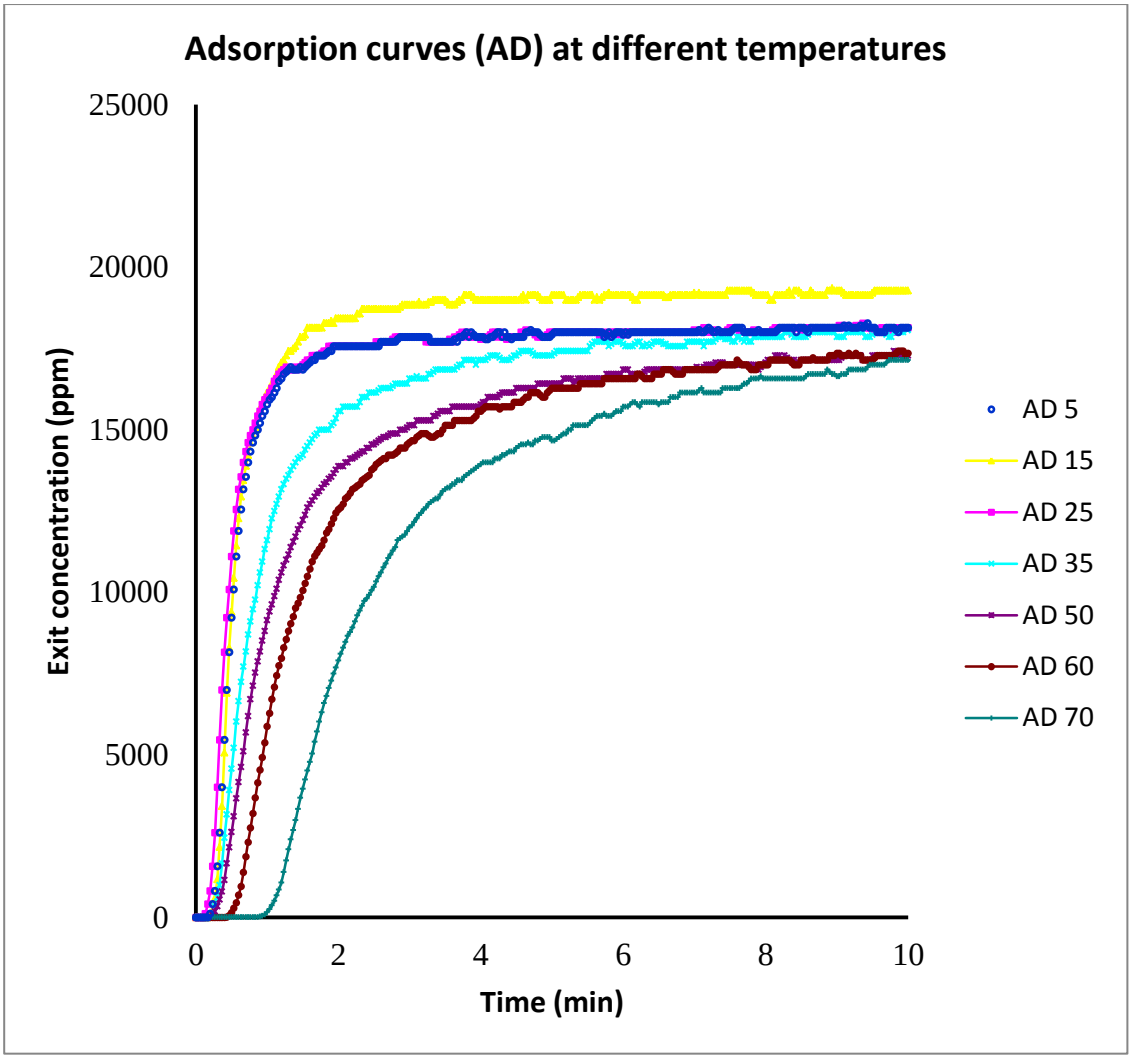

Figure 32 Effect of temperature on the adsorption of treated kaolin.

4.7 Effect of initial concentration

Figure 33 shows the breakeven curves for adsorption of CO_2 by treated kaolin at different initial concentrations of CO_2 at room temperature, 4 L/min flow rate and 1 atm. The adsorption capacity is proportional to both the initial concentration of CO_2 and time needed to reach the saturated value, because of the increase in the driving force between the gas concentration in bulk and others in the surface of the adsorbent. At an initial concentration of 18700 ppm, the adsorption capacity is high because of the high value of the initial concentration. The adsorption capacity is high at an initial concentration of

`

1600 ppm because of the high value of time needed to get saturated, but not as high as the first case since the initial concentration is much higher.

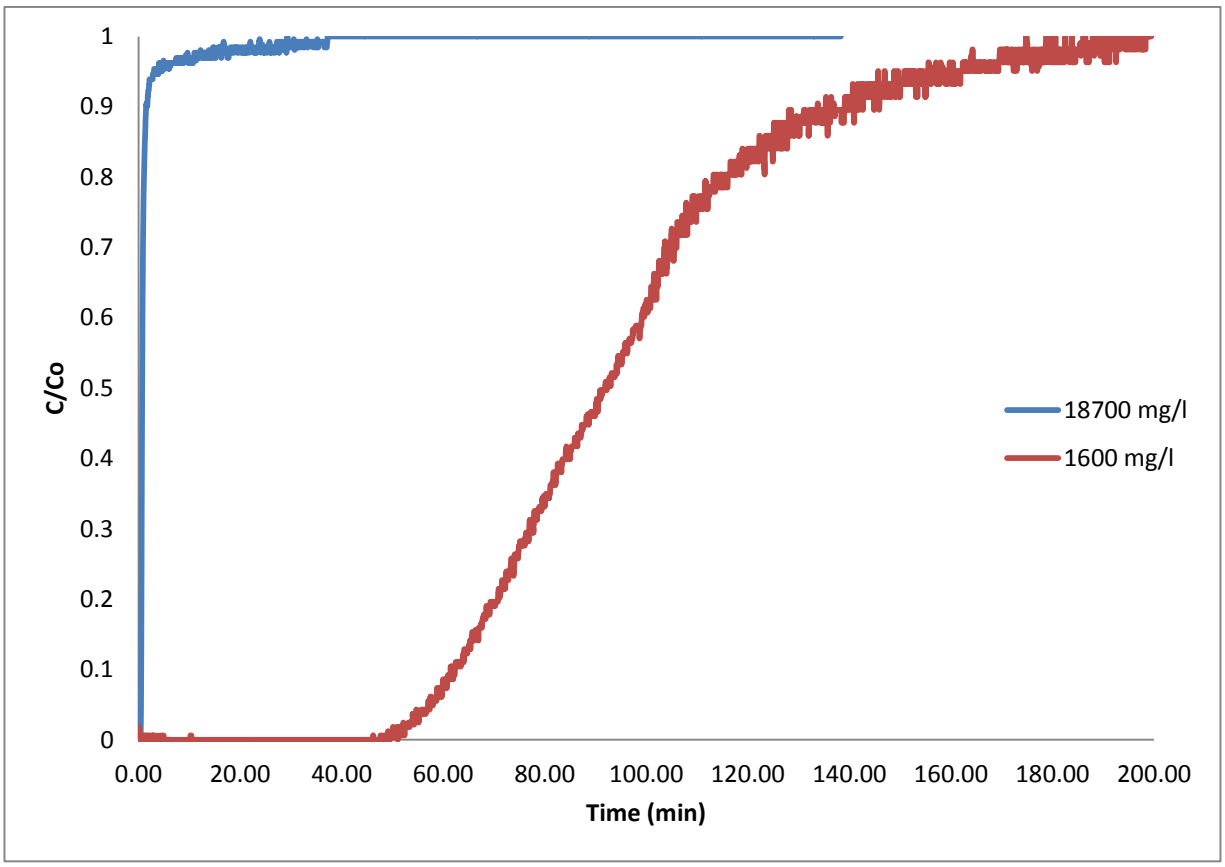

Figure 33 Effect of initial concentration on the adsorption of treated kaolin.

4.8 Results of characterization of regenerated material

This section deals with studying the results of characterization of the treated sample after five cycle regeneration. Table 9 shows the elemental analysis of the sample using SEM instrumental. It is obvious that after using five cycles, more Na is linked with aluminosilicate structure because of the treatment with NaOH, and this proves the increase in adsorption capacity with an increase in the regeneration cycles.

`

The structure of the treated sample after five cycles was examined by using scanning electron microscopy (SEM). Figures 34, 35 and tables 8, 9 show the SEM image and their related peaks. The analysis confirmed the conclusion that was obtained about the increase in the percentage of Na in the structure after regeneration of the material at different times using NaOH. The sample is composed of spherical like particles and in the form of aggregates.

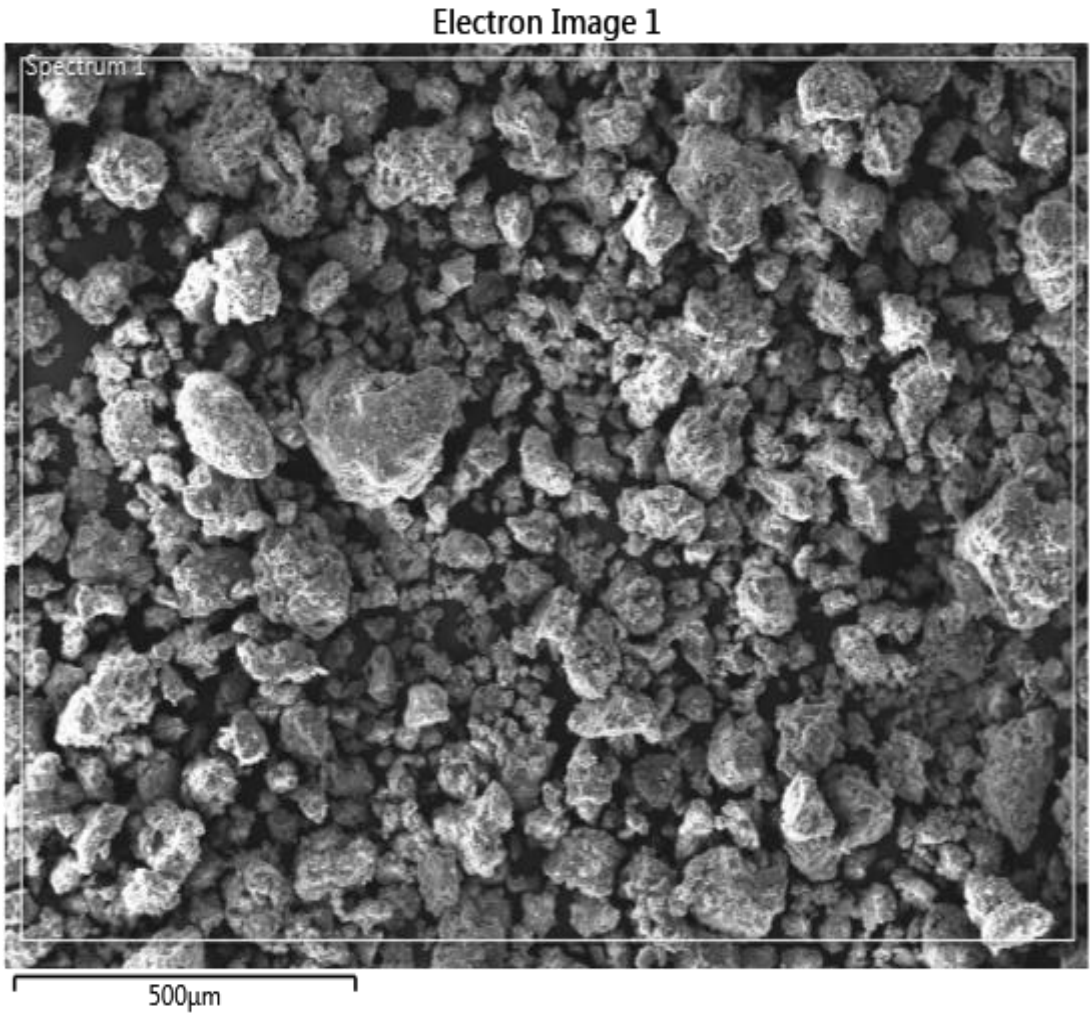

Figure 34 SEM micrographs of the treated sample after five cycles.

`

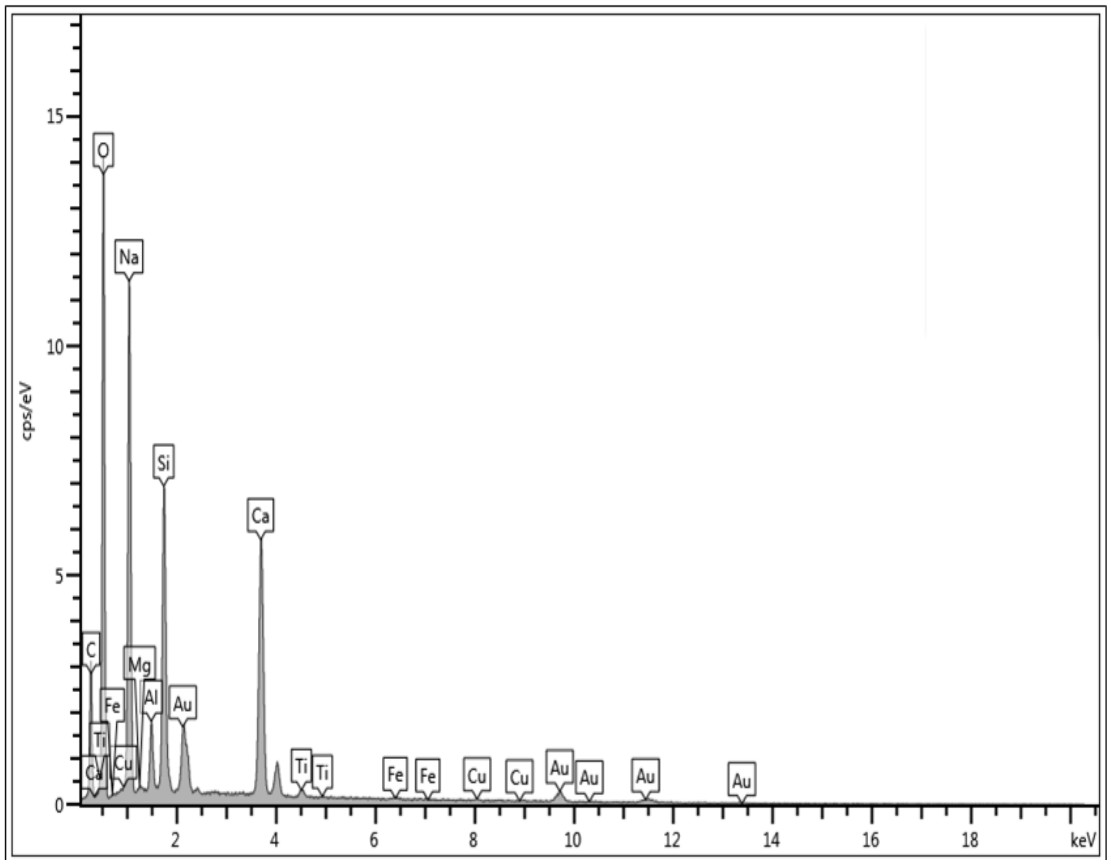

Figure 35 Spectrum of x-rays for treated sample after five cycles.

Table 8 Statistical analysis of elemental data.

Statistics	O	Na	Mg	Al	Si	Ca	Ti	Fe	Cu
Max	55.61	21.23	0.15	2.11	8.41	11.44	0.51	0.21	0.34
Min	55.61	21.23	0.15	2.11	8.41	11.44	0.51	0.21	0.34
Average	55.61	21.23	0.15	2.11	8.41	11.44	0.51	0.21	0.34
Standard Deviation	0.00	0.00	0.00	0.00	0.00	0.00	0.00	0.00	0.00

`

Table 9 Elemental analysis from SEM results for sample after five cycles.

Element	Weight %
O	55.61
Na	21.23
Si	8.41
Al	2.11
Ti	0.51
Fe	1.02
Ca	11.44
Cu	0.34
Mg	0.15
Total	100

`

4.9 Effect of humidity

It is very important to study the effect of humidity on the adsorption capacity for CO_2 gas and humidity on the surface of the treated kaolin material since the adsorbent is a hydrophilic material. During all previous experiment results, the material was exposed to the atmosphere, so it was saturated with water (20 % RH), and the adsorption capacity was good. That enhancement of the adsorption capacity may be due to the water vapor making a link between the CO_2 and calcium and sodium oxide in such way that the adsorption is enhanced. The adsorption can also be improved by increasing the humidity in the inlet CO_2 gas by passing the gas through a controlled relative humidity water vapor. Figure 36 shows the breakthrough curve of different relative humidity values for inlet gas at constant temperature, flow rate, and concentration. The adsorption time that is needed for the material to get saturated for 63% relative humidity is higher than that for 20%. Figure 37 shows the adsorption capacities value at different sets of humidity conditions.

The rise in the adsorption capacity with humid gas is still a matter of discussion. There are different literatures which discuss the effect of water vapor on the adsorption capacity for different adsorbents. Yazaydin et al [71] studied the effect of the humidity on the adsorption on MOF, he found that molecules of water opened the metal sites on the framework and increased the adsorption capacity.

Baroz Aziz [72] studied the effect of humid CO_2 on the adsorption capacity of the APTES modified silica; he found that the uptake of CO_2 was enhanced when the humidity was applied. He claimed that carbamateammonium ions react further with CO_2 and H_2O and may form bicarbonate groups.

`

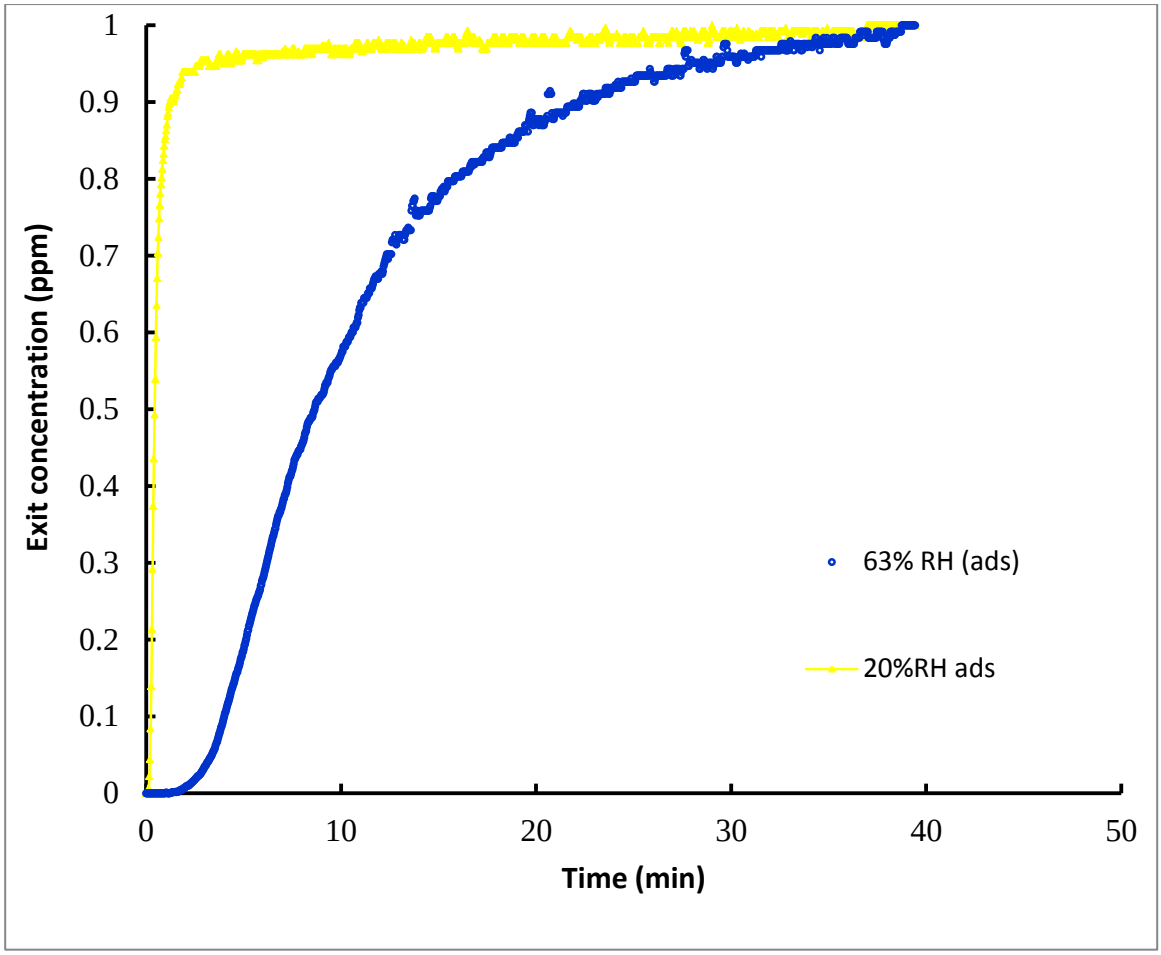

Figure 36 Breakthrough curve for treated kaolin at relative humidity of 63% and 20%.

`

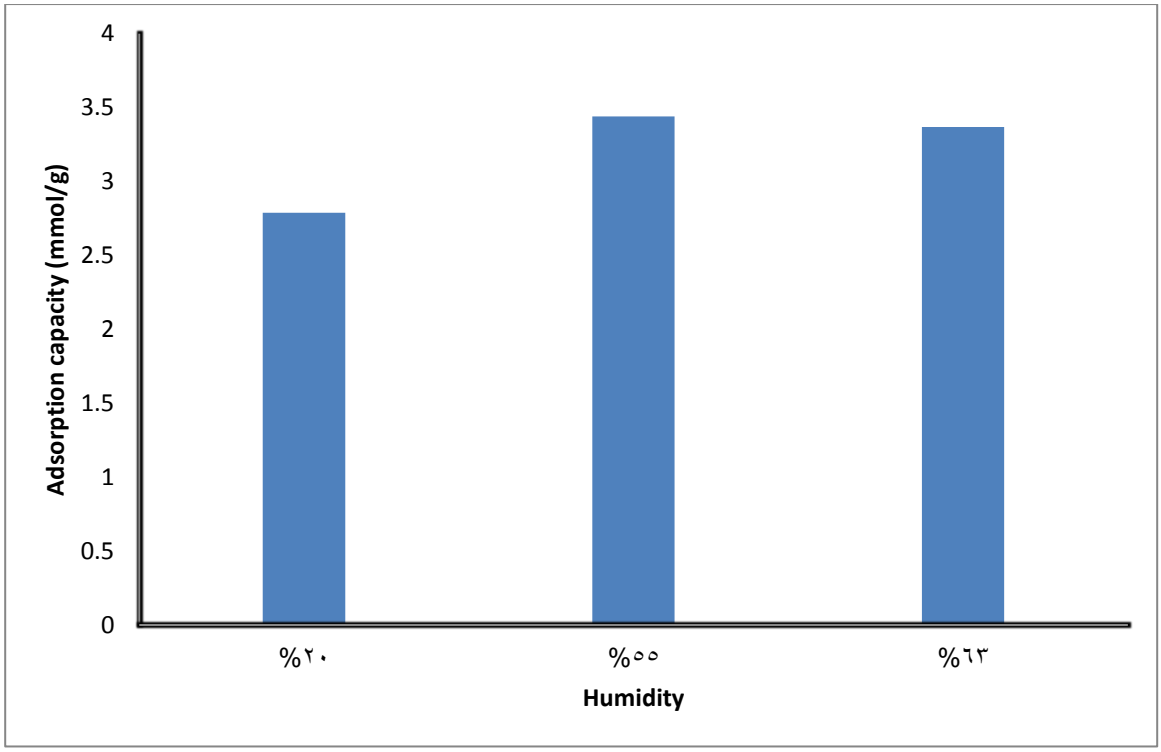

Figure 37 Adsorption capacity at different sets of humidity conditions.

`

CHAPTER 5

MATHEMATICAL IINTERPRETATION

5.1 Breakthrough curve analysis

The mean residence time or average residence time (space time) t_m is defined as volume over volumetric flow rate. It can be described by the residence time distribution function E(t) that describes how much time different gas elements have spent in the column:

$$E(t) = \frac{C(t)}{\int_0^\infty C(t)\,dt}$$

$$t_m = \int_0^\infty tE(t)\,dt$$

The mean residence time (MRT) is a very important parameter to estimate the average time that gas molecules are present in the adsorption column. For treated kaolin at room temperature initial concentration and flow rate of 1630 ppm and 4 L/min respectively, the MRT is (figure 38):

$$t_m = 143.9\text{min}$$

`

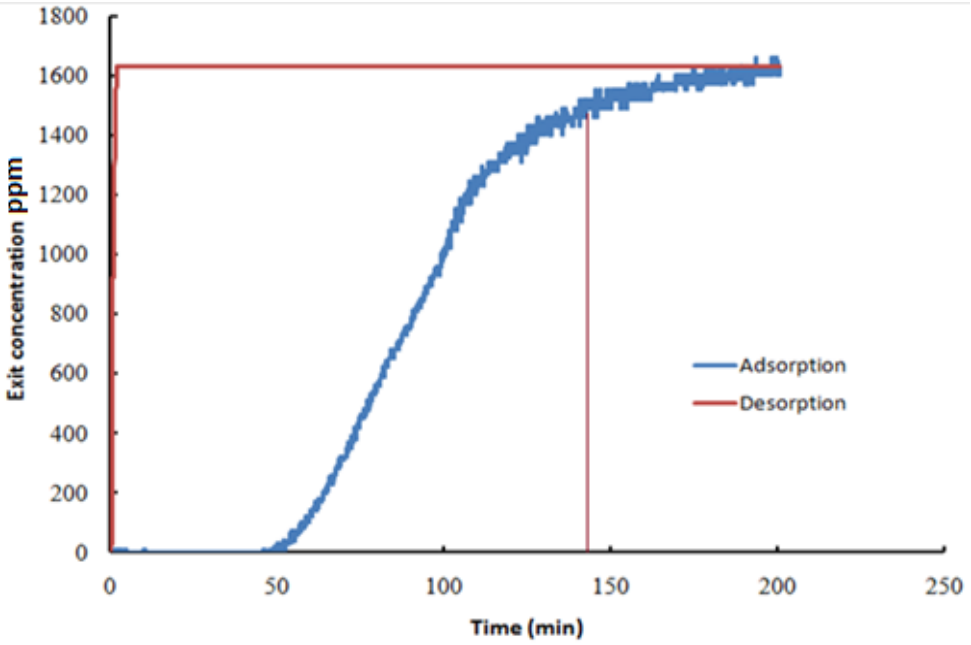

Figure 38 Definition of mean reciedence time on the breakthrough curve.

5.2 CO_2 adsorption isotherm analysis

Figure 39 shows the CO_2 adsorption isotherm after applying the vacuum condition for the treated kaolin sample, so the humidity in the solid sample and the gas feed is almost zero and the adsorption is not as much as the one with humidity conditions.

The isotherm has a form of type II in BDTT classification where BET mechanism is applicable. N-layer BET equation can be applied in case the adsorption layer is limited by n layers. The form of n-layer equation is:

$$\frac{q}{q_m} = \frac{CX}{1-X}\frac{1-(n+1)X^n+nX^{n+1}}{1+(C-1)X-CX^{n+1}}$$

`

When n equal 1 the equation will reduce to the Langmuir equation form, and when n is infinity, the equation will reduce to the BET equation. Figure 40 shows the linearization of the isotherm data to get the BET constants and after getting the isotherm parameters, the isotherm data was fitted with n-layer equation to get the number of layers n (figure 41). The parameters obtained are listed below:

n (layers)	6.164553
c	27
q_m (mg/g)	11.22

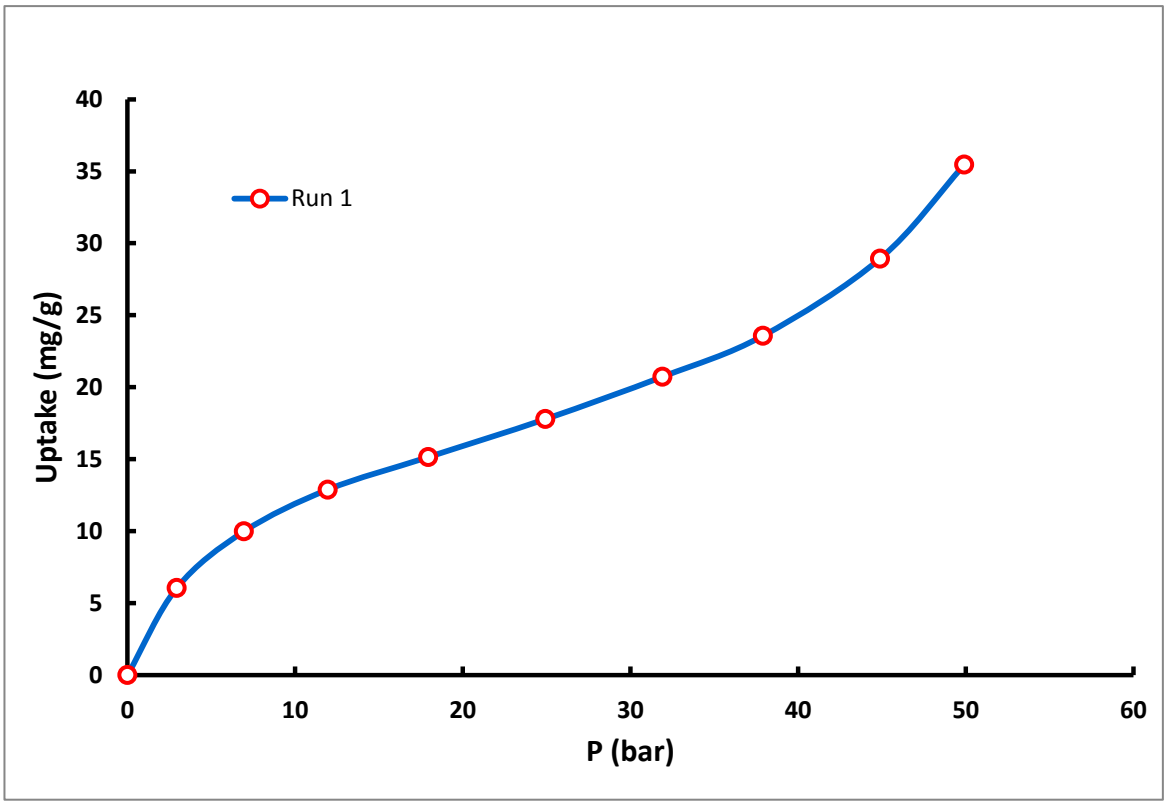

Figure 39 CO_2 adsorption isotherm at 22 C.

`

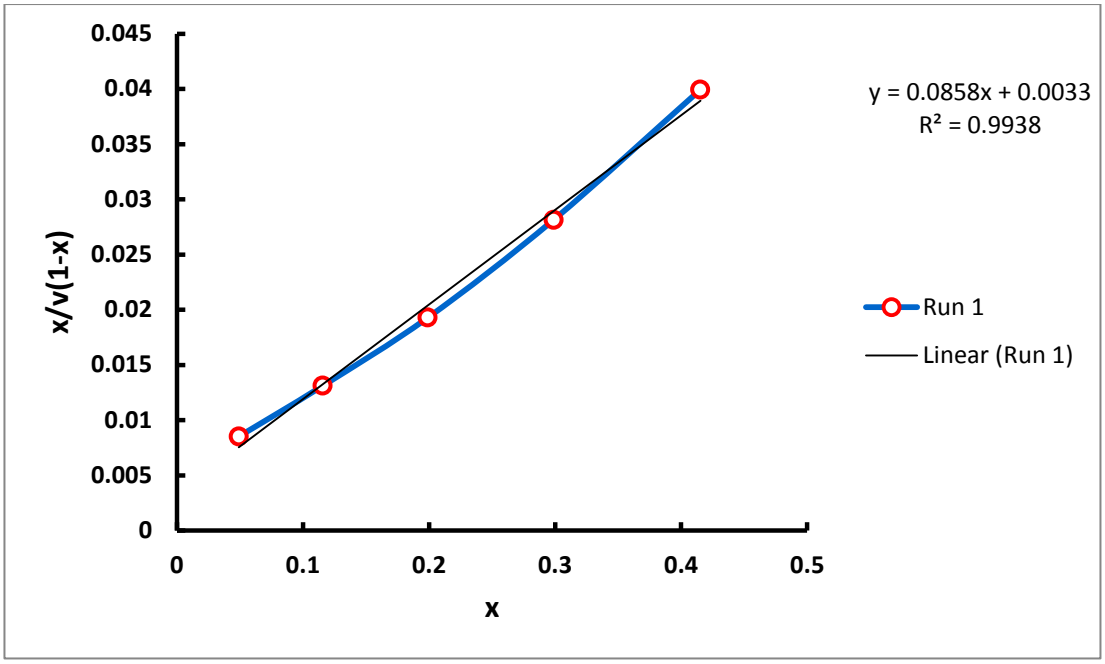

Figure 40 Linear form of BET isotherm for CO_2 adsorption on treated kaolin at 22C.

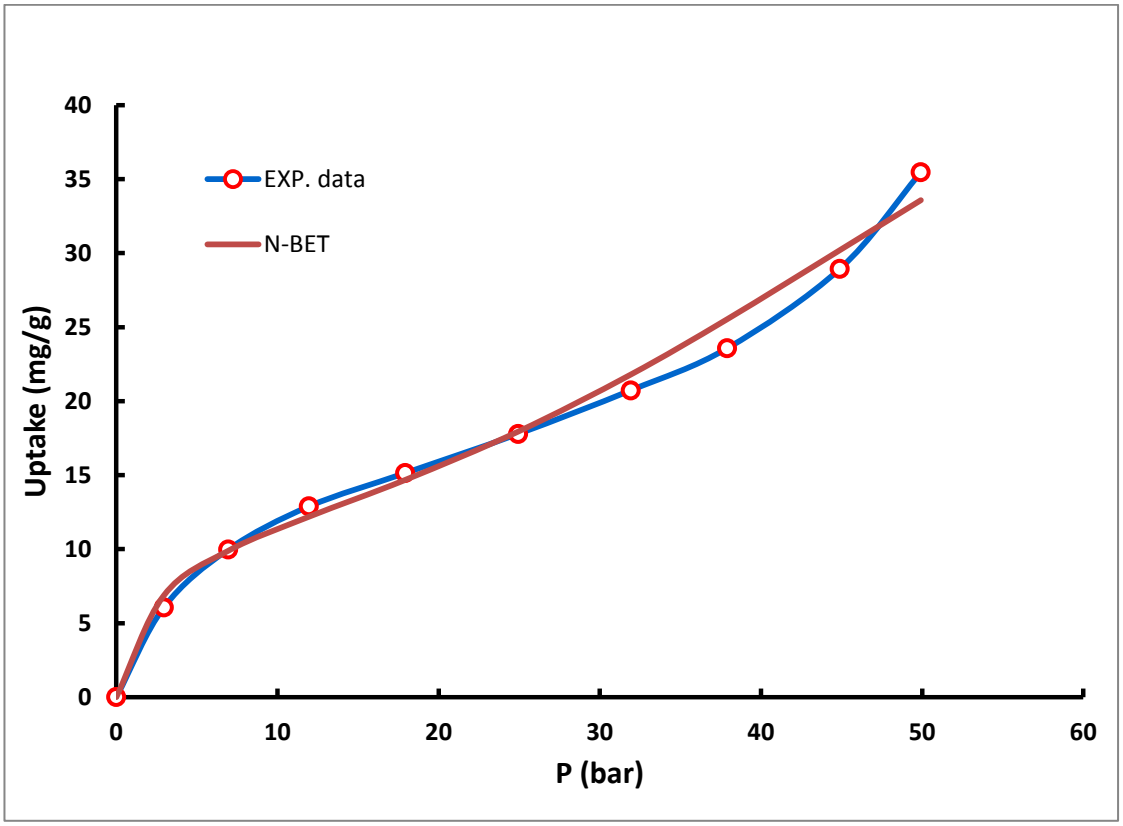

Figure 41 Fitting between experimental isotherm data and n-BET equation.

`

5.3 Thermodynamic parameters

Since the pseudo first order model was considered acceptable, its kinetic parameters at different temperatures were used to calculate the thermodynamic parameters. In the previous actions, the effect of temperature was studied at different values of temperature (15, 25, 35, 50, 60, and 70) at flow rate of 4 L/min and constant initial concentration and humidity. As we saw that an increase of the temperature caused an increase in the CO_2 adsorption capacity, this means that there is an endothermic interaction between the CO_2 molecules and the surface of the treated kaolin, where chemisorption and physisorption takes place. Although the increase in temperature makes the gas molecules active energized and harder to be adsorbed, but an increase in flow rate and the negligible effect of pressure makes this effect disappear and an increase in the temperature will increase the rate of the reaction on the surface and increase the adsorption capacity. The following equations were used to evaluate the thermodynamic properties as the heat of adsorption (ΔH°), slandered free energy change (ΔG°) and slandered entropy (ΔS°) [77-81]:

$$\Delta G_0 = \Delta H_0 - T\Delta S_0$$

$$\Delta G_0 = -R\,T\,ln\,k_f$$

$$ln\,k_f = \frac{\Delta S_0}{R} - \frac{\Delta H_0}{R\,T}$$

Where kf is the equilibrium constant from pseudo first order model, R is the gas constant (8.314 J/mol K), and T is the temperature in K.

The plot of ln kf versus 1/T was made to get the slope and the intercept which are heat of adsorption and entropy respectively. Plot is shown in figure 42.

`

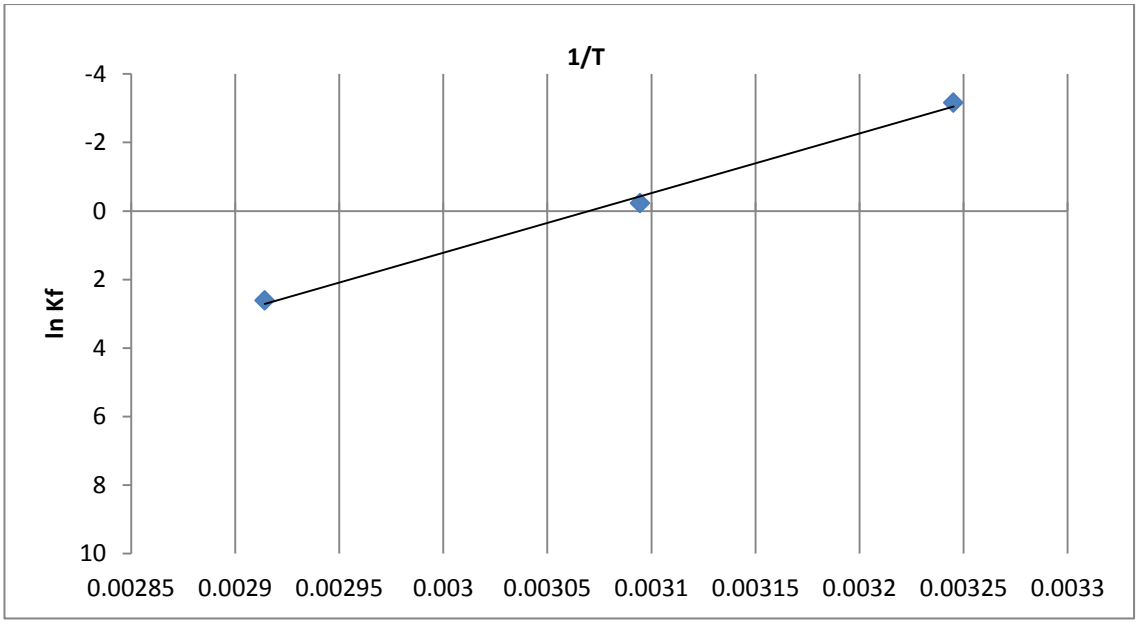

Figure 42 Relationship between equilibrium constant and temperature for treated kaolin.

The equilibrium constant increases with an increase in the temperature, hence the number of active sites increases while the adsorption capacity increases. The table below lists the values of thermodynamics parameters (ΔHads, ΔSads and ΔGads). The value of ΔHads is positive (+144.6 kJ/mol) indicating that the nature of the adsorption is endothermic, which explains the enhancement in the adsorption capacity with temperature. The positive value of ΔSads (444.1 J/mol.K) confirmed the randomness and disorder during the adsorption process at solid/gas interface. The low and negative values of ΔGads indicate the spontaneity of the adsorption process, so it does not need an external energy source for the adsorption system.

The physical and chemical adsorption can be classified based on the value of the heat of adsorption, when the value is less than 84 kJ/mol, the physical adsorption is dominant, while the chemical adsorption bond strength ranges from 84 to 420 kJ/mol [82,83].

`

From the evaluated value of heat of adsorption, it was found that the adsorption of CO_2 on treated kaolin follows the chemical adsorption process.

Temperature (K)	delta G (kJ/mol)	delta H (kJ/mol)	delta S (J/mol.K)
308	8.090		
323	0.599	144.6	444.1
343	-7.46		

`

5.4 Fixed Bed Adsorption Column Modeling

It is very important for the given adsorption system to obtain the breakthrough curve by mathematical modeling. Different mathematical models have been used to predict the breakthrough curves in fixed bed adsorption column. For adsorption of CO_2 on treated kaolin, the dispersion model was selected. Considering the system as an axial dispersed plug flow, the following equation was used for convective-diffusion-reaction:

$$\frac{\partial C_A}{\partial t} + u\frac{\partial C_A}{\partial z} = D_{\mathrm{AB}}[\frac{1}{r}\frac{\partial[r(\partial C_A/\partial r]}{\partial r} + \frac{\partial^2 C_A}{\partial z^2}] - R_A$$

Where C_A is the CO_2 concentration and D_{AB} is the diffusion coefficient. The following assumptions can be made:

- The system is uniform in temperature and has a constant pressure drop.
- The radial dispersion is negligible.
- Adsorption, surface reaction, and internal diffusion resistances are involved in chemical adsorption.
- The velocity of the gas is assumed to be constant.

Based on the above assumptions, the equation and the initial boundary conditions are described as following:

$$\frac{\partial C_A}{\partial t} + u\frac{\partial C_A}{\partial z} - D_{\mathrm{AB}}\frac{\partial^2 C_A}{\partial z^2} + \frac{K_A {C_A}^a}{1 + K_B {C_A}^b} = 0$$

The initial and boundary conditions are:

$C_A[t\ ,\ 0] = C_0$

`

$C_A[0, z] = 0$

$\partial_z x[t, L] = 0$

Where C_0 is the initial concentration (1630 ppm), L is the length of the column (10 cm), and t_s is the time when the adsorbent becomes saturated and the inlet concentration is the same as that of the outlet from the column (194 min).

The model can be solved numerically using the finite difference method:

$$\frac{C_{i+1,j,k} - C_{i,j,k}}{\Delta t} + u_i \frac{C_{i,j,k+1} - C_{i,j,k}}{\Delta z} - D_{AB} \frac{C_{i,j+1,k} - 2C_{i,j,k} + C_{i,j-1,k}}{\Delta z^2} + \frac{K_A {C^a}_{i,j,k}}{1 + K_A {C^a}_{i,j,k}} = 0$$

$$\frac{C_{i+1,j,k}}{\Delta t} - \frac{C_{i,j,k}}{\Delta t} - \frac{u_i C_{i,j,k}}{\Delta z} + 2D_{AB} \frac{C_{i,j,k}}{\Delta z^2} = u_i \frac{C_{i,j,k+1}}{\Delta z} - \frac{K_A {C^a}_{i,j,k}}{1 + K_A {C^a}_{i,j,k}} + D_{AB} \frac{C_{i,j+1,k} + C_{i,j-1,k}}{\Delta z^2}$$

$$\frac{C_{i+1,j,k}}{\Delta t} - C_{i,j,k}\left(\frac{u_i}{\Delta z} - \frac{2D_{AB}}{\Delta z^2} + \frac{1}{\Delta t}\right) = C_{i,j+1,k}\left(\frac{D_{AB}}{\Delta z^2}\right) + \frac{D_{AB} C_{i,j-1,k}}{\Delta z^2} + \frac{u_i}{\Delta z} C_{i,j,k+1} - \frac{K_A {C^a}_{i,j,k}}{1 + K_A {C^a}_{i,j,k}}$$

$$C_{i+1,j,k} = C_{i,j,k}\left(\frac{u_{i\Delta t}}{\Delta z} - \frac{2\Delta t D_{AB}}{\Delta z^2} + 1\right) + C_{i,j+1,k}\left(\frac{D_{AB}\Delta t}{\Delta z^2}\right) + C_{i,j-1,k}\left(\frac{D_{AB}\Delta t}{\Delta z^2}\right) + \frac{u_i}{\Delta z} C_{i,j,k+1} - \frac{K_A {C^a}_{i,j,k}}{1 + K_A {C^a}_{i,j,k}}$$

$$\emptyset = \left(\frac{D_{AB}\Delta t}{\Delta z^2}\right)$$

$$C_{i+1,j,k} = C_{i,j,k}\left(\frac{u_{i\Delta t}}{\Delta z} - 2\emptyset + 1\right) + C_{i,j+1,k}\emptyset + C_{i,j-1,k}\emptyset + \frac{u_i}{\Delta z} C_{i,j,k+1} - \frac{K_A {C^a}_{i,j,k}}{1 + K_A {C^a}_{i,j,k}}$$

The constants in the equation were written as a function of temperature, so the model was fitted with different sets of experimental data at different temperatures.

`

Where:

$$D_{\mathrm{AB}} = D_0\, e^{\frac{-E0}{R_0 * T_{\mathrm{g}}}}$$

$$K_{\mathrm{A}} = K_1\, e^{\frac{-E1}{R_0 * T_{\mathrm{g}}}}$$

$$K_{\mathrm{B}} = K_2\, e^{\frac{-E2}{R_0 * T_{\mathrm{g}}}}$$

$$\frac{\partial C_A}{\partial t} + u\frac{\partial C_A}{\partial z} - D_0\, e^{\frac{-E0}{R_0 * T_{\mathrm{g}}}}\frac{\partial^2 C_A}{\partial z^2} + \frac{K_1\, e^{\frac{-E1}{R_0 * T_{\mathrm{g}}}}\, {C_A}^a}{1 + K_2\, e^{\frac{-E2}{R_0 * T_{\mathrm{g}}}}\, {C_A}^b} = 0$$

The model was fitted with experimental data by MATHEMATICA V.9 software, and the parameters were found as following:

D_{eff}=2.8x10^{-3} cm^2/s
K_1=1x10^{-13} s^{-1}
K_2=5.1x10^{-10} s^{-1}
$E0$ =19.0 KJ/mol
$E1$ =16.0 KJ/mol
$E2$ =6.8 KJ/mol
a= 0.96
b= 1.5

The dispersion model is used to describe actual reactors (non-ideal) when axial dispersion is covered.

`

The dispersion number is the reciprocal of Peclet number (Pe) and measures the ratio between the rate of transport by diffusion or dispersion to the rate of transport by convection, and shows the deviation from plug flow in the adsorption column.

$$\text{Dispersion number} = \frac{D_{\text{eff}}}{uL}$$

The value of dispersion number was found to be $7\text{x}10^{-6}$, when dispersion number approaches zero, the dispersion can be considered as negligible, and the system behaves as a plug flow reactor (PFR). Figure 43 shows the fitted experimental data with the dispersion model.

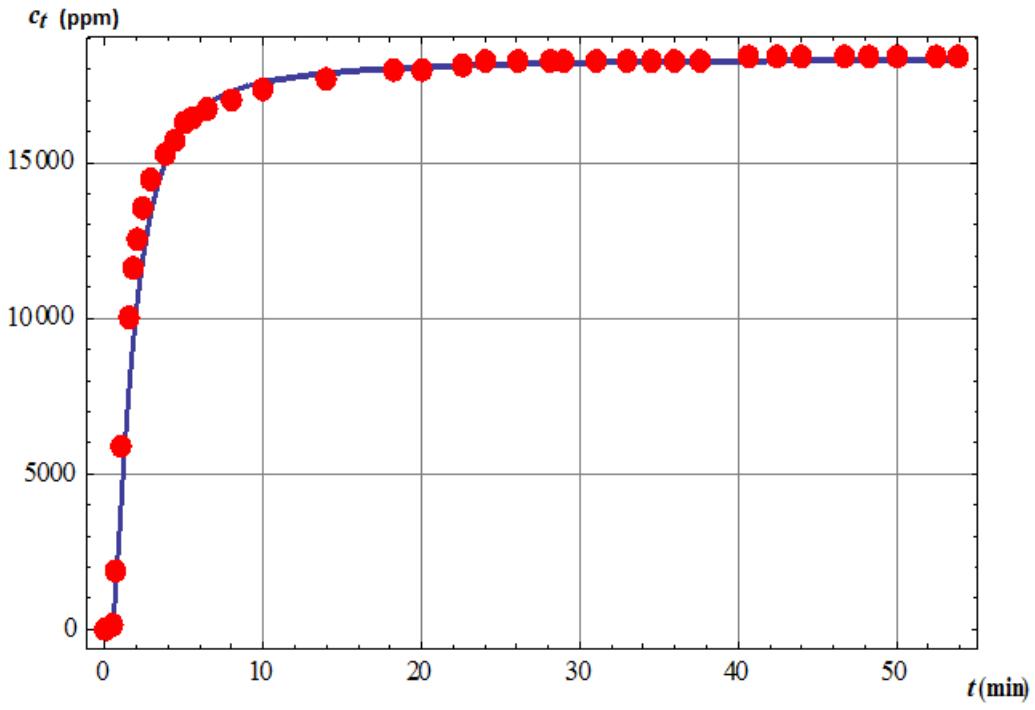

Figure 43 Experimental and dispersion model for CO_2 adsorption

`

CHAPTER 6

CONCLUSIONS AND RECOMMENDATIONS

6.1 Conclusions

A new Ca-Na-Al_2O_3-SiO_2 adsorbent was prepared from low cost raw materials composed of kaolinite and limestone. This material was characterized according to its surface area, morphology, and pore size distribution. Then it was used for adsorption of carbon dioxide from gas stream. The following are the main conclusions drawn from this research work:

1. The produced adsorbent composition was sodium-calcium-aluminosilicate composition and comprised of a mixture of Gehlenite $Ca_2Al(Al_{1.22}Si_{0.78}O_{6.78})OH_{0.22}$ and Stilbite $Na_{5.76}Ca_{4.96}(Al_{15.68}Si_{56.32}O_{144})$ with weight percentage of 43 and 57 respectively, when the hydrothermal reaction was carried out at a constant temperature and pressure of 200 ^{0}C and 15 bar respectively and optimum concentration of NaOH of 36 M. Another produced sample showed the presence of Gehlenite, Stilbite, and Lawsonite $CaAl_2Si_2O_7OH_2(H_2O)$ with weight percentages of 4.1, 7.1, and 88 respectively, obtained at a reaction temperature of 50 ^{0}C, pressure of 4 bar, and sodium hydroxide concentration of 4 M. The mechanism of the hydrothermal reaction of kaolin and limestone mixture in alkali solution can be summarized in three steps; the first step is the dissolution of Al and Si in the kaolinite by OH^- and keeping them in an alkali solution, second step is the formation of aluminosilicate gel and

`

the linking of the calcium and sodium in their structure, and the third step is the crystallization of the gel to form Ca-Na-SiO_2-Al_2O_3 structure.

2. Characterization of the produced adsorbent showed a maximum surface area of 5.8 m^2/g and pore volume of 0.045 cm^3/g with mesoporous structure. The nitrogen adsorption/desorption isotherm showed that the treated adsorbent has narrow and uniform pore size distribution. The BJH pore sized distribution method showed that the produced adsorbent has a higher adsorption cumulative pore volume than raw materials.
3. The produced adsorbent's performance was tested for the removal of CO_2 from a gas stream. A method of adsorption of a sample of CO_2 was carried out by placing a fixed amount of sample in an isothermal column. The CO_2/N_2 mixture was passed over water vapor to gain the desired humidity, and then the mixture was introduced to the column. The concentration of CO_2 at the exit stream was measured at different periods of time. A similar procedure of desorption was carried out by introducing N_2 to the column. For a given mass of sample of 10 g, an initial flow rate and concentration of CO_2 of 4 L/min and 1630 ppm, respectively, the breakthrough adsorption curves showed that the produced sample took about 55 min to get saturated with CO_2 with an adsorption capacity of 2.79 mmol/g, while limestone and kaolin took 0.27 and 0.23 min respectively to reach the same saturated value with an adsorption capacity of 0.013 mmol/g.
4. The effect of humidity was tested to investigate the effect of water molecules on the adsorption performance. It was noticed that by increasing the humidity up to 55%, the breakthrough time required to achieve the saturation capacity increased. However, further increase in humidity resulted in lowering the adsorption capacity

`

as a result of competitive adsorption between CO_2 and water molecules on the adsorbent surface.

5. The adsorption of CO_2 by the treated samples follows the chemisorption process where a chemical reaction between the CO_2 and the surface took place. This adsorption was enhanced with increasing bed temperature which suggests an endothermic nature at the surface of the produced samples. Although the increasing of the temperature makes the gas molecules active energized and harder to be adsorbed, with an increase in the flow rate and negligible effect of pressure, this effect will disappear. Additionally, increasing the temperature will increase the rate of the reaction on the surface of the adsorbent. The obtained experimental data were fitted according to axial dispersion model with assumptions that the system is uniform in temperature and has a constant pressure drop, the radial dispersion is negligible, and the surface reaction, adsorption, and initial diffusion resistances are involved in chemical adsorption. The model was solved using the finite difference method by MATHEMATICA V.9 software and found that effective diffusivity and reaction constants have a noticeable effect on the rate of adsorption. The effective diffusivity was calculated to be $2.8*10^{-3}$ cm^2/s. The value of ΔH (+144 kJ/mol) confirmed that the chemical adsorption is dominant and the adsorption process was endothermic in nature. The positive value of ΔS (444 kJ/mol) confirmed the randomness and the disorder during the adsorption process at solid/gas interface. By increasing the temperature, the adsorption process becomes more spontaneous and the value of ΔG becomes negative.

`

6. The produced adsorbent was tested after several regeneration cycles with 14 M NaOH and it was found that its capacity increases with an increase in the regeneration cycles as a result of more Na oxide linked aluminosilicate structure with the treatment of NaOH. When the initial concentration was 1.87% and the flow rate was 4 L/min, the maximum adsorption capacity after fifth regeneration cycle was 4.7 mmol/g, which is twice the adsorption capacity after the first regeneration. The weight percentages of Na in the produced adsorbent after the first and fifth regeneration are 12.07 and 21.23, respectively.
7. The produced adsorbent has a number of significant practical advantages over other adsorbents. It is naturally available and inexpensive relative to other solid adsorbents. Despite its low surface area, it has a high adsorption capacity when compared with others at the same operational conditions. It is regenerable as its adsorption capacity increases after several regeneration cycles, and its performance can be enhanced with increasing humidity. Thus the produced adsorbent can be commercially and economically viable in industry.

`

6.2 Recommendations

The recommendations of great value to this work would be the following:

1. The same experimental procedure can be done for adsorption/desorption of the other gases which may be found in natural gas such as H_2S. It is also recommended to perform the experiments for competitive adsorption/desorption of CO_2, CH_4, and H_2S.
2. It is recommended to perform experiments on treated kaolin adsorbent with different particle sizes to study the effect of this factor on adsorption capacity. It is also important to study the effect of the adsorption column diameter.
3. The method of treatment can be changed using different types of alkaline solutions with different amounts.
4. In-depth pilot scale experiment using the same working conditions should be conducted similarly with the previous method to design the scale up.

`

APPENDIX

Appendix A: CO_2 uptake Graph

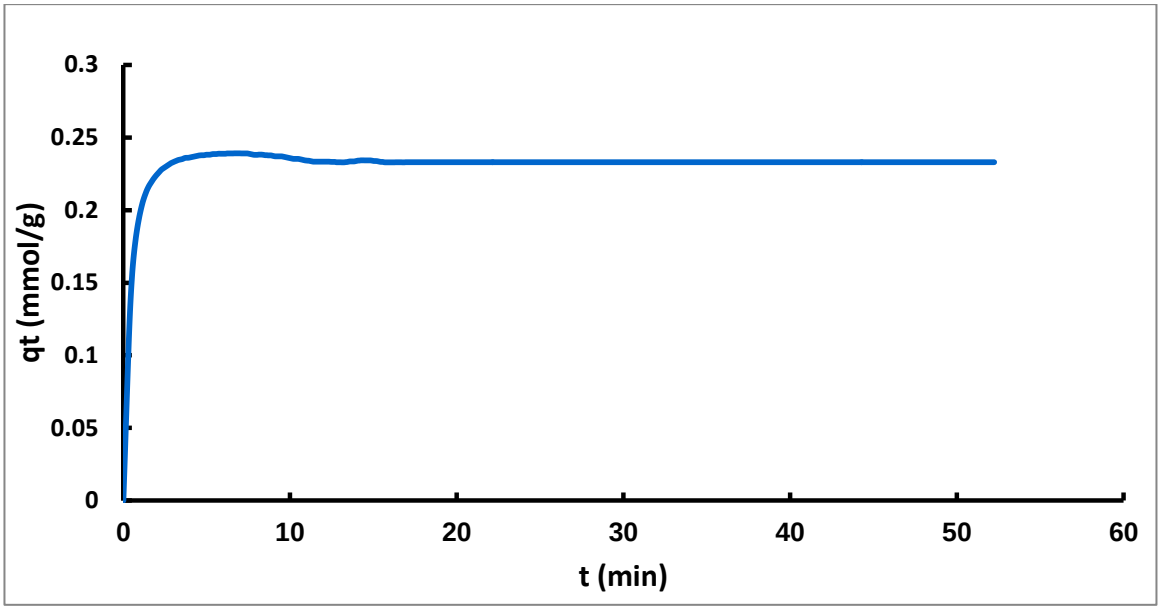

Figure 44 CO_2 uptake of treated kaolin (4 L/min, 19140 ppm, 20% RH,15 C).

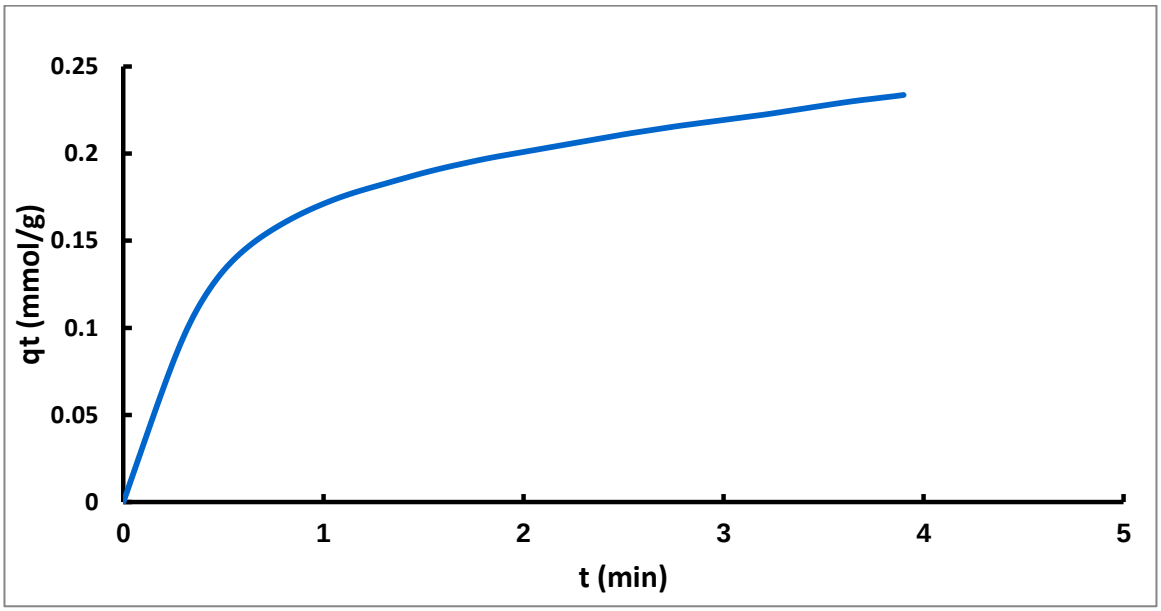

Figure 45 CO_2 uptake of treated kaolin (4 l/min, 18710 ppm, 20% RH,25 C).

`

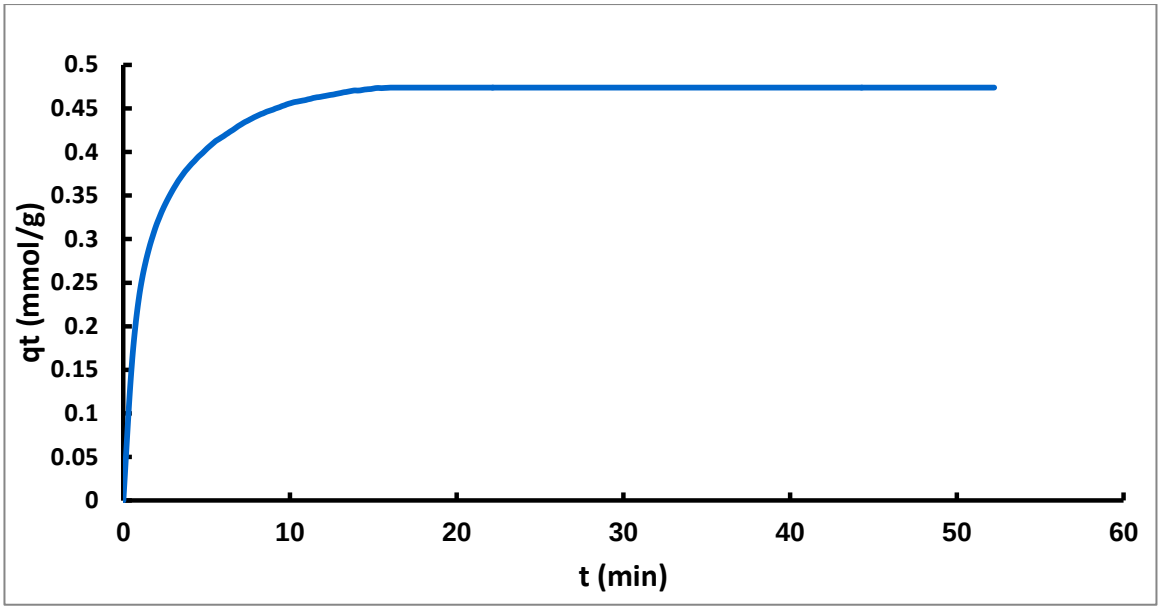

Figure 46 CO_2 uptake of treated kaolin (4 l/min, 18350 ppm, 20% RH,35 C).

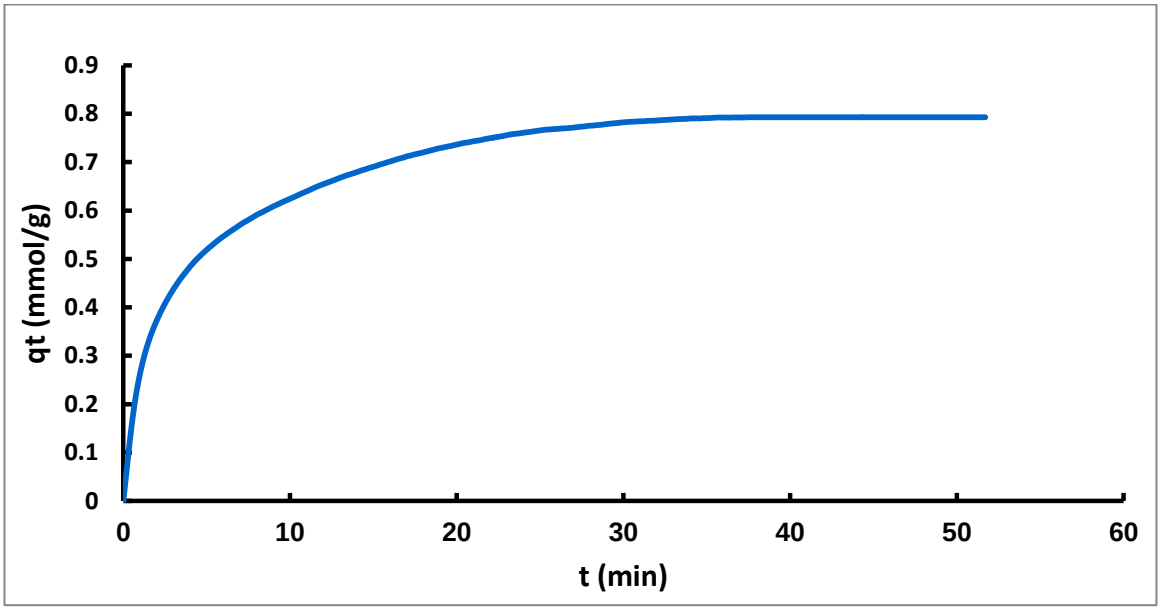

Figure 47 CO_2 uptake of treated kaolin (4 l/min, 18140 ppm, 20% RH,50 C).

`

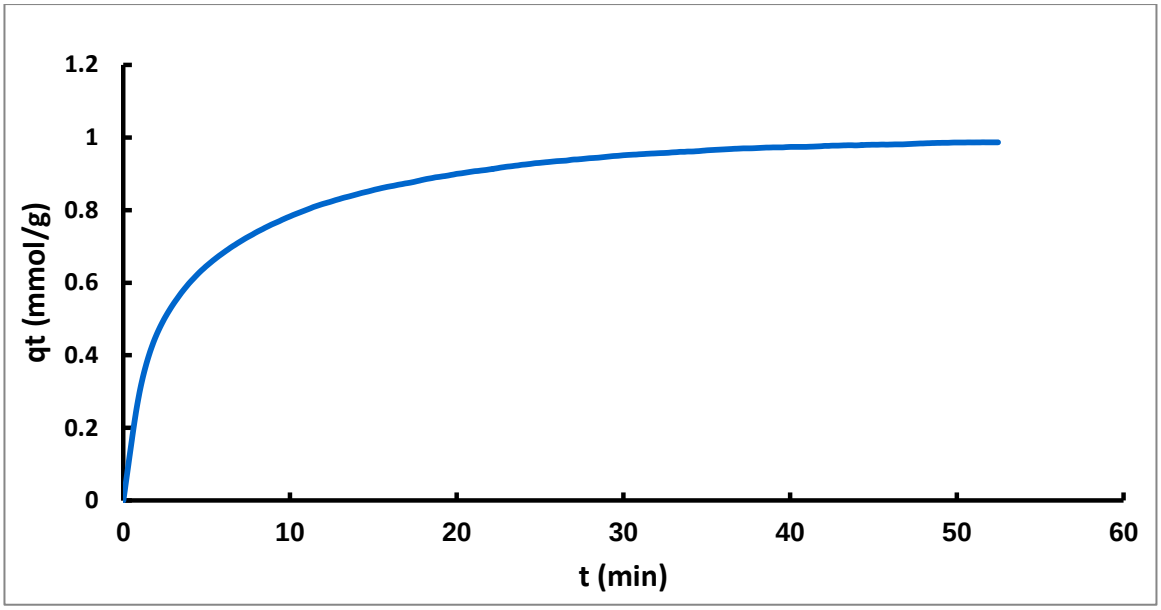

Figure 48 CO_2 uptake of treated kaolin (4 l/min, 18420 ppm, 20% RH,60 C).

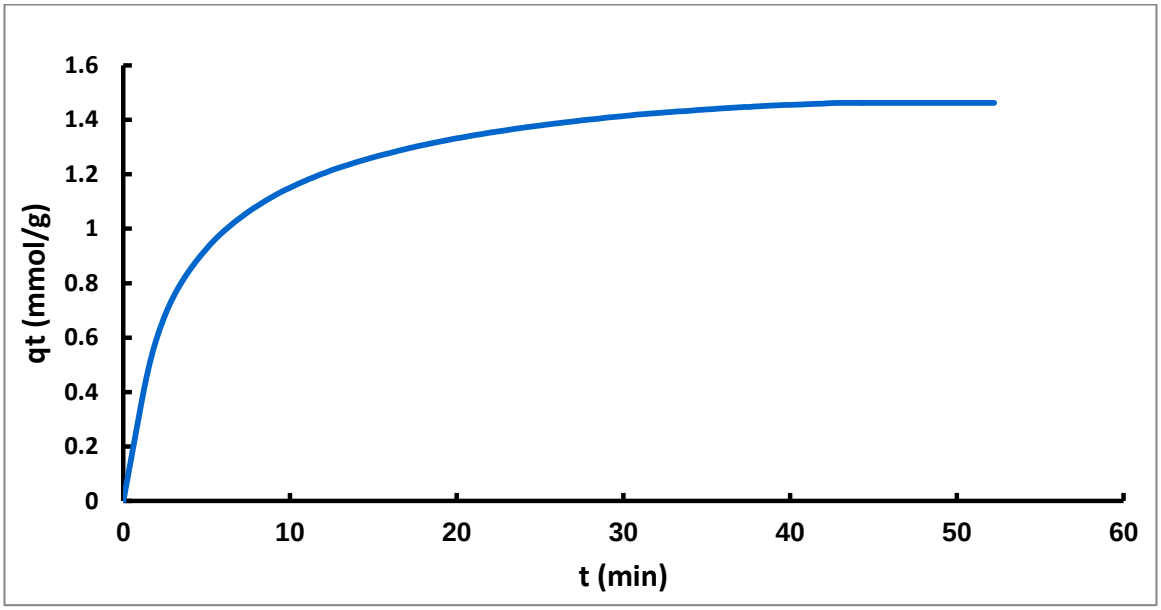

Figure 49 CO_2 uptake of treated kaolin (4 l/min, 18710 ppm, 20% RH,70 C).

`

Appendix B: CO_2 Adsorption/Desorption Graph

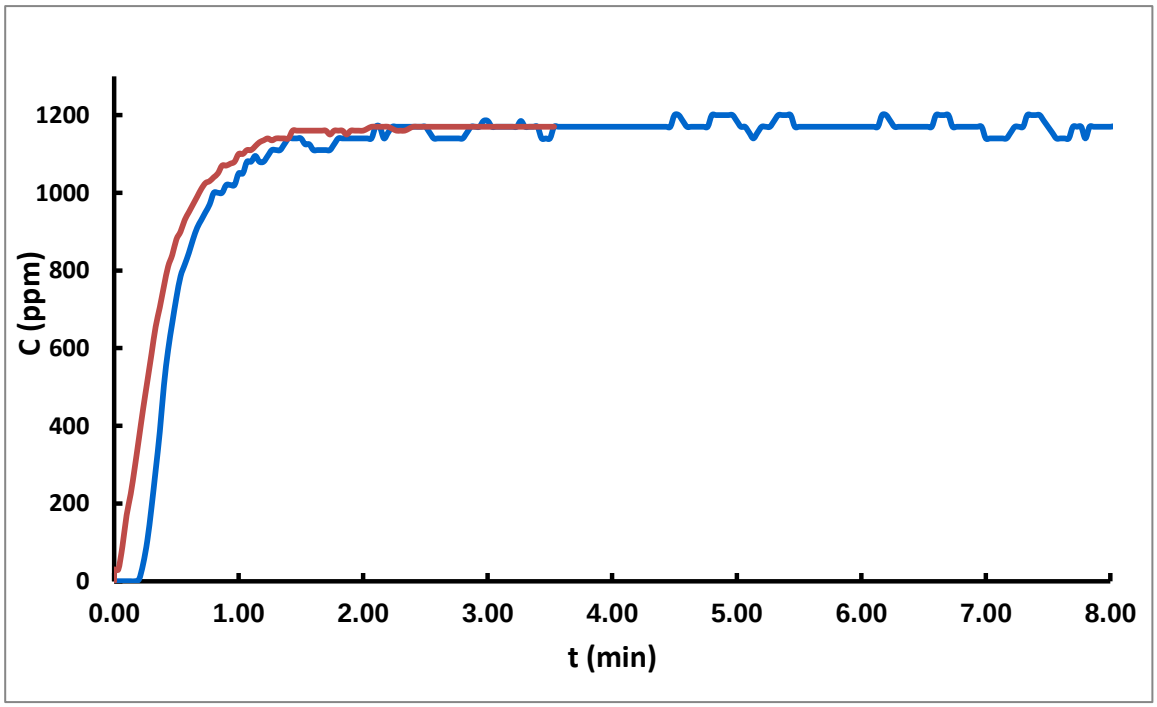

Figure 50 Adsorption-desorption curve for raw kaolin at %RH = Low, Conc= 1200ppm, flowrate= 4 L/min and Temp=25 C.

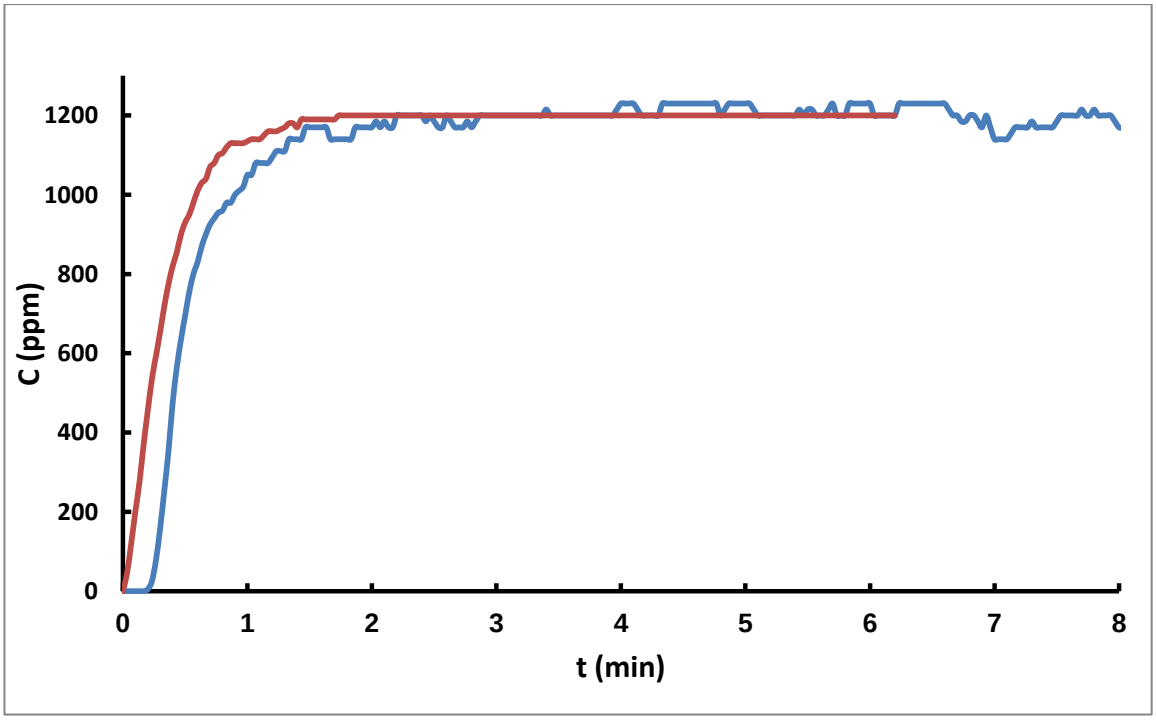

Figure 51 Adsorption-desorption curve for raw limestone at %RH = Low, Conc= 1200ppm, flowrate= 4 L/min and Temp=25 C.

`

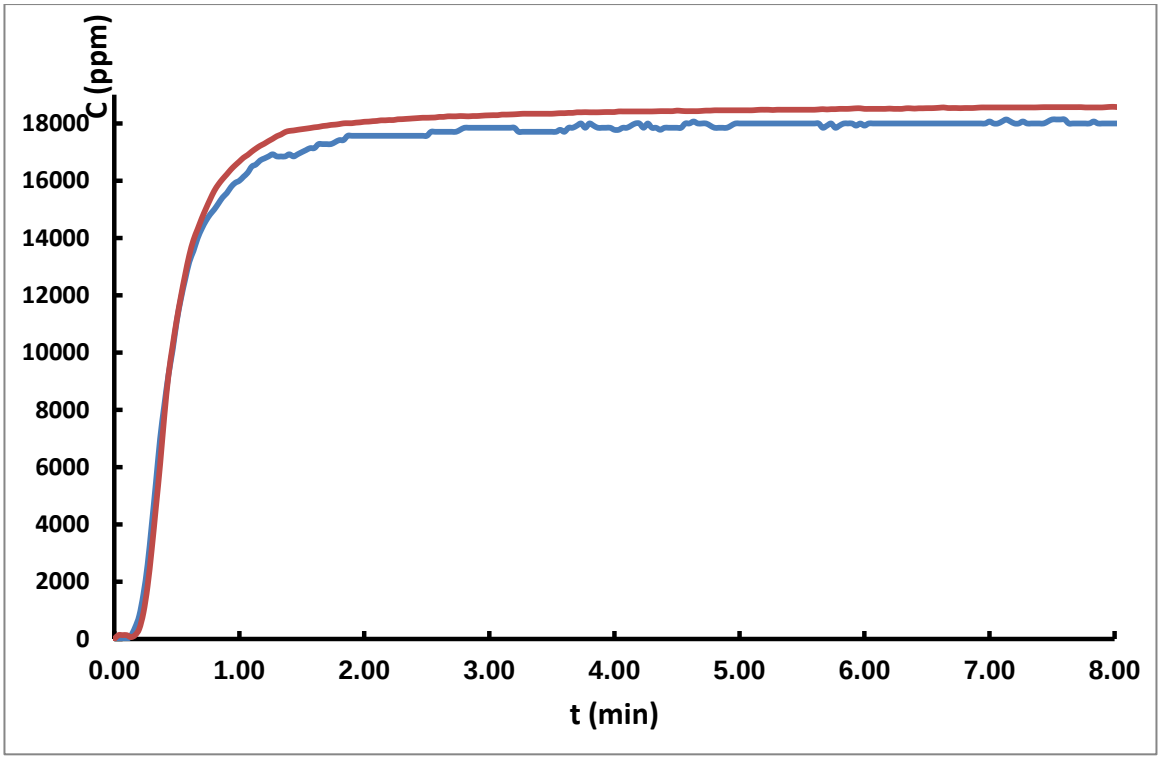

Figure 52 Adsorption-desorption curve for treated kaolin at fresh regeneration cycle.

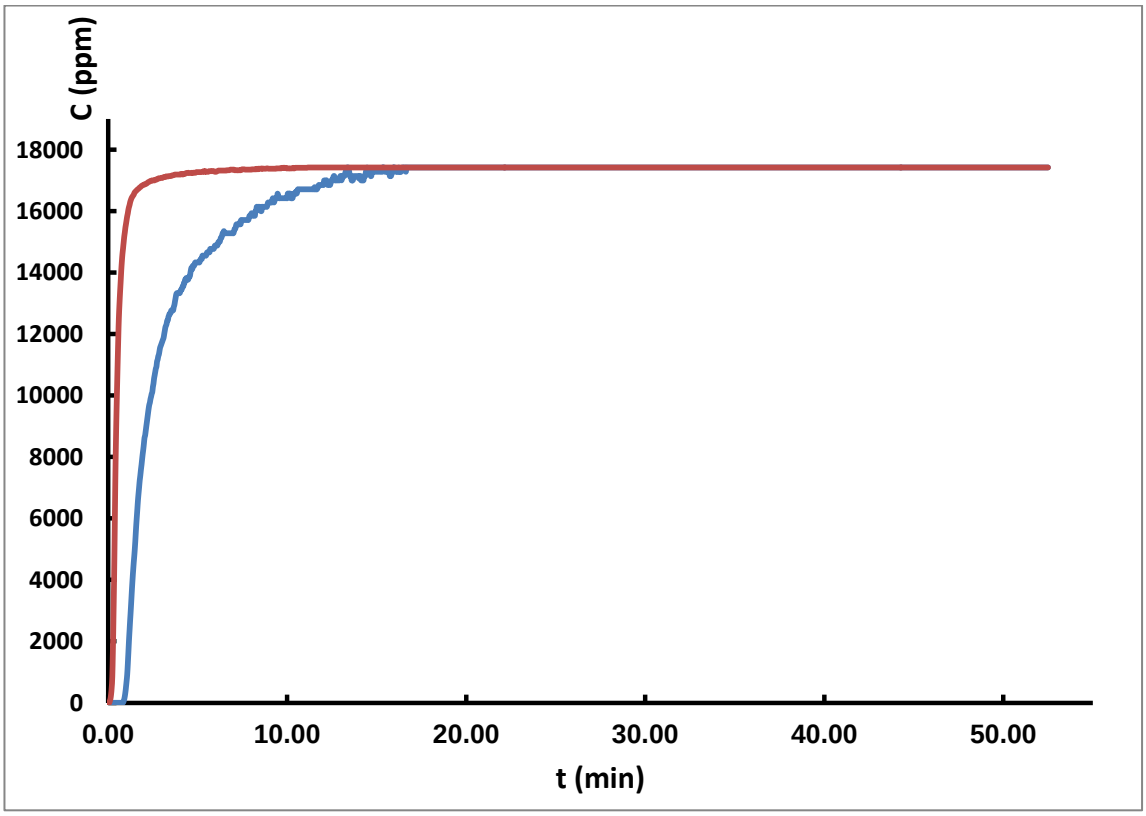

Figure 53 Adsorption-desorption curve for treated kaolin at first regeneration cycle.

`

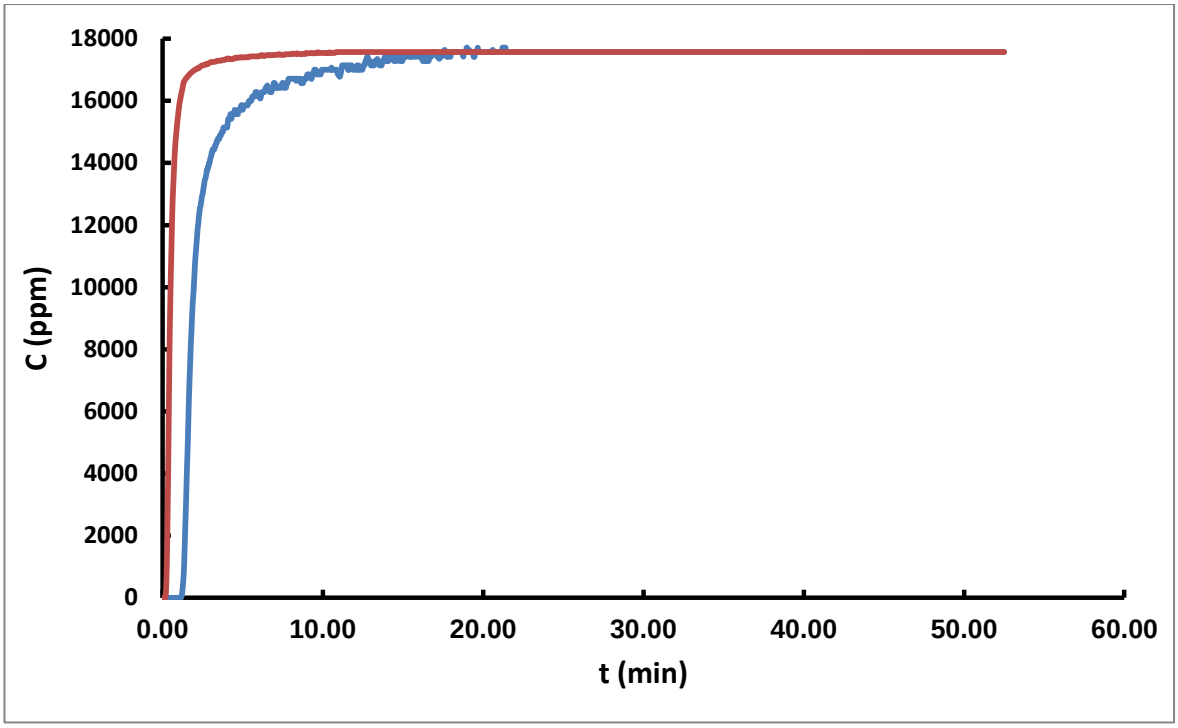

Figure 54 Adsorption-desorption curve for treated kaolin at second regeneration cycle.

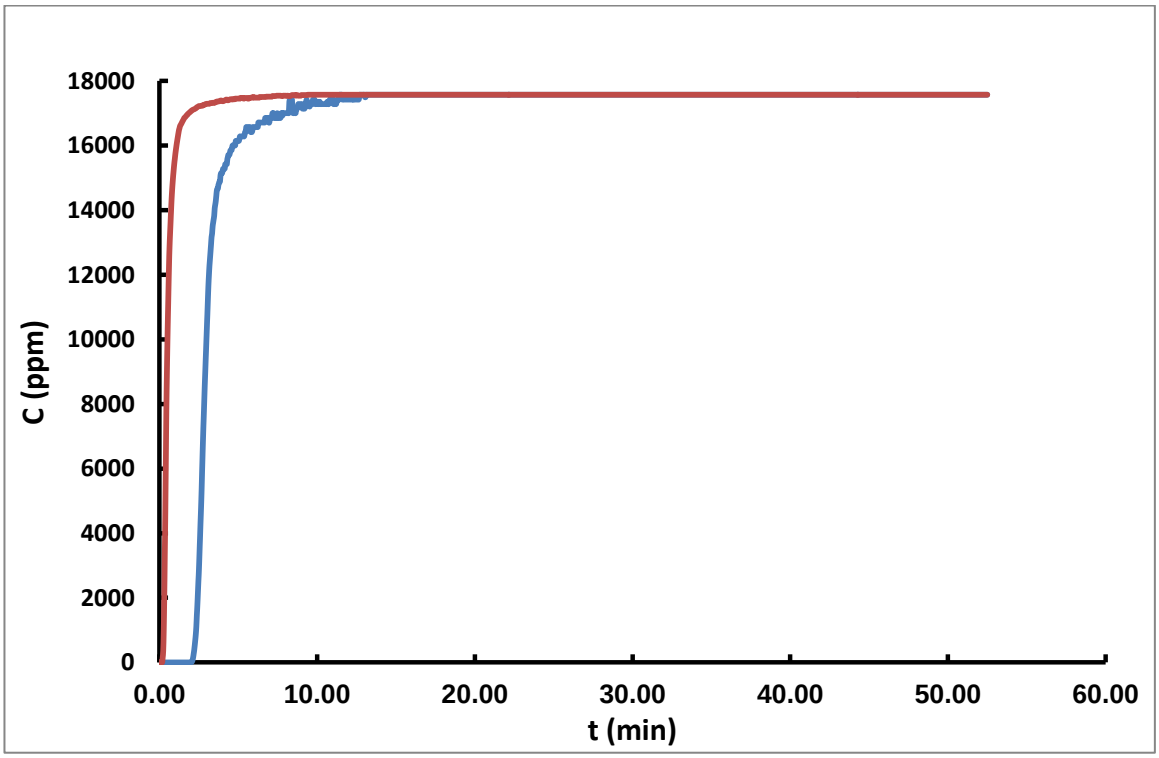

Figure 55 Adsorption-desorption curve for treated kaolin at third regeneration cycle.

`

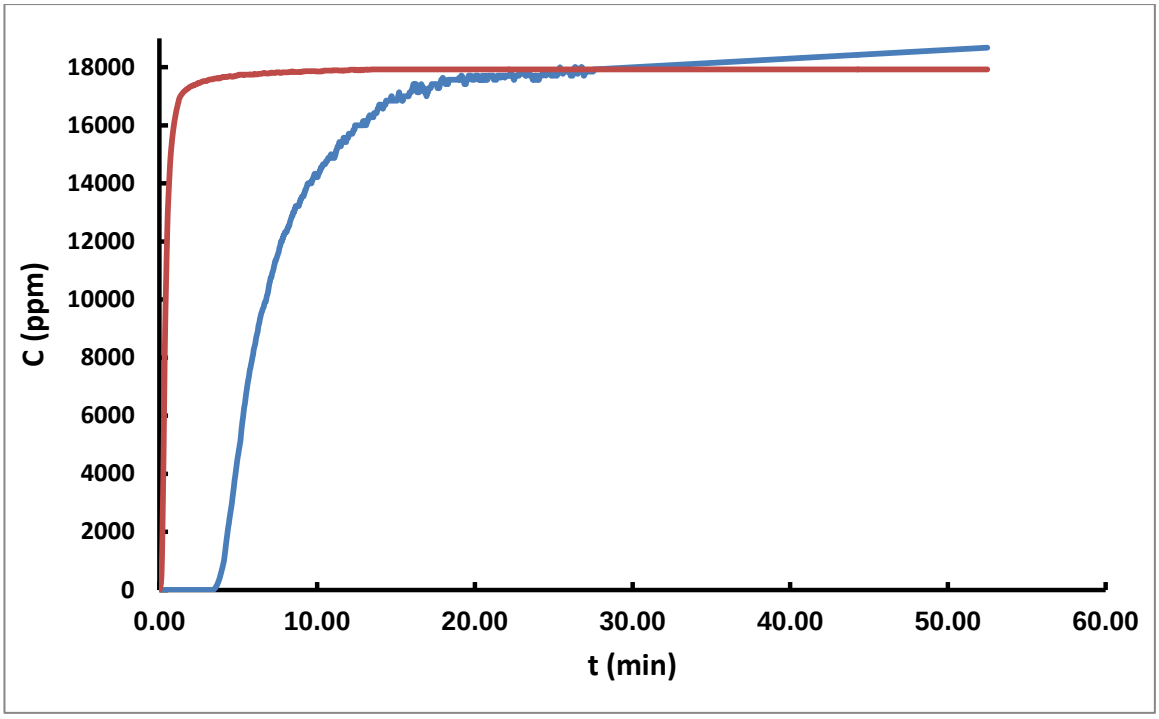

Figure 56 Adsorption-desorption curve for treated kaolin at fourth regeneration cycle.

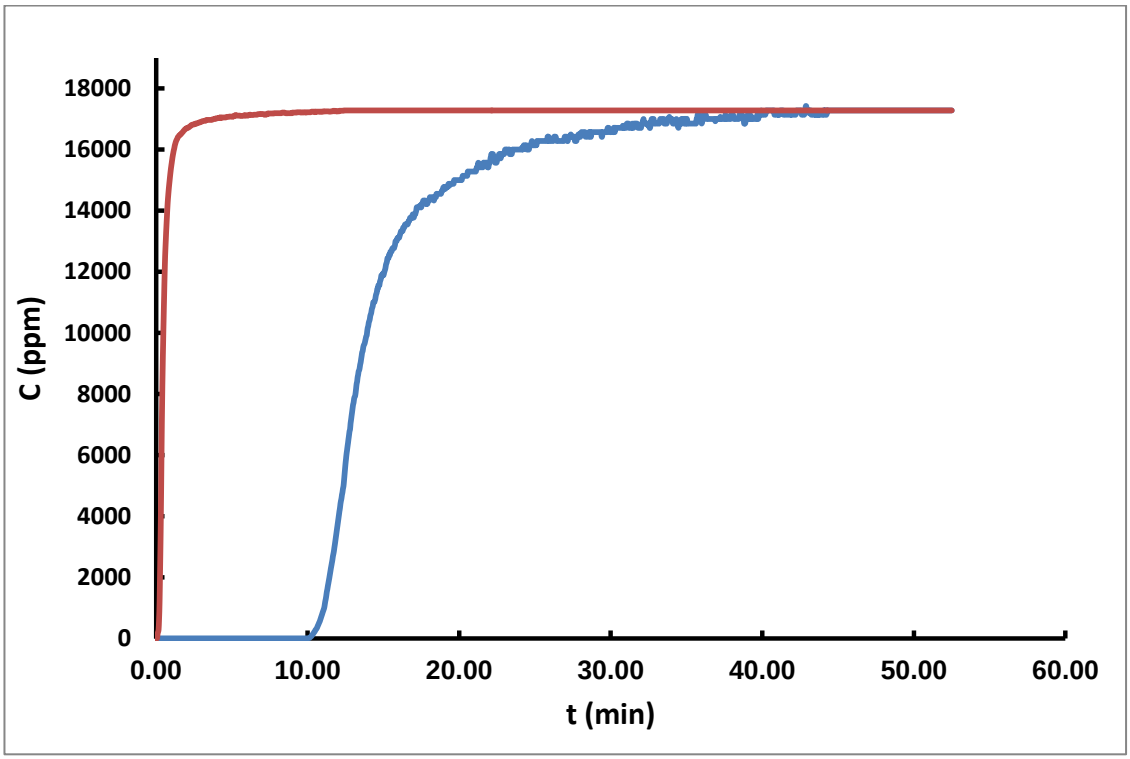

Figure 57 Adsorption-desorption curve for treated kaolin at fifth regeneration cycle.

`

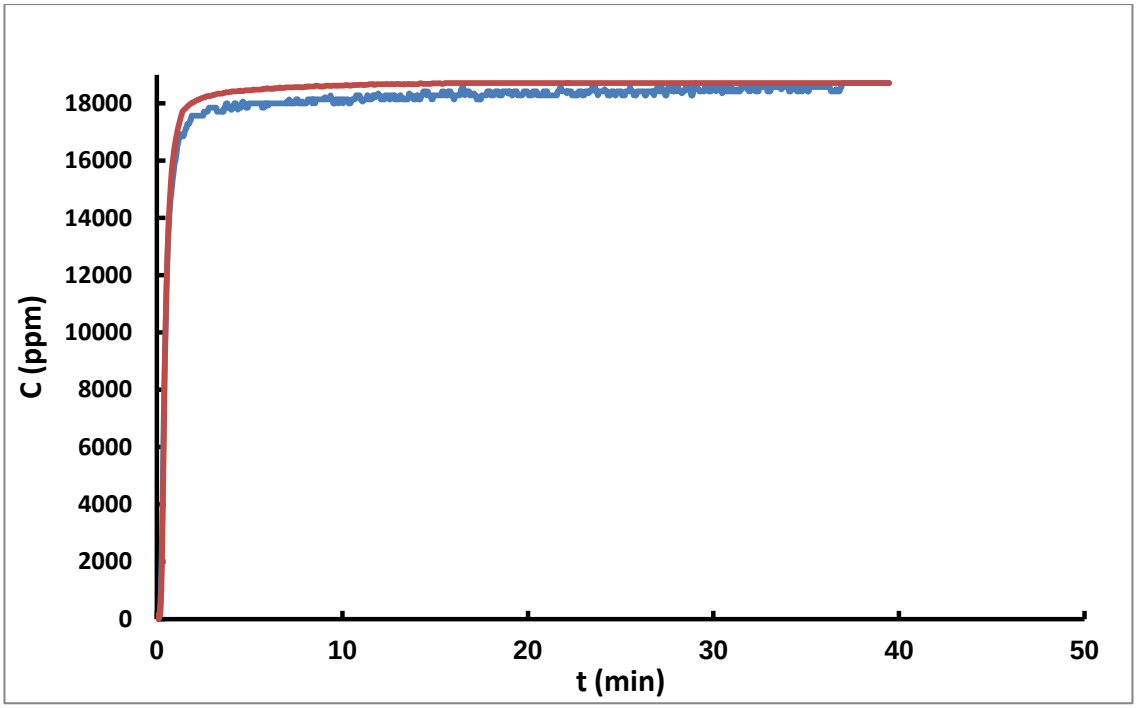

Figure 58 Adsorption-desorption curve for treated kaolin at low humidity.

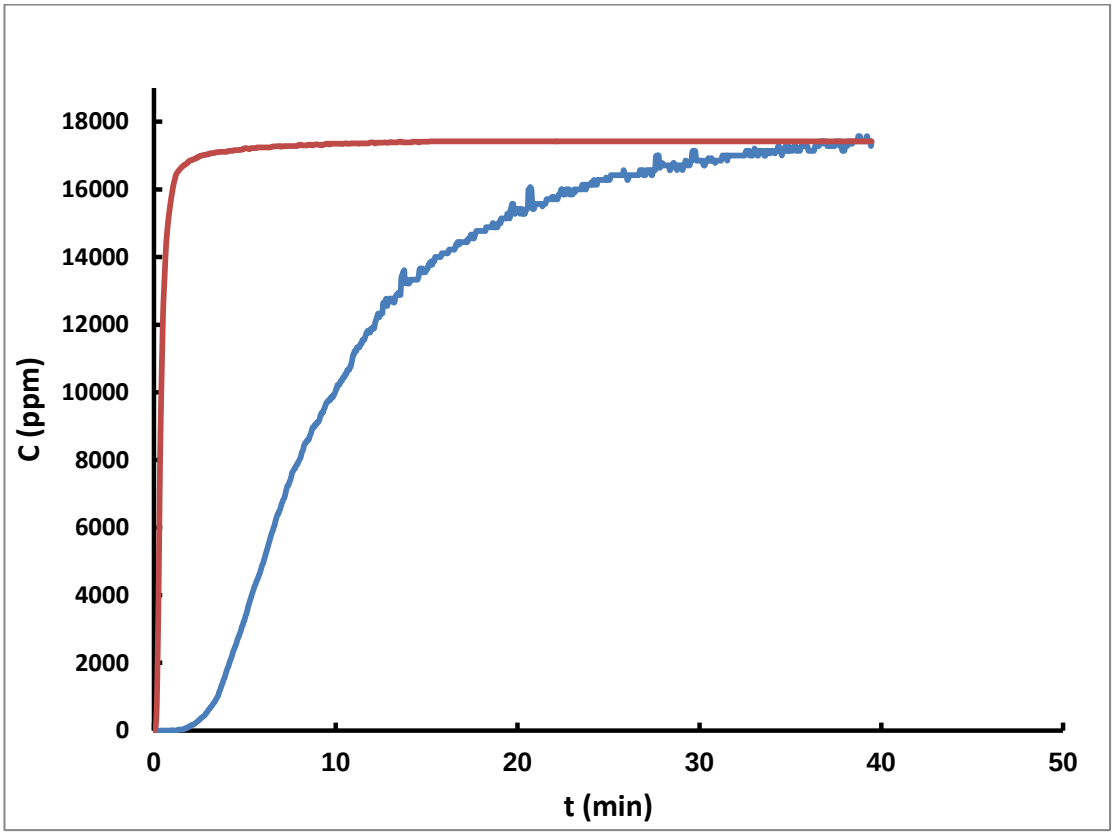

Figure 59 Adsorption-desorption curve for treated kaolin at high humidity.

`

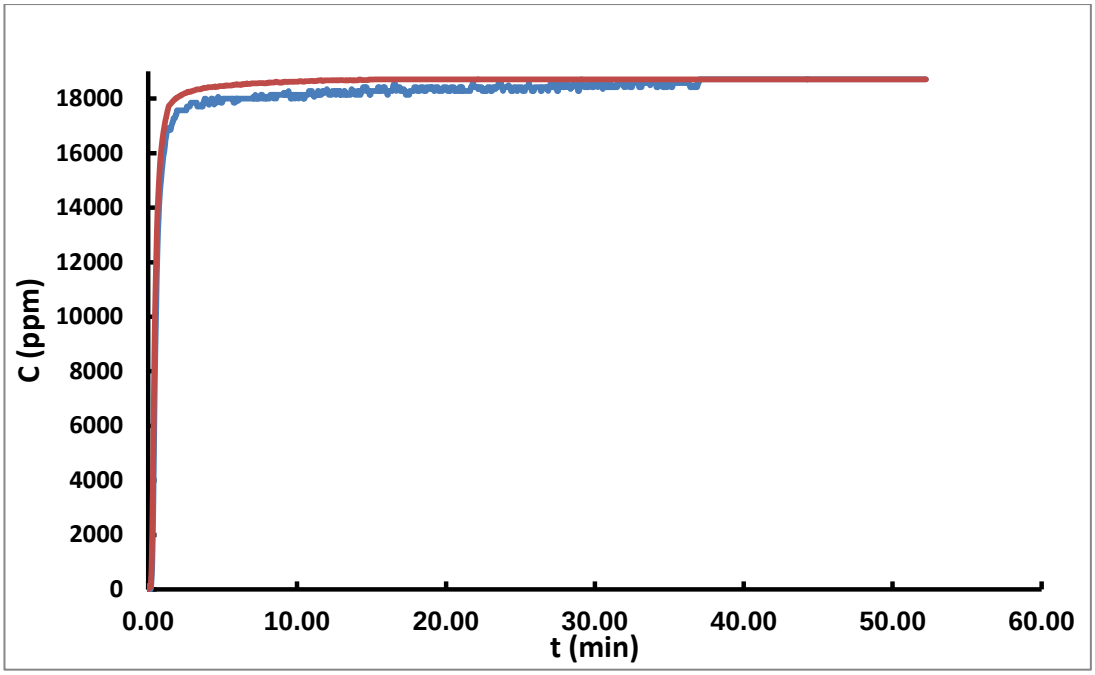

Figure 60 Adsorption-desorption curve for treated kaolin at 5 C.

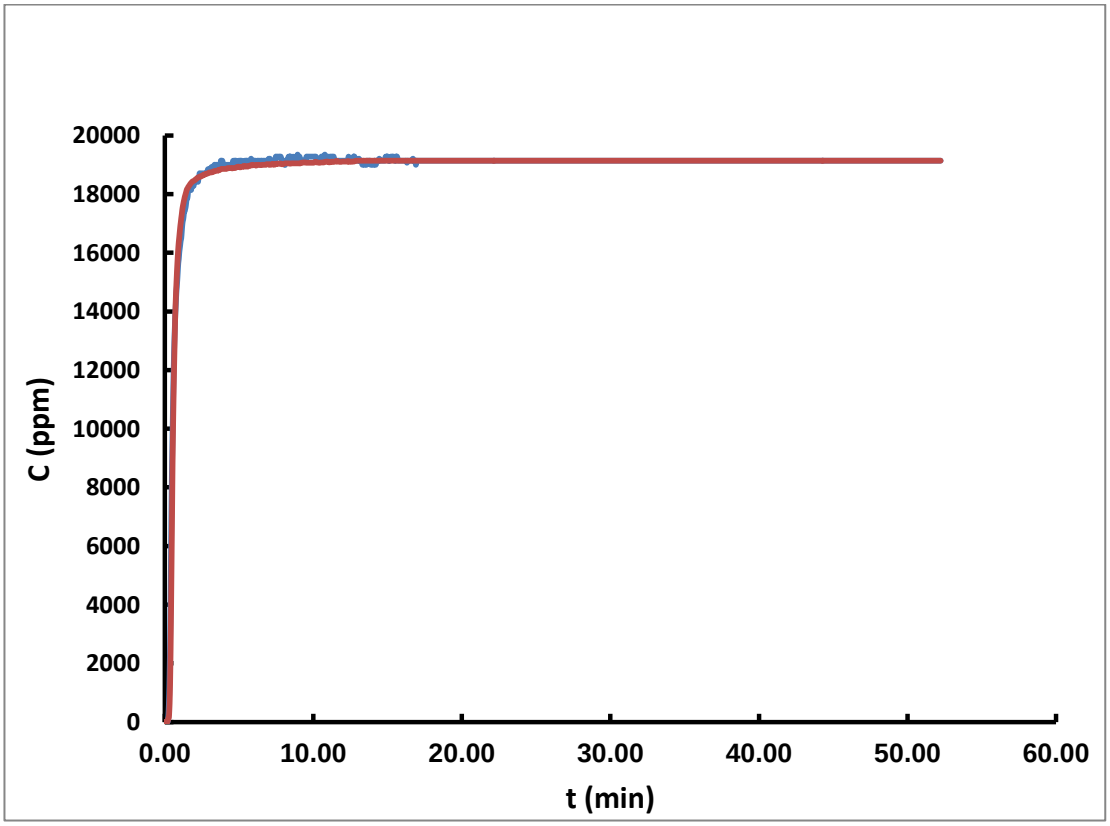

Figure 61 Adsorption-desorption curve for treated kaolin at 15 C.

`

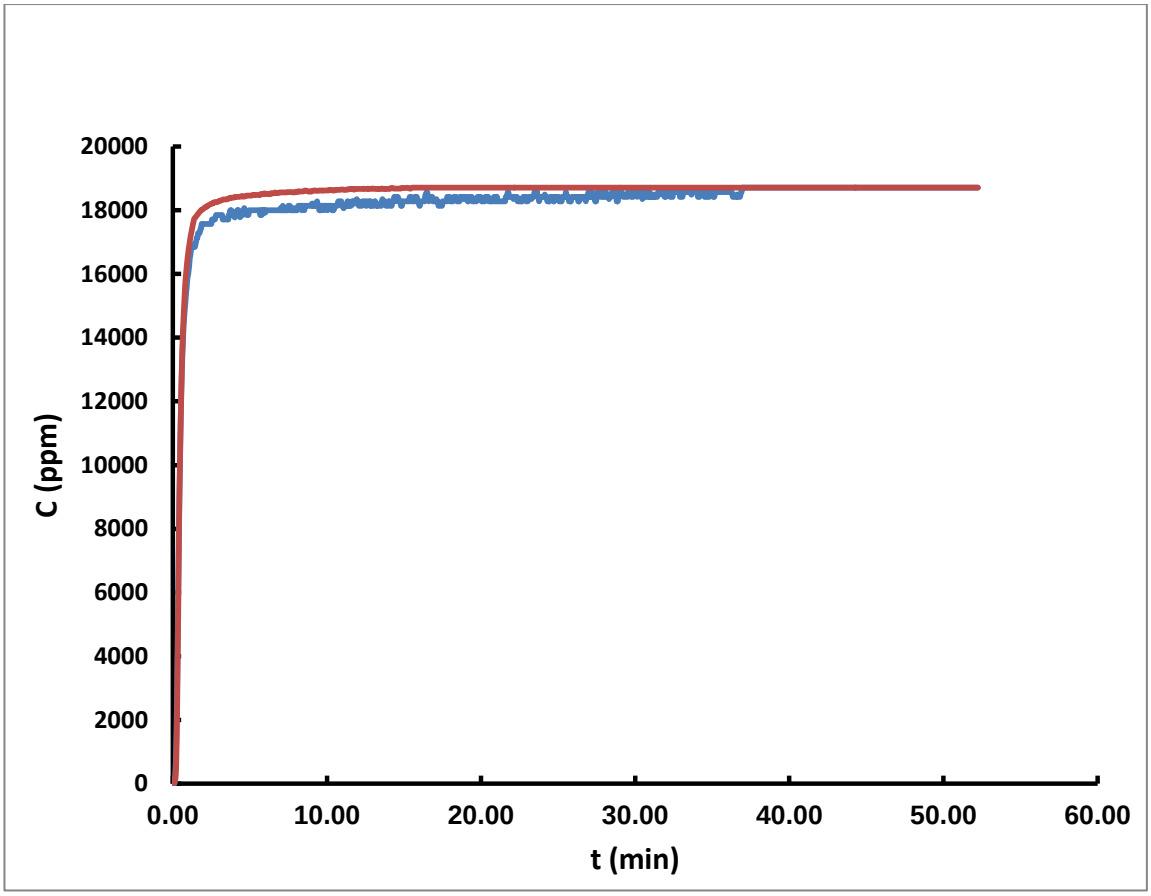

Figure 62 Adsorption-desorption curve for treated kaolin at 25 C.

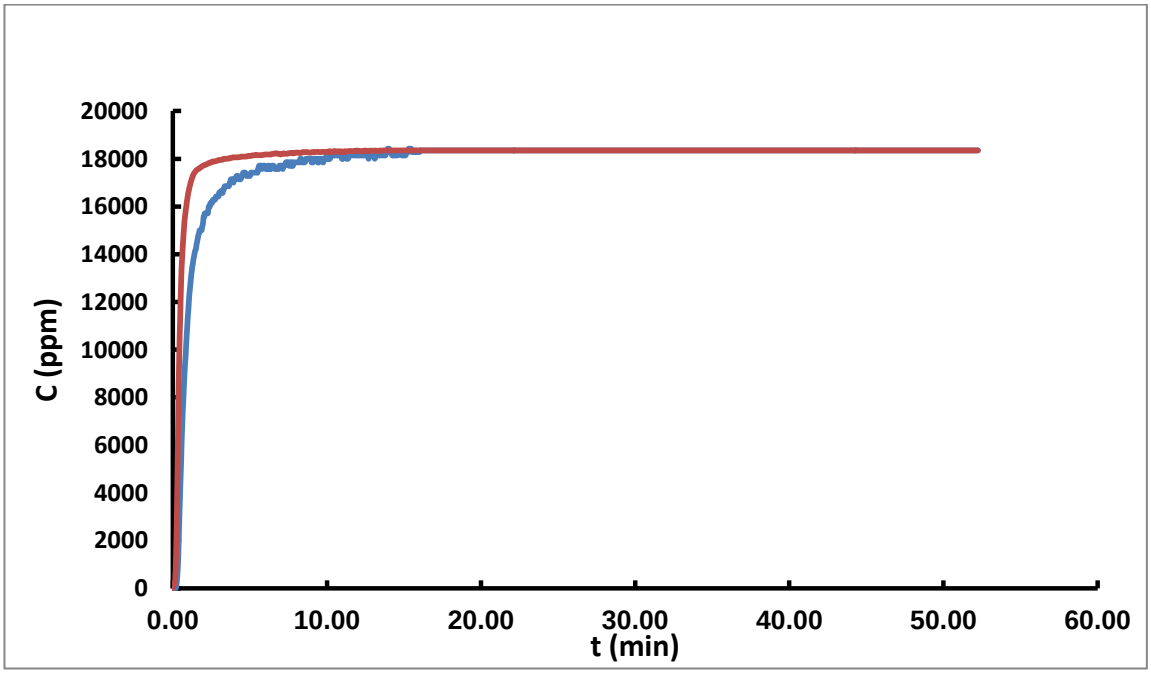

Figure 63 Adsorption-desorption curve for treated kaolin at 35 C.

`

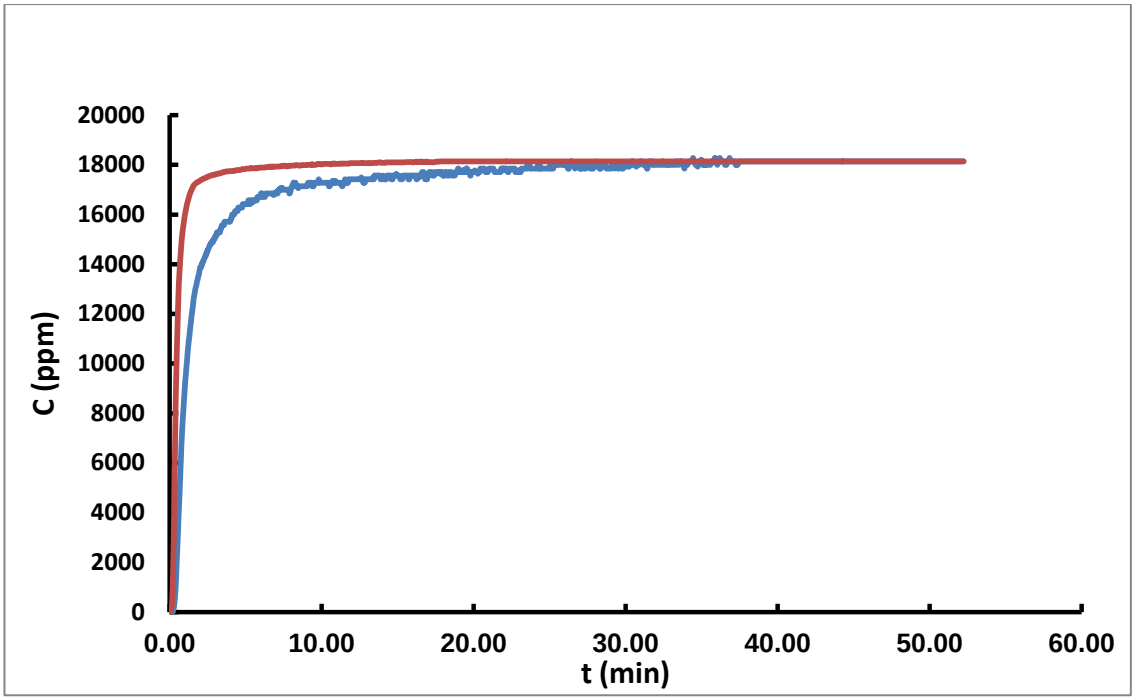

Figure 64 Adsorption-desorption curve for treated kaolin at 50 C.

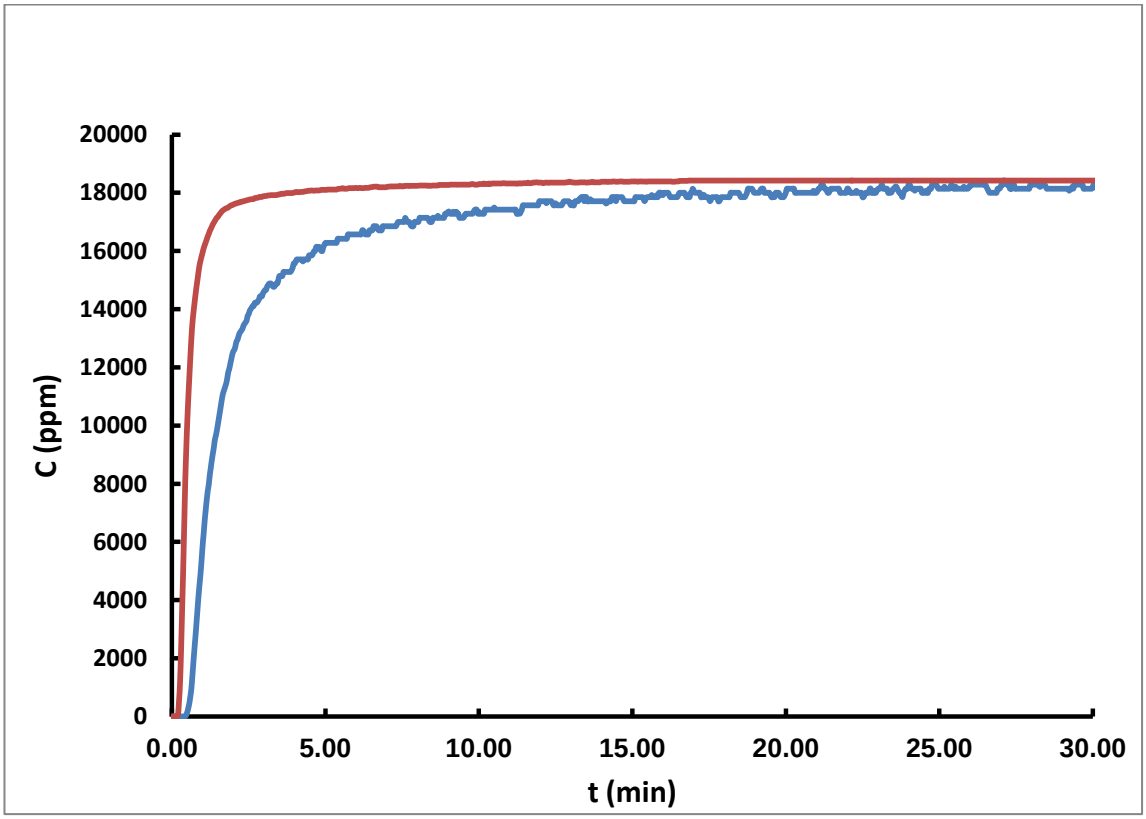

Figure 65 Adsorption-desorption curve for treated kaolin at 60 C.

`

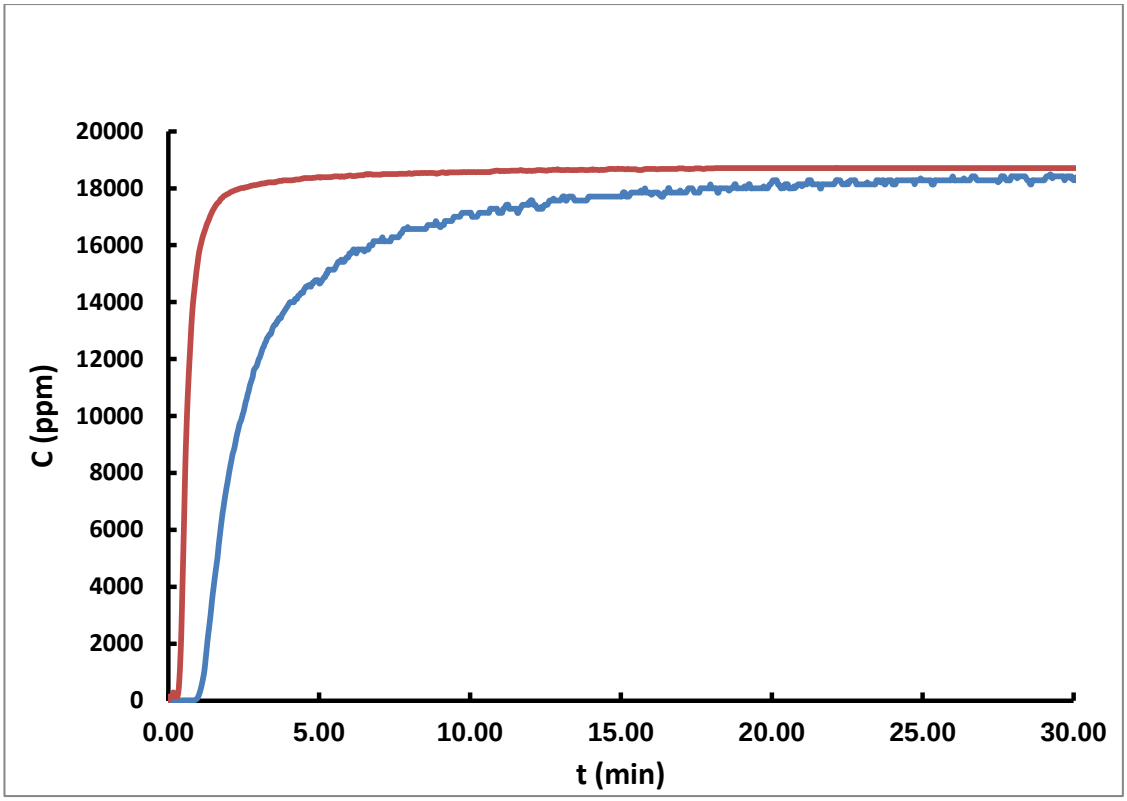

Figure 66 Adsorption-desorption curve for treated kaolin at 70 C.

`

Appendix C: Breakthrough curve analysis

Table 10 Residence time calculations.

t (s)	C(t) g/cm3	E(t) 1/min	t E(t)
5714	890	8.7063E-05	0.497477
5716	890	8.7063E-05	0.497651
5718	890	8.7063E-05	0.497825
5720	895	8.7552E-05	0.500797
5722	890	8.7063E-05	0.498173
5724	900	8.8041E-05	0.503947
5726	900	8.8041E-05	0.504123
5728	900	8.8041E-05	0.504299
5730	900	8.8041E-05	0.504475
5732	900	8.8041E-05	0.504651
5734	900	8.8041E-05	0.504827
5736	900	8.8041E-05	0.505003
5738	900	8.8041E-05	0.505179
5740	900	8.8041E-05	0.505355
5742	900	8.8041E-05	0.505531
5744	900	8.8041E-05	0.505708
5746	900	8.8041E-05	0.505884

`

Table 11 Adsorption capacity calculations sample.

t(min)	C(t)	1-C(t)/C0	INTEGRATION tq	Capacity mmol/g
0	0	1	0	0
0.033333	0	1	0.033333333	0.011117053
0.066667	0	1	0.066666667	0.022234106
0.1	0	1	0.1	0.033351159
0.133333	120	0.993586317	0.133226439	0.044432561
0.166667	410	0.978086585	0.166087654	0.055392157
0.2	820	0.956173169	0.198325316	0.066143791
0.233333	1575	0.915820417	0.229525209	0.076549317
0.266667	2605	0.860769642	0.259135044	0.08642454
0.3	4000	0.786210583	0.286584714	0.095579323
0.333333	5465	0.707910208	0.311486727	0.103884433
0.366667	6995	0.626135756	0.333720827	0.111299762
0.4	8155	0.564136825	0.353558703	0.117915924
0.433333	9220	0.507215393	0.371414573	0.123871064
0.466667	10090	0.460716195	0.387546766	0.129251337
0.5	11105	0.40646713	0.401999822	0.134071598
0.533333	11885	0.364778193	0.414853911	0.138358586
0.566667	12550	0.329235703	0.426420809	0.14221628
0.6	13165	0.29636558	0.436847497	0.145693702
0.633333	13550	0.275788348	0.446383396	0.148874034
0.666667	13995	0.252004276	0.455179939	0.151807784
0.7	14330	0.234099412	0.463281668	0.154509804
0.733333	14605	0.21940139	0.470840014	0.1570306
0.766667	14825	0.207642972	0.47795742	0.159404337
0.8	15000	0.198289685	0.484722965	0.161660725
0.833333	15210	0.18706574	0.491145555	0.163802733
0.866667	15420	0.175841796	0.497194014	0.165819964
0.9	15570	0.167824693	0.502921789	0.167730244
0.933333	15780	0.156600748	0.508328879	0.169533571

`

Appendix D: Experimental and dispersion model for CO_2 adsorption.

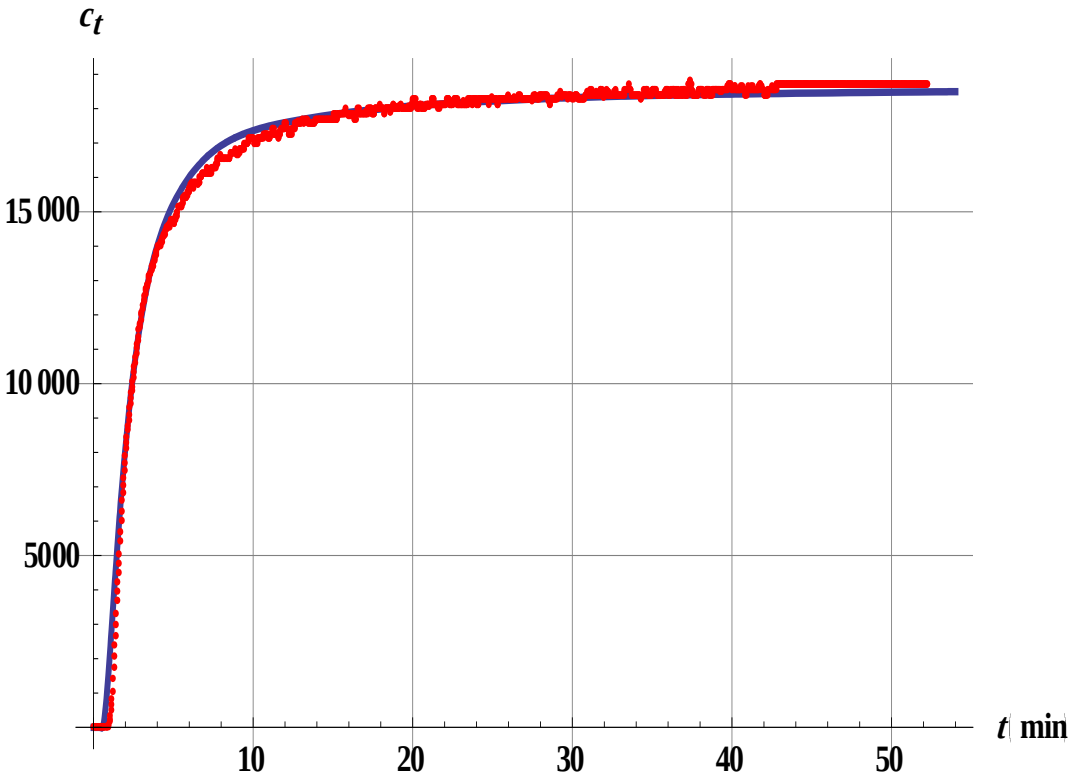

Figure 67 Experimental and dispersion model isotherm for CO_2 adsorption (70 C).

`

References

[1] J. Albo, P. Luis, A. Irabien, Carbon Dioxide Capture from Flue Gases Using a Cross-Flow Membrane Contactor and the Ionic Liquid 1-Ethyl-3-methylimidazolium Ethylsulfate, Ind. Eng. Chem. Res., 49, (2010), 11045-11051.

[2] D.J. Hofmann, J.H. Butler, P.P. Tans, A new look at atmospheric carbon dioxide, Atmos. Environ., 43 (2009), pp. 2084–2086

[3] Taub, D. (2010) Effects of Rising Atmospheric Concentrations of Carbon Dioxide on Plants. Nature Education Knowledge 3(10):21

[4] IPCC. Climate Change 2007: The Physical Science Basis. Contribution of Working Group I to the Fourth Assessment Report of the Intergovernmental Panel on Climate Change. Cambridge, UK: Cambridge University Press, 2007.

[5] A. Sayari, Y. Belmabkhout, R. Serna, Flue gas treatment via CO2 adsorption, Chem. Eng. Jo. 171 (2010) 760-774

[6] T. Dantas, A. Rodrigues, R. Moreira, Separation of carbon dioxide from flue gas using adsorption on porous solids, Greenhouse Gases - Capturing, Utilization and Reduction, Dr Guoxiang Liu (Ed.), ISBN: 978-953-51-0192-5, InTech, DOI: 10.5772/31917.

[7] M. Wanga, A. Lawala, P. Stephensonb, J. Siddersb, C. Ramshawa, H. Yeunga, Post-combustion CO2 Capture with Chemical Absorption: A State-of-the-art Review, Chem. Eng. Res. Desi. 89 (2011) 1609-1624

[8] Kvamsdal HM, Jakobsen JP, Hoff KA. Dynamic modelling and simulation of a CO2 absorber column for post combustion CO2 capture. Chem Eng Process 2008. doi:10.1016/j.cep.2008.03.00.

[9] A. Lawal, M. Wanga, P. Stephensonb, H. Yeung, Dynamic modelling of CO2 absorption for post combustion capture in coal-fired power plants, Fuel 88 (2009) 2455–2462.

[10] Kenig EY, Schneider R, Górak A. Reactive absorption: optimal process design via optimal modelling. Chem Eng Sci 2001;56(2):343–50

`

[11] A. Aroonwilas, A. Veawab, Characterization and comparison of the CO2 absorption performance into single and blended Alkanolamines in a packed column, Ind. Eng. Chem. Res. 2004, 43, 2228-2237.

[12] E. Keskes, C. Adjiman, A. Galindo, G. Jackson, A physical absorption process for the capture of CO2 from CO2 rich natural gas sreams,

[13] T. Rufford, S. Smart, G. Watson, B. Graham, J. Boxall, J. Costa, E. May, The removal of CO2 and N2 from natural gas: A review of conventional and emerging process technologies, of Petroleum Science and Engineering 94-95 (2012) 123–154.

[14] IEA GHG(1993), The capture of carbon dioxide from fossil fuel fired power stations. eltenham, UK: IEA GHG; IEA GHG/SR2.

[15] Xin, Haoliang, Deliang, Jingtian, Ying, Huiling, Yueping, Yuehua, Zhua, Adsorption of CO2 on heterostructure CdS(Bi2S3)/TiO2 nanotube hotocatalysts and their photocatalytic activities in the reduction of CO2 to methanol under visible light irradiation, Chemical Engineering Journal 180 (2012) 151– 158.

[16] Dincă , Dailly ,Liu , Brown ,Neumann , Long, Hydrogen Storage in a Microporous Metal−Organic Framework with Exposed Mn2+ Coordination Sites, J. Am. Chem. Soc., 2006, 128 (51), pp 16876–16883

[17] Yaghi, Guangming, Hailian, Selective binding and removal of guests in a microporous metal–organic framework, Nature 378, 703 - 706 (14 December 1995); doi:10.1038/378703a0.

[18] A.R. Millward, O.M. Yaghi, Metal-organic frameworks with exceptionally high capacity for storage of carbon dioxide at room temperature, J. Am. Chem. Soc. 127 (2005) 17998–17999.

[19]Llewellyn, P.L.,Bourrelly,S.,Serre,C.,Vimont,A.,Daturi,M.,Hamon,L.,Weireld, G.D., Chang,J.-S.,Hong,D.-Y.,Hwang,Y.K.,Jhung,S.H.,Fe´ rey, G.,2008.High uptakes ofCO2 and CH4 in mesoporousmetal-organicframeworksMIL-100 and MIL-101.Langmuir24,7245–7250.

[20] Hayashi, H.,Cˆote´ , A.P.,Furukawa,H.,O'Keeffe,M.,Yaghi,O.M.,2007.Zeolitea imidazolate frameworks.Nat.Mater.6,501–506.

[21]Banerjee,R.,Phan,A.,Wang,B.,Knobler,C.,Furukawa,H.,O'Keeffe,M.,Yaghi,O.M., 2008. High-throughputsynthesisofzeoliticimidazolateframeworksand application to CO2 capture. Science319,939–943.

`

[22] Z. Zhang, S. Xian, H. Xi, H. Wang, Z. Li, Improvement of CO2 adsorption on ZIF-8 crystals modified by enhancing basicity of surface, Chem. Eng. Sci. 66 (2011) 4878–4888.

[23] N. Konduru, P. Lindner, N.M. Assaf-Anid, Curbing the greenhouse effect by carbon dioxide adsorption with zeolite 13X, AIChE J. 53 (2007) 3137–3143.

[24] M.Rad, S. Fatemi, S. Mirfendereski, Development of T type zeolite for separation of CO2 from CH4 in adsorption processes, chemical engineering research and design 9 0 (2012) 1687–1695.

[25] A. Hirotani, R. Mizukami, H. Miura, T. Takaba, A. Miya, A. Fahmi, A. Stirling, M. Kubo, A. Miymoto, Grand Canonical Monte Carlo of the dsorption of CO2 on silicalite and NaZSM-5, Appl. Surf. Sci. 120 (1997) 81–84.

[26] A. Zukal, J. Pawlesa, J. Cejka, Isosteric heats of adsorption of carbon dioxide on zeolite MCM-22 modified by alkali metal cations, Adsorption 15 (2009) 264–270.

[27] I. Deroche, L. Gaberova, G. Maurin, P.L. Llewellyn, M. Castro, P. Wright, Adsorption of carbon dioxide in SAPO STA-7 and AlPO-18: Grand anonical Monte Carlo simulations and microcalorimetry measurements, Adsorption 14 (2008) 207–213.

[28] Z. Zhang, M. Xu, H. Wang, Z. Li, Enhancement of CO2 adsorption on high surface rea activated carbon modified by N2, H2 and ammonia, Chem. Eng. J. 160 (2010) 571–577.

[29] W.Isahak, Z. Ramli, M.Ismail, K.Ismail, R.Yusop, M.Hisham, M.Yarmo, Adsorption–desorption of CO2 on different type of copper oxides surfaces: Physical and chemical ttractions studies, Journal of CO2 Utilization 2 (2013) 8–15.

[30] Elkhalifah, A.E.I., et al., Effects of exchanged ammonium cations on structure characteristics and CO2 adsorption capacities of bentonite clay, Applied Clay Science (2013), http://dx.doi.org/10.1016/j.clay.2013.07.016.

[31] Chungsying Lu, Fengsheng Su , Shih-Chieh Hsu, Wenfa Chen, Hsunling Bai,Jyh Feng Hwang, Hsiu-Hsia Lee, Thermodynamics and regeneration of CO2 adsorption on mesoporous spherical-silica particles, Fuel Processing Technology 90 (2009) 1543–1549

[32] A. L. Yaumi, I. A. Hussien, R. A. Shawabkeh, Surface modification of oil fly ash and its application in selective capturing of carbon dioxide, Applied Surface Science 266 (2013) 118– 125.

`

[33] M. Olivares-Marıˇın, T.C. Drage, M. Mercedes Maroto-Valer, Novel lithium-based sorbents from fly ashes for CO2 capture at high temperatures, International Journal of Greenhouse Gas Control 4 (2010) 623–629.

[34] H.R. Abid, G.H. Pham, H.M. Ang, M.O. Tade, S. Wang, Adsorption of CH4 and CO2 on Zr-metal organic frameworks, Journal of Colloid Interface Science 366 (1) (2012) 120–124.

[35] X. Yan, L. Zhang, Y. Zhang, Ke Qiao, Z. Yan, S. Komarneni, Amine-modified mesocellular silica foams for CO2capture, Chemical Engineering Journal 168 (2) (2011) 918–924.

[36] O.G. Nik, X.Y. Chen, S. Kaliaguine, Functionalized metal organic framework polyimide mixed matrix membranes for CO2/CH4 eparation, Journal of Membrane Science 413–414 (2012) 48–61.

[37] Z.B. Bao, L.A. Yu, Q.L. Ren, X.Y. Lu, S.G. Deng, Adsorption of CO2 and CH4 on a magnesium-based metal organic framework, Journal of Colloid and Interface Science 353 (2) (2011) 549–556.

[38] X. Xu, C. Song, J.M. Andresen, G.M. Bruce, A.W. Scaroni, Preparation and characterization of novel CO2 “molecular basket” adsorbents based on polymer-modified mesoporous molecular sieve MCM-41, Microporous and Mesoporous Materials 62 (2003) 29–45.

[39] G. Qi, Y. Wang, L. Estevez, X. Duan, N. Anako, A.-H.A. Park, W. Li, C.W. Jones, E.P. Giannelis, High efficiency nanocomposite sorbents for CO 2 capture based on amine-functionalized mesoporous capsules ,Energy Environ. Sci. 4 (2011) 444–452.

[40] A. Somy, M.R. Mehrnia, H.D. Amrei, A. Ghanizadeh, M. Safari, Adsorption of carbon dioxide using impregnated activated carbon promoted by Zinc, Int. J. Greenhouse Gas Control, 3 (2009), pp. 249–254

[41] Vic DiVenere, The Greenhouse Effect and Global Warming, http://www.columbia.edu/~vjd1/greenhouse.htm.

[42] Anthes, R.A., Corell, R.W., Holland, G., Hurrell, J.W., MacCracken, M.C., & Trenberth, K. (2010, February 12). Hurricanes and Global Warming—Potential Linkages and Consequences. Bulletin of the American Meteorological Society, 87: 623-628. Accessed April 15, 2010.

[43] Meehl, G.A., et al., "Ch 10: Global Climate Projections", Sec 10.7.2 Climate Change Commitment to Year 3000 and Beyond to Equilibrium, in IPCC AR4 WG1 2007.

`

[44] Hansen, J.E. and M. Sato (July 2011), NASA GISS: Science Briefs: Earth's Climate History: Implications for Tomorrow, New York City, New York, USA: NASA GISS.

[45] IPCC, "Summary for Policymakers", Sec. 1. Observed changes in climate and their effects, p. 5, in IPCC AR4 SYR 2007.

[46]http://wattsupwiththat.com/2014/04/23/march-2014-global-surface-landocean-temperature-anomaly-update/

[47] U.S. Energy Information Administration (2011). Electricity Explained - Basics.

[48] Kahn Ribeiro, S., S. Kobayashi, M. Beuthe, J. Gasca, D. Greene, D. S. Lee, Y. Muromachi, P. J. Newton, S. Plotkin, D. Sperling, R. Wit, P. J. Zhou (2007). Transport and its infrastructure. In Climate Change 2007: Mitigation.

[49] Rao A.B, Rubin E.S. (2002), A technical, economic, and environmental assessment of amine-based CO2 capture technology for power plant greenhouse gas control. Environmental Science and Technology, 36:4467-4475.

[50] CO2CRC, CO2 capture/separation technologies, http://www.co2crc.com.au/aboutccs/cap_membranes.html.

[51] thermo Nicolet corporation, "introduction to Fourier transform infrared spectroscopy" 2010, http://mmrc.caltech.edu/FTIR/FTIRintro.pdf.

[52] http://www.ammrf.org.au/myscope/xrd/background/whatisxrd/.

[53] Klug, H. P.; Alexander, L. E. X-ray Diffraction Procedures for Polycrystalline and Amorphous Materials, 2nd ed.; John Wiley & Sons: New York, 1974.

[54] Lauriat, J.-P. Introduction a` la cristallographie et a` la diffraction Rayons XsNeutrons, Paris Onze e´dition N° K 150; Universite´ de Paris- Sud: Orsay, France,1998.

[55]http://www.greenwood.wa.edu.au/resources/Physics%203B%20WestOne/content/004_em_fields_force/page_12.htm.

[56] Shimadzu Scientific Instruments Inc., "Shimadzu: Application News – Energy Dispersive X-Ray Fluorescence Spectroscopy", 2012.

[57] S. Gregg, L. Sing, Adsorption, Surface Area and Porosity, 2nd ed., Academic Press, London, 1982.

`

[58] K. Sing, D. Everett, R. Haul, L. Moscou, R. Pierotti, J. Rou- querol, and T. Siemieniewska, Pure Appl. Chem. 57, 603 (1985).

[59] Recommendations: Reporting Physisorption Data for Gas/Solid Systems with Special Reference to the Determination of Surface Area and Porosity, IUPAC Commission on Colloid and Surface Chemistry Including Catalysis, Pure Appl. Chem., 57 (1985) 603; Recommendations for the Characterization of Porous Solids, IUPAC Commission on Colloid and Surface Chemistry, Pure Appl. Chem., 66 (1994) 1739.

[60] Characterisation of Porous Solids; Dubinin, M.M., Ed.; Society of Chemical Industries: London, 1979; Vol. 1.

[61] Christian Lastoskie , Keith E. Gubbins , Nicholas Quirke, Pore size distribution analysis of microporous carbons: a density functional theory approach, J. Phys. Chem., 1993, 97 (18), pp 4786–4796.

[62] Brunauer, S., Emmett, P.H., Teller, E., J. Amer. Chem. Soc., 1938, 60, pp. 309.

[63] Jura, G., Harkins, W.D., J. Amer. Chem. Soc., 1944, 66, pp. 1856.

[64] K.S. Low, C.K. Lee, B.F. Tan, Quaternized wood as sorbent for reactive dyes, Appl. Biochem.Biotechnol., 87 (2000), pp. 233–245.

[65] M. Najafia, Y. Yousefib, A.A. Rafatib, Synthesis, characterization and adsorption studies of several heavy metal ions on amino-functionalized silica nano hollow sphere and silica gel, Separation and Purification Technology 85 (2012), pp. 193-205.

[66] Shawabkeh, R. and Tutunji, M., Experimental study and modeling of basic dye sorption by diatomaceous clay, Invited publication in Experimental Earth Journal, 1 (5), 2003.

[67] Bear, F.E., 1965. Chemistry of the Soil, 2nd ed. Reinhold Publishing, New York.

[68] ALAIN MEUNIER, Clays, ISBN 3-540-21667-7 Springer Berlin Heidelberg New York.

[69] http://www.separationprocesses.com/Adsorption/AD_Chp02c.htm.

[70] http://chemelab.ucsd.edu/aeronex02/model.html.

[71] Yazaydın Aozr, Benin AI, Faheem SA, Jakubczak P, Low JJ, Willis RR and Snurr RQ, Enhanced CO2 adsorption in metal-organic frameworks via occupation of open-metal sites by coordinated water molecules. Chem Mater 21:1425–1430 (2009).

`

[72] BAROZ AZIZ, " Synthesis and modification of potential CO2 adsorbents, Amine modified silica and calcium carbonates" Ms thesis, Stockholm University

[73] C.J. Geankoplis, Transport Processes and Unit Operations, third ed., Prentice-Hall, New Jersey, 1993.

[74] Maroto-Valer .M.M., Tang Z. and Zhang Y., 2005: CO2 capture by activated and impregnated anthracites. Fuel Processing Technology 86(14–15), 1487–1502

[75] V.J. Inglezakis, S.G. Poulopoulos, Adsorption, Ion Exchange and Catalysis. Designof Operations and Environmental Applications, Elsevier, The Netherlands, 2006.

[76] R.M.A. Roque-Malherbe, Adsorption and Diffusion in Nanoporous Materials,CRC Press, Florida, 2007.

[77] Monier, M. and D. A. Abdel Latif : Adsorption of Hg 2+, Cu 2+ and Zn 2+ ions from aqueous solution using formaldehyde cross-linked modified chitosan hioglyceraldehyde Schiff's base (2012) International Journal of Biological Macromolecules, 50 (3), pp. 773-781.

[78] Reyad Shawabkeh, Equilibrium study and kinetics of Cu2+ removal from water by zeolite prepared from oil shale ash Process, Safety and Environmental Protection 87 (2009) 261–266.

[79] C. Namasivayam and D. Kavitha1: Removal of Congo Red from water by adsorption onto activated carbon prepared from coir pith, an agricultural solid waste Dyes and Pigments 54 (2002) 47–58.

[80] I.A.W. Tan, B.H. Hameed and A.L. Ahmad: Equilibrium and kinetic studies on basic dye adsorption by oil palm fibre activated carbon Chemical Engineering Journal 127 (2007) 111–119.

[81] V.K. Gupta, I. Ali,b Suhas, and Dinesh Mohan: Equilibrium uptake and sorption dynamics for the removal of a basic dye (basic red) using low-cost adsorbents Journal of Colloid and Interface Science 265 (2003) 257–264.

[82] Yahya S. Al-Degs a, Musa I. El-Barghouthi a, Amjad H. El-Sheikh and Gavin M.Walker: Effect of solution pH, ionic strength, and temperature on adsorption behavior of reactive dyes on activated carbon Dyes and Pigments 77 (2008) 16-23.

[83] Faust S and Aly O: Adsorption processes for water treatment. Butterworth Publishers; 1987.

[84] http://www.eia.gov/environment/emissions/co2_vol_mass.cfm

`

[85] Danlu Tong, Geoffrey C. Maitland, Martin J.P. Trusler, Paul S. Fennell, Solubility of carbon dioxide in aqueous blends of 2-amino-2-methyl-1-propanol and piperazine, Chemical Engineering Science, Volume 101, 20 September 2013, Pages 851-864, ISSN 0009-2509.

[86] Young Eun Kim, Sung Jun Moon, Yeo Il Yoon, Soon Kwan Jeong, Ki Tae Park, Shin Tae Bae, Sung Chan Nam, Heat of absorption and absorption capacity of CO2 in aqueous solutions of amine containing multiple amino groups, Separation and Purification Technology, Volume 122, 10 February 2014, Pages 112-118, ISSN 1383-5866.

[87] Yamini Sudha Sistla, Ashok Khanna, CO2 Absorption Studies in Amino Acid-Anion Based Ionic Liquids, Chemical Engineering Journal, Available online 27 October 2014, ISSN 1385-8947, http://dx.doi.org/10.1016/j.cej.2014.09.043.

[88] Norihiro Murayama, Hideki Yamamoto, Junji Shibata, Mechanism of zeolite synthesis from coal fly ash by alkali hydrothermal reaction, International Journal of Mineral Processing, Volume 64, Issue 1, February 2002, Pages 1-17, ISSN 0301-7516.

[89] W. Franus, charactiriczation of X- type zeolite prepared from coal fly ash, Pol. J. Environ. Stud. Vol 21, No. 2(2012), 337-343.

[90] Maria Bentabol, Maria Dolores Ruiz Cruz, Francisco Javier Huertas and Jose Linares, Hydrothermal synthesis of Mg-rich and Mg-Ni-rich kaolinite, Clays and Clay Minerals(December 2006), 54(6):667-677

[91] M. Bentabol, M.D. Ruiz Cruz, F.J. Huertas, Hydrothermal synthesis (200 °C) of Co–kaolinite and Al–Co–serpentine, Applied Clay Science, Volume 42, Issues 3–4, January 2009, Pages 649-656, ISSN 0169-1317, http://dx.doi.org/10.1016/j.clay.2008.06.001.

[92] Mousa Gougazeh, J.-Ch. Buhl, Synthesis and characterization of zeolite A by hydrothermal transformation of natural Jordanian kaolin, Journal of the Association of Arab Universities for Basic and Applied Sciences, Volume 15, April 2014, Pages 35-42.

[93] Ghorab, H.Y.; Rizk, M.; Ibrahim, B.; Allam, M.M. (2014) High belite cement from alternative raw materialsMater. Construcc. 64 [314], e012 http://dx.doi.org/10.3989/mc.2014.01913.

[94] Petr Ptáček, Tomáš Opravil, František Šoukal, Jaromír Havlica, Radek Holešinský, Kinetics and mechanism of formation of gehlenite, Al–Si spinel and anorthite from the mixture of kaolinite and calcite, Solid State Sciences, Volume 26, December 2013, Pages 53-58, ISSN 1293-2558, http://dx.doi.org/10.1016/j.solidstatesciences.2013.09.014.

`

[95] Karfa Traoré, Tibo Siméon Kabré, Philippe Blanchart, Gehlenite and anorthite crystallisation from kaolinite and calcite mix, Ceramics International, Volume 29, Issue 4, 2003, Pages 377-383, ISSN 0272-8842, http://dx.doi.org/10.1016/S0272-8842(02)00148-7

[96] Hua Xu, Jannie S.J. Van Deventer, Microstructural characterisation of geopolymers synthesised from kaolinite/stilbite mixtures using XRD, MAS-NMR, SEM/EDX, TEM/EDX, and HREM, Cement and Concrete Research, Volume 32, Issue 11, November 2002, Pages 1705-1716, ISSN 0008-8846, http://dx.doi.org/10.1016/S0008-8846(02)00859-1.

[97] Yen-Hua Chen, De-Long Lu, Amine modification on kaolinites to enhance CO2 adsorption, Journal of Colloid and Interface Science, Volume 436, 15 December 2014, Pages 47-51, ISSN 0021-9797, http://dx.doi.org/10.1016/j.jcis.2014.08.050

[98] Castellano, M., Turturro, A., Riani, P., Montanari, T., Finocchio, E., Ramis, G., Busca, G. Bulk and surface properties of commercial kaolins (2010) Applied Clay Science, 48 (3), pp. 446-454.

[99] N. Emre Altun, Assessment of marble waste utilization as an alternative sorbent to limestone for SO2 control, Fuel Processing Technology, Volume 128, December 2014, Pages 461-470, ISSN 0378-3820, http://dx.doi.org/10.1016/j.fuproc.2014.08.009.

[100] KALMYKOVA, Y., PEREZ-HOLMBERG, J., ABBAS, Z. AND STEENARI, B-M, UTILIZATION OF PAPER INDUSTRY WASTE IN CONTAMINATED WATER TREATMENT, http://www.srcosmos.gr/srcosmos/showpub.aspx?aa=14241

[101] Kalliopi K. Aligizaki, Pore Structure of Cement-Based Materials: Testing, Interpretation and requirements, modern concrete technology sereie, V 12.

[102] E. P. Barrett, L. G. Joyner, P. P. Halenda, The determination of pore volume and area distributions in porous substances. I. Computations from nitrogen isotherms, J. Am. Chem. Soc. (1951), 73, 373–380.

[103] Moaaz K. Seliem, S. Komarneni, M. Park, H. Katsuki, M.G. Shahien, A.A. Khalil, I.M. Abd El-Gaid, Hydrothermal synthesis of Mn-kaolinite using NaOH or KOH and characterization, Applied Clay Science, Volume 49, Issues 1–2, June 2010, Pages 74-79, ISSN 0169-1317, http://dx.doi.org/10.1016/j.clay.2010.04.006.

[104] L. Heller-Kallai, I. Lapides, Reactions of kaolinites and metakaolinites with NaOH—comparison of different samples (Part 1), Applied Clay Science, Volume 35, Issues 1–2, January 2007, Pages 99-107, ISSN 0169-1317, http://dx.doi.org/10.1016/j.clay.2006.06.006.

`

[105] M. Murat, A. Amokrane, J. P. Bastide and L. Montanaro, Synthesis of zeolites from thermally activated kaolinite; some observations on nucleation and growth Clay Minerals(March 1992), 27(1):119-130

[106] Rios, Carlos A. Williams, Craig D. Maple, Martin J., Synthesis of Zeolites and Zeotypes by Hydrothermal transformation of Kaolinite and Metakaolinite, BISTUA, V.5, 15-26

[107] Z Aksu, Equilibrium and kinetic modelling of cadmium(II) biosorption by C. vulgaris in a batch system: effect of temperature, Separation and Purification Technology, Volume 21, Issue 3, 1 January 2001, Pages 285-294, ISSN 1383-5866, http://dx.doi.org/10.1016/S1383-5866(00)00212-4.

[108] Ramiro J.E. Martins, Rosana Pardo, Rui A.R. Boaventura, Cadmium(II) and zinc(II) adsorption by the aquatic moss Fontinalis antipyretica: effect of temperature, pH and water hardness, Water Research, Volume 38, Issue 3, February 2004, Pages 693-699, ISSN 0043-1354, http://dx.doi.org/10.1016/j.watres.2003.10.013.

[109] C. Namasivayam, D. Kavitha, Removal of Congo Red from water by adsorption onto activated carbon prepared from coir pith, an agricultural solid waste, Dyes and Pigments, Volume 54, Issue 1, July 2002, Pages 47-58, ISSN 0143-7208, http://dx.doi.org/10.1016/S0143-7208(02)00025-6.

[110] Mahir Alkan, Çiğdem Hopa, Zürriye Yilmaz, Halil Güler, The effect of alkali concentration and solid/liquid ratio on the hydrothermal synthesis of zeolite NaA from natural kaolinite, Microporous and Mesoporous Materials, Volume 86, Issues 1–3, 28 November 2005, Pages 176-184, ISSN 1387-1811, http://dx.doi.org/10.1016/j.micromeso.2005.07.008.

`

Vitae

Name : **Qusay Yousef I. Bkour**

Nationality : **Jordanian**

Date of Birth : **11/28/1990**

Email :**qousi4@hotmail.com**

Address : **Irbid, Jordan**

Academic Background :

***Bachelor in Chemical Engineering, from Jordan University of Science and Technolgy (JUST), Irbid, Jordan, 2012.**

***Certificate Examination of General Secondary Education (Tawjihi) (GPA: 89.3%).**

Research Interest, experience and projects:

- **Adsorption of carbon dioxide from natural gas using kaolin based material**
- **synthesis of nano structured material**
- **Production of activated carbon from waste fly ash and application for selective removal of hydrogen sulfide from natural gas.**
- **Removing of the multi-components heavy metals in water by using treated fly ash.**
- **polymerization of natural kaolinite to make strong construction materials.**

`

- **Making hybrid organic-inorganic nanocomposites by functionalization of kaolinite and other natural clays with different materials to removal of hydrogen sulfide from natural gas.**

- **Polymer nanocomposite.**

Publications:

- R.Shawabkeh, N.Faqir, Q.Bkour," Synthesis of CO2-ONE adsorbent for CO2 removal", Patent Pending, # 424688US.

- Q.Bkour, N.Faquir, R.Shawabkeh, A. Ul-Hamid, Hans-JörgBart, " Adsorption of CO2 by chemically treated kaolin-based materials", Under submission.